THERMO-ELECTRO-HYDRODYNAMIC INVESTIGATIONS OF ALL-VANADIUM REDOX FLOW BATTERY USING LUMPED MODEL AND NUMERICAL SIMULATION

A thesis submitted in partial fulfillment of the requirements for the degree of

DOCTOR OF PHILOSOPHY

By

SATHISHA H.M.

DEPARTMENT OF MECHANICAL ENGINEERING

INDIAN INSTITUTE OF TECHNOLOGY GUWAHATI

GUWAHATI 781039, INDIA

OCTOBER 2015

THERMO-ELECTRO-HYDRODYNAMIC INVESTIGATIONS OF ALL-VANADIUM REDOX FLOW BATTERY USING LUMPED MODEL AND NUMERICAL SIMULATION

A thesis submitted in partial fulfillment of the requirements for the degree of

DOCTOR OF PHILOSOPHY

By

SATHISHA H.M.

(Roll No. 10610327)

DEPARTMENT OF MECHANICAL ENGINEERING

INDIAN INSTITUTE OF TECHNOLOGY GUWAHATI

GUWAHATI 781039, INDIA

OCTOBER 2015

CERTIFICATE

It is certified that the work contained in the thesis entitled **"Thermo-Electro-Hydrodynamic Investigations of All-Vanadium Redox Flow Battery Using Lumped Model and Numerical Simulation"** by **Sathisha H.M.**, has been carried out under my supervision and that this work has not been submitted elsewhere for a degree.

(Amaresh Dalal)
Associate Professor
Department of Mechanical Engineering
Indian Institute of Technology Guwahati

October, 2015

ABSTRACT

Renewable energy technology is needed urgently due to crisis and challenges against conventional energy's. However, intermittent and random nature of the non-conventional energy sources like solar and wind leads to low quality electricity output and a poor stability in the grid. The electricity energy storage (EES), storing and releasing electricity, is available temporarily to resolve those problems. Among all the EES technologies all-vanadium redox flow battery (VRFB) is a promising option. The VRFBs have many advantages including long cycle life, active thermal management, elimination of electrolyte cross-contamination, high energy efficiency, low cost for large energy storage systems, etc. Most important feature of redox flow batteries is its power flexibility. Also, capacity design of a battery is not coupled making more efficient design of the battery configurations. Hence, the redox flow batteries are preferred for the applications of peak shaving, load leveling, grid integration and frequency regulation. Compared to other flow batteries, VRFB is more preferred since it does not suffer from the problem of electrolyte cross-contamination due to the fact that both the half cells of the battery employ different species of vanadium in the electrolyte. As a result, electrolyte lifetime is increased significantly. It has been observed that the disposal of vanadium ions from VRFB do not create any environmental issues in comparison with conventional lead acid battery. However, a few challenges have to be taken into account to implement this technology. As of now, there are only a few lumped and comprehensive models developed for VRFBs which explain system performances and characteristics at steady and unsteady states under different operating conditions.

The present thesis employs lumped dynamic model for the all-vanadium redox flow battery, using the conservation equations of charge and mass combined with the effects of major resistances, electrochemical reactions and recirculation of the electrolyte through external reservoirs. The same model is extended by adding the effects of crossover of vanadium ions through membrane and mass transfer. This model is able to predict the cell voltage variation and capacity loss of cell for different membrane materials. One more lumped thermal model is used, which is based on conservation of energy to predict the temperature variation of cell and reservoir

as a function of time, surrounding air temperature and battery structure.

A comprehensive numerical model is used for two-dimensional, three-dimensional steady and unsteady simulations. The model is based on the conservation laws along with the fundamental modes of transport and kinetic model for reactions involving the vanadium species. The processes in the redox flow batteries are described by the equations of electrodynamics, electrochemistry and fluid mechanics. The electrolyte flow through porous electrodes and diffusion of proton ions through the membrane can be modeled by the laws of conservation of mass and momentum. By solving the Poisson equations, the distributions of electric potential for VRFB can be determined. Using Nernst equation and Butler-Volmer law, the electrochemical interaction of species in the cell can be obtained. Combination of these processes makes the solution of equations more complicated. The same model is also extended by including the concentration over potential and ohmic losses and predicts various efficiencies accurately for different parameters.

There are many issues which need to be addressed in order to make it commercially viable application. These issues include optimization and scale-up which encompasses flow geometries assemblage and operation conditions, membrane fouling, development of electrode materials resistant to oxidation and improvement in electrolyte stability. Modeling and simulation are cost-effective methods for solving these problems, which can minimize the time and costs of the laboratory experiments. In addition to this, modeling and simulation can reveal the detailed information about fundamental processes inside the vanadium redox flow battery, which is useful for optimizing the design and operating condition. Moreover, there is a need to develop control oriented models that can capture the performance accurately.

Keeping these motivations in mind, this doctoral thesis focuses on development of lumped and comprehensive numerical models. The objectives of this work are two folds. Firstly, it is to develop a lumped model which includes lumped dynamic model incorporating with and without crossover effects and thermal modeling. The other objective is to develop two and three-dimensional steady and transient numerical model encompassing theoretical analysis which will be helpful for fundamental understanding of the underlying mass and charge transport characteristics in the porous electrode. A primary focus is to gain more detailed coupled characteristics of mass and charge for the operation of vanadium redox flow battery to optimize the performance of the battery. The detailed research objectives are given below.

A lumped dynamic model simulation has been carried out. The model is able to predict the effects of flow rate, applied current density, concentration, porosity, temperature on the performance of an all-vanadium redox flow battery. It is observed that higher electrolyte flow rate gives longer charging time and higher cell performance. The lower applied current density yields better potential difference than

higher applied current densities. The higher vanadium concentration shows increase in cell voltage which leads to high performance. The lower porosity of the electrode gives little less potential difference than higher porosity electrode during charging, while discharging it gives higher potential difference, but overall lower porosity electrode gives better performance. The higher operating temperature leads to poor performance of the cell. These parametric studies help to optimize the performance of the all-vanadium redox flow battery.

The above model is extended by adding the effects of mass transfer and crossover of vanadium ions through membrane. The model predicts the capacity loss for different membrane materials. The simulation results show that reaction rate constants and diffusion coefficients depends on temperature and it affects cell performance. The model is able to predict the capacity loss of the battery due to the diffusion of vanadium ions across the membrane over many cycles at different temperatures. The effect of temperature and porosity on concentration change is studied for three membrane materials such as, Selemion AMV membrane, Selemion CMV membrane and Nafion 115 membrane and the temperature ranging from 10° C and 40° C. The effects of temperature on diffusion coefficients and reaction rate constants have also been studied. It is observed that the capacity loss for Selemion AMV membrane and Selemion CMV membrane shows linear variation with number of cycles and it does not stabilize. In the case of Nafion 115 membrane, capacity loss is experienced initially up to 77 cycles, then stabilizes with increase in number of cycles. The simulation results show that crossover and mass transfer effects have significant impact on the performance of the cell potential response.

A thermal model is developed for the vanadium redox flow battery system based on the conservation of energy for transient conditions. The model has three energy balance equations. One energy balance equation for the battery stack and the other two energy balance equations for electrolyte reservoirs are solved. One stack with 19 cells and two electrolyte reservoirs are considered for simulations. The model formulation considers the pump power loss, chemical power loss and power loss due to cell internal resistance. The dynamic model is able to predict the stack and tank temperatures for various working conditions. The results show that the stack and reservoir temperature are very much sensitive to the effects of flow rate, surrounding air temperature. Therefore, this model can be more useful to design the battery system for specific location of the installation.

A two-dimensional transient, isothermal model for the all-vanadium redox flow battery is developed. In this context, earlier efforts reported in the literature were mainly focused on simulation of the variation of the charge/discharge characteristics of the cell. There is a need to optimize the cell parameters so that the cell performance can be improved. This model is used to predict the effects of change in concentration, electrolyte flow rate, electrode porosity and applied current. Numer-

ical model results are validated with the available experimental result which shows good agreement. It is observed from the results that higher vanadium concentration shows increase in cell voltage which leads to higher performance. The higher electrolyte flow rate gives longer charging time, so it gives also higher coulombic efficiency and higher cell performance. Lower applied current yields better potential difference than higher applied current. It is also seen that decrease of the electrode porosity by a very small amount can lead to a significant increase in coulombic efficiency and reduction in the rates of oxygen and hydrogen gas evolution reaction. One of the main features of the numerical model is the ability to predict various parameters, such as, velocity, pressure, concentration etc. These quantities are difficult to measure and sometimes not possible by laboratory experimentation. This information could be useful in extending the life of battery.

This investigation is further extended by incorporating concentration overpotential and ohmic losses into the model. Concentration overpotential of an electrode occurs due to the formation of a diffusion layer adjacent to the electrode surface, where there is a gradient of the concentration of ion. Ohmic losses associated with current collector, membrane and the electrolyte are considered. Due to these overpotentials, there is considerable amount of voltage drop taking place inside the cell. Therefore, significant amount of variation in efficiencies can be observed. Using the model effect of concentration, electrolyte flow rate, electrode porosity and applied current on the performance of the cell are analyzed. Simulations have predicted that concentration $C_3^0 = 1260\ mol/m^3$ gives maximum voltage and energy efficiency. Hence, it can be considered as optimum value. Also, it is observed that increasing the electrolyte flow rate gives better cell performance. Lesser the value of electrode porosity values, higher the efficiencies of the cell due to uniform distribution of concentration inside the porous electrode. Higher coulombic, voltage and energy efficiencies can be observed for lesser value of applied current because there are no side reactions.

A three-dimensional numerical simulation can provide the detailed information, which is helpful to optimize the cell performance. The steady isothermal model includes concentration overpotential and ohmic losses which have significant contribution to predict performance accurately. The effects of electrolyte flow rate, concentration, electrode porosity and applied current density with state of charge are studied. It is observed that electrolyte distribution has symmetric pattern in the domain of porous electrode. The higher velocity of electrolyte leads to lower overpotential, therefore, less chances of side reactions. Higher flow rate shows higher energy efficiency due to more uniform distribution of vanadium ions in the porous electrode. Also, it is observed that for higher initial concentration gives higher voltage for both charging and discharging conditions. From the results, it is seen that lower electrode porosity gives better performance due to lower polarization and lower hydrogen and oxygen gas evolution side reactions. The higher current density increases the over-

potential in both half of the cell leading to side reactions and therefore performance decreases. It can be concluded that electrode properties, current density vary with state of charge and these parameters have significant impact on the energy efficiency.

The previous model is further extended for transient conditions. This model is used to predict the effects of change in electrolyte flow rate, concentration and electrode porosity. For the given geometry of the cell, the model is able to predict the distributions of velocity, pressure and concentration in sections parallel and perpendicular to the direction of the applied current. It is observed from the results that higher vanadium concentration shows increase in cell voltage and uniform distribution of concentrations inside the cell, which lead to higher performance. The higher electrolyte flow rate gives longer charging time, higher coulombic efficiency and also better cell performance. This is because a higher flow rate minimizes the contact time for reaction in the electrode, which results in longer time for the exit solution to reach the required state of charge.

The thesis is concluded with a summary of the main findings and recommendations for future work.

Dedicated to my parents

Sri. Mallesha Gowda
and
Smt. Kamalamma

Acknowledgements

I would like to express my sincere gratitude to my advisor Dr. Amaresh Dalal for the continuous support of my Ph.D study and research, for his motivation, patience, enthusiasm, and immense knowledge. His guidance helped me in all the time of research and writing of this thesis. His willingness to help whenever I had problems is fascinating. Also he was always keen to help me to understand a few more things about batteries and CFD. I could not have imagined having a better advisor and mentor for my Ph.D study.

I am grateful to Dr. Partha P. Mukherjee from Texas A & M, USA, who inspired me to begin the research on vanadium redox flow battery and mentored during my dissertation work. My thanks go to Professor Pinakeshwar Mahanta, Dr. Ganesh Natarajan and Dr. Nanda Kishore for their service on my doctoral thesis committee and for their suggestions and insightful comments on my work.

I would also like to extend my sincerest appreciation and thanks to Professor Anup Kumar Das, Dr. Arnab K. De, Dr. Vinayak Kulkarni and Dr. Pankaj Biswas from IIT Guwahati for motivating me during this study. Also I want to thank to Pro. S. R. Mahadeva Prasanna and Dr. Arup Kumar Das for their constant encouragement throughout my Ph.D. research.

I wish to acknowledge a great many friends and colleagues who made my study enjoyable: Prashant, Basant Kumar Rana, Jai Manik, Mukul, Saurabh, PreetiRekha, Simon Peeter, Mukesh, Mruthyunjay, Ravi Kant and Jitendra patel. These people have taught me many good values and habits for which I will be always indebted to them.

I would also like to thank my parents and two elder sisters. They were always supporting me and encouraging me with their best wishes.

Finally, I would like to thank my wife, Dr.Kavya. She was always there cheering me up and stood by me through the good times and bad. I would like to dedicate this thesis to my parents whose endless encouragement and love made it possible to

finish this research work.

Contents

List of Figures

List of Tables

Nomenclature

Symbol	Definition	Unit
A	Cross sectional area	m^2
A_1	Inside area of the cylindrical wall	m^2
A_2	Area of the top or bottom circular wall	m^2
B	Amplitude of the air temperature	
b_e	Breadth of the electrode	m
C	Concentration	mol/m^3
C	Minimum of the air temperature	$^\circ C$
C_D	Drag coefficient	Dimensionless
C_p	Specific heat capacity at constant pressure	J/kgK
D	Diffusion coefficient	m^2/s
D	Unit outer normal	Dimensionless
d_g	Bubble diameter	m
E	Potential	V
E_{cell}	Cell voltage	V
eff	Coulombic efficiency	
E_0	Open circuit voltage	V
F	Faradays constant	C/mol
h	electrode height	m
h_e	Height of the electrode	m
H	Height of the tank	m
h_{11}	Convection heat transfer coefficient for the inner cylinder surface	$W/m^2\ K$
h_{12}	Convection heat transfer coefficient for the inner top or bottom surface	$W/m^2\ K$

h_{21}	Convection heat transfer coefficient for the outer cylinder surface	$W/m^2\ K$
h_{22}	Convection heat transfer coefficient for the outer top or bottom surface	$W/m^2\ K$
I	Current	A
$\overrightarrow{j}$	Current density	A/m^2
k	Thermal conductivity of the polypropylene	$W/m\ K$
K	Kozeny-Carman constant(i=1,2)	$Dimensionless$
k_i	Reaction rate constants	m/s
num	Number of cell	
$\overrightarrow{n}$	Thickness/width	m
p	pressure	$Pascal$
Q	Outlet flow rate	m^3/s
Q_{heat}	Heat transfer rate	J/s
r	Height of the tank	m
R	Molar gas constant	$J/molK$
R_1	Overall stack resistance	Ω
R_{co}	Charging average cell resistivity	Ω
R_{do}	Discharge average cell resistivity	Ω
S	Specific surface area for reaction	m^-1
S_i	Source flux term	mol/m^3s
t	time	s
T	Temperature	K
$\overrightarrow{u}$	Phase velocity	m/s
U	Overall heat transfer coefficient	$W/m^2\ K$

U_1	Overall heat transfer coefficient for the cylindrical wall of the tank	$W/m^2\ K$
U_2	Overall heat transfer coefficient for the top circular wall of the tank	$W/m^2\ K$
v	electrolyte velocity	m/s
V_r	Volume of electrolyte in the reservoir	m^3
w_c	Width of the current collector	m
w_e	Width of the electrode	m
w_m	Width of the membrane	m
x	x-coordinate	m
y	y-coordinate	m
z	Electrons involved in the reaction	

Greek Symbols

α	Transfer coefficient	Dimensionless
β	Volume fraction	Dimensionless
$\triangle G$	Change in Gibbs free energy	J/mol
$\triangle H$	Change in enthalpy	J/mol
$\triangle S$	Change in entropy	$J/molK$
ϵ	Porosity	Dimensionless
η	Overpotential	V
θ	Tank thickness	m
μ	Dynamic viscosity	kg/ms
ρ	Density	kg/m^3
σ	Electronic conductivity	S/m
ϕ	Electrostatic potential	V
ϕ_1	Phase	rad
ω	Flow rate	m^3/s
ω_1	Angular frequency	rad/s

Subscripts

air	surrounding air
c	charging
cell	cell
coll	Current collector
d	discharging
H^+	Proton property
H_2O	Water property
in	inlet value
s	stack
t	tank
0	initial or equilibrium value
+	positive electrode property/quantity
−	negative electrode property/quantity

Abbreviations

CFD	Computational Fluid Dynamics
ESS	Energy Storage Systems
ODE	Ordinary Differential Equations
PEM	Proton Exchange Membrane
PSB	PolySulphide-Bromine
RFB	Redox Flow Battery
SIMPLE	Semi Implicit Method for Pressure Linked Equations
TDMA	Tridiagonal Matrix Algorithm
UDF	User Defined Function
VRFB	Vanadium Redox Flow Battery
ZBB	Zinc Bromine Battery

Chapter 1

Introduction

World populations are facing the energy crisis of fossil fuels. The use of fossil fuels creates the problem of pollution leading to global warming, acid rain etc. So there is a scope of developing the renewable energy sources which include tidal energy, biomass energy, wind energy and solar energy etc. From renewable energy sources, the energy cannot be produced continuously. Hence there is a need to store energy, which can be used whenever required. Batteries, the energy storage device, can be used to store the energy. It stores energy in the form of chemical energy and converts to electrical energy. Presently available technology batteries in the market i.e., lead acid battery, lithium ion batteries are more toxic and pollutant to the environment. Therefore, it is essential to develop battery which should be environmental friendly, high efficiency, cheap and simple in construction and operation. Now a days use of redox flow batteries is coming up due to their ability to store large amounts of electrical energy efficiently and economically [1]. A redox flow battery employs liquid battery active materials. The positive and negative active materials are circulated in liquid permeable electrolytic cells, where an oxidation-reduction reaction takes place and it allows charge and discharge [2]. Types of redox flow batteries include all-vanadium, bromide-polysulphide, vanadium/bromine, soluble lead acid cells and zinc-cerium, of which the all-vanadium redox flow battery is most developed [3]. Redox flow secondary batteries have following advantages in comparison with conventional secondary batteries [2].

1. The energy storage capacity of the battery can be increased by simply increasing the volume of the storage tanks and the quantity of the active materials.

2. Redox flow batteries have positive and negative active materials, which are stored completely and separately in different tanks, hence there is less possibility of self discharge than the batteries of other types in which two active materials are in contact with their respective electrodes.

3. During charge and discharge reaction of active material, only ions exchange electrons on the surface of the liquid-permeable carbon porous electrodes used in the redox flow batteries. Therefore, the active materials do not deposit on the electrodes unlike zinc ions in zinc-bromine batteries, hence the cell reaction is simple.

1.1 Batteries

A battery is an electric cell or a device that generates electricity from a chemical reaction. It converts chemical energy stored into electrical energy by redox (reduction/oxidation) reactions. Redox reactions are chemical reactions in which electrons are produced by the chemical reaction. It includes two or more cells connected in parallel or series. A cell consists of a negative electrode, positive electrode, a separator, an electrolyte which conducts ions and an ion conductor. The electrolyte used in the battery can be aqueous or non aqueous in solid, liquid or paste form. If the external load is disconnected from the cell, the reaction process stops, when the external load connected to the cell, the negative electrode supplies a current of electrons that flow through the load and are accepted by the positive electrode. The main parameters that predict most of the basic characteristics of the battery are the materials employed for the electrode and electrolyte for both the reduction and oxidation reactions. The electrode is the main location where core of the reduction and oxidation reactions take place. Most of the battery systems, containing alkaline and lead acid batteries, the electrode is not only where the electron transfer takes places, but also a component in the chemical reaction that generates or uses the electron. In some other kind of battery systems the electrode material is itself inert i.e., no reaction takes place at the electrode and it is the only place for the electron transfer from one reactant to another, this phenomena can be observed in fuel cells.

During discharging process oxidation reaction occurs at the positive electrode called anode and it has positive voltage, reduction reaction during charging process occurs at the negative electrode called cathode, which is having negative voltage. While recharging process the cathode has a positive charge and the anode has a negative charge. The redox reaction occurs not only in the porous electrode, because a redox reaction includes the interaction of more than one component. The other component involving chemical reactions is the electrolyte. Most of the battery system, the electrolyte is an aqueous solution. Main reason for having an aqueous solution is the reduced or oxidized form of the electrode which exists in an aqueous solution. Also another reason is that the chemical species in the electrolyte can flow freely inside the porous electrode where the chemical reaction occurs and ion species can move from one electrode to the other.

1.1.1 Types of Batteries

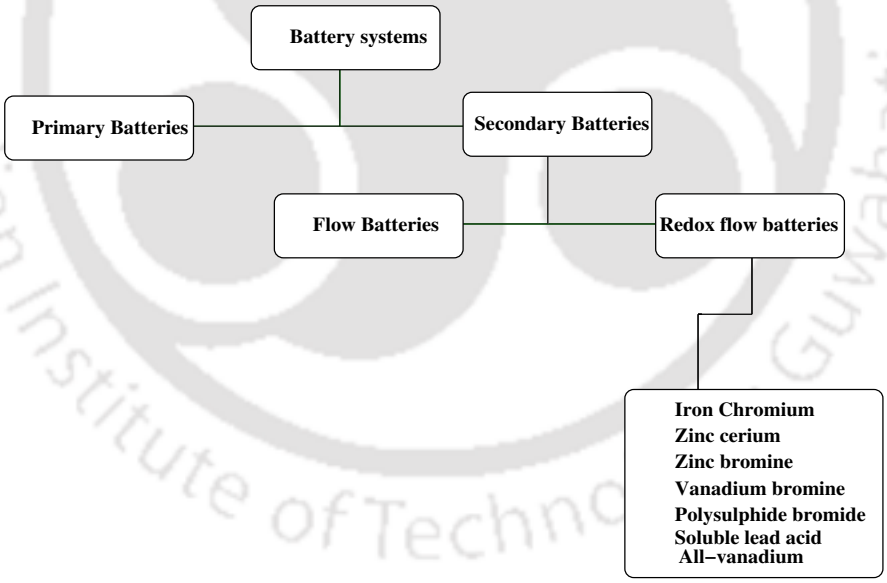

Figure 1.1: Flow chart shows types of battery system

There are two types of batteries, primary and secondary batteries. In primary battery electrical energy conversion from chemical energy is one way process. Even though there are those types of batteries, which transforms irreversibly from chemical energy to electrical energy, if the initial supply of reactants, is exhausted, energy cannot be restored to the battery. Therefore, the process is irreversible and electri-

cal energy cannot be converted to chemical energy. It is understood that a primary battery cannot be recharged, it will convert its chemicals into electricity one time only, then it should be discarded. There are few types of primary batteries such as, telegraph circuits, which can be restored to operation by replacing few components of the battery consumed by the chemical reaction. Figure 1.1 shows types of battery systems. In secondary batteries energy conversion process is reversible, it means that chemical energy can be convert into electrical energy and vice versa. Also these batteries are rechargeable. Battery chemical reactions can make reversed by supplying the electrical energy to the cell, therefore it can restore to the original condition. In secondary batteries the electrodes can be reconstituted by transferring electricity back through it, hence it is called a rechargeable or storage battery. Examples of secondary batteries are lithium-ion batteries employed in higher power consumer electronic equipment such as camcorders, computer laptops, some digital cameras and mobile telephones and lead acid batteries used in cars. Silver zinc battery developed in 1960's was one of the first space battery dominates in most of the industries. This battery has high specific energy and power but it is little costly due to the use of silver. Nowadays these batteries are still used in few s.elected applications, such as torpedoes and space launch vehicles. Silver zinc battery also employed in Mars pathfinder, but it was designed as a rechargeable battery. This type of battery has a relatively short cycle life and can not be used for multi year missions. This battery are also commonly used in hearing aid applications.

1.1.2 Flow Batteries

Flow batteries are also known as redox flow batteries. Redox stands for reduction/oxidation reaction. The name redox flow battery is based on the redox reaction between the two electrolytes in the system. The chemical reactions encompass all chemical processes in which atoms have their oxidation number changed. A flow battery is a form of battery in which electrolyte consisting one or more dissolved electroactive species flows through a cell or porous electrodes and the reactor in which chemical energy is converted to electrical energy. Generally the electrolytes are stored externally by reservoirs/tanks and pumped through the cell of the reactor. A flow battery is designed in such a way that it is more flexible, because energy and power capacity of the cell can be changed very easily. Also the flow battery can be designed for high capacity electrical energy storage as well as for high power

applications. There are many kinds of electrical energy storage devices, such as flywheels and conventional batteries that may not show the flexibility and have few limitations. Flywheels are generally employed for short durations of less than 300 seconds and high power storage more than 0.5×10^6 W, and conventional batteries are used for power less than 0.5×10^6 W and durations more than 1 hour. Large scale projects need high power storage and capacity storage, so preferably flow batteries are used. Therefore, flow batteries are used in the application of grid-connected electricity storage at solar photovoltaic systems and wind farms. There are many kinds of flow batteries using aqueous electrolytes. These include polysulphide bromine, iron chromium cell, all-vanadium redox flow cell and zinc bromine cell. All flow cells use different electrolytes in the negative and positive half cells but cells have same design. Each cell is different in terms of energy efficiency, coulombic efficiency, cycle life and open circuit potential but cells face similar challenges such as electrolyte management and membrane failure. Flow battery is charged and discharged by a reversible chemical reaction process between the two liquid electrolytes of the battery. These electrolytes are stored in the separate storage tanks, but in the case of conventional battery the electrolytes are stored in the power cell of the battery. While operation the electrolytes are supplied from tank using pump through the electrochemical reactor in which chemical reduction and oxidation reaction occur and electricity is generated. Electrolytes are stored outside the reactor, so the design specifications of the cells are flexible, therefore energy content and power of the system can be described separately. It is easy to replace the electrolytes or to increase the amount of electrolytes. Furthermore, the design of the power can be optimized for the power required, this is independent of the amount of electrolyte used. Flow batteries can be more attractive for future applications, particularly for large-scale applications, like peak power support at wind farms or solar photovoltaic cells.

1.1.3 Redox flow battery

A redox flow battery (RFB) is an electrochemical system that permits energy to be stored in two solutions encompassing different redox couples. RFBs are stationary storage batteries that operate continuously pumping two electrolytes through a pair of high surface area electrodes that are separated by the ion exchange membrane. The energy is harvested and stored by the reduction/oxidation reactions of redox

active solutes in the two electrolytes. The redox flow battery system capacity is increased by simply increasing the volume of the electrolyte reservoirs or increasing the concentration of the electrolytes but the conventional secondary batteries storage capacity depends on the size of the electrodes. The redox flow battery technology is developing and having future, three alternative systems have recently been commercialized like, zinc-cerium system, polysulphide-bromine system and all-vanadium system. Figure 1.2 describes redox flow battery which consists of a battery cell and

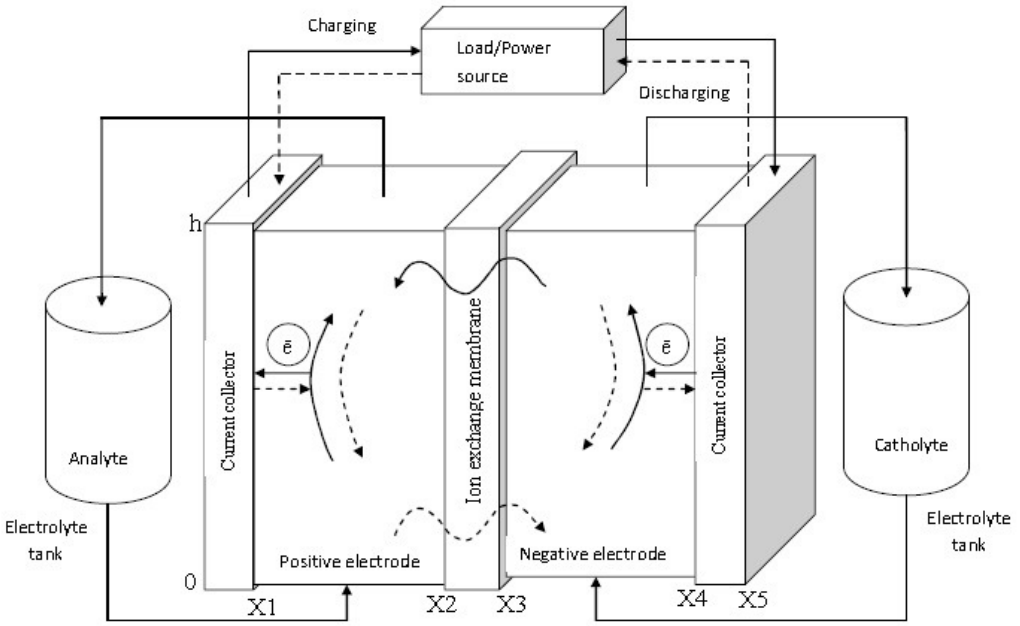

Figure 1.2: Schematics of the vanadium redox flow battery

storage tanks for positive and negative electrolytes. The battery cell is separated by a membrane to provide positive and negative cell, each cell having a liquid permeable porous electrode [3, 4, 5, 6, 7, 8]. The electrolyte is prepared by mixing the electroactive materials with sulphuric acid aqueous solutions. The positive and negative electrolytes are circulated from the storage tanks to the positive and negative cells, respectively [3]. In the battery the reduction and oxidation reactions take place on both sides of the membrane. While the discharge, electrons are removed from the anolyte and passed through the external circuit to the catholyte. While charging flow direction of electron is reversed, the reduction occurs in the anolyte and the oxidation process takes place in the catholyte [9].

1.2 Types of flow batteries

1.2.1 Zinc bromine redox system

The zinc bromine battery (ZBB) is a hybrid flow battery, since one of its electrodes is involved in the reaction. This technology is presently being developed for commercial stationary energy storage applications, but also used for electric vehicle applications. The main advantage of the system is high energy density (65-84 Wh/kg) and can withstand maximum 2000 cycles. The concept of zinc bromine battery initially started since 1880s, but due to technical difficulties the development was very slow until the 1970s. ZBBs are preferred as a rechargeable power source because of their high degree of reversibility, high cell voltage, high energy density, and the materials cost is low [5]. Similar to other redox flow cells, the aqueous electrolytes including reactive species are stored separately in external reservoirs and circulated through each cell in the stack. Each cell consists of two electrodes at which reversible electrochemical redox reactions takes place. During charging process the electrolyte contains zinc bromide salt dissolved in water, so zinc is plated on the negative electrode, therefore capacity of the battery decreases. At the positive electrode, bromine is generated and sinks to the bottom of the positive electrolyte reservoir. While discharging process, bromide ions are formed at the positive electrode and zinc is redissolved to form zinc ions. One more extra pump is needed to re-circulate the bromine complex. The efficiency of the ZBB is around 60-75%.

1.2.2 The iron-chromium redox system

The iron-chromium redox system first studied by the NASA research group. The negative reactant is a solution of the chromous-chromic couple while positive reactant is an aqueous solution of ferric-ferrous redox couple, both reactant acidified with hydrochloric acid solution. In this type of redox flow cell the flow rate of each reactant must be higher than the stoichiometric flow requirement, which leads to total reactant utilization in a single pass through the cell. Each cell consists of cationic and anionic ion exchange membrane, that separates the two flowing reactant solutions. In principle, the membrane does not allow the crossover of chromium and iron ions, it only allows chloride and hydrogen ions for completion of the electrical circuit through the cell [6].

1.2.3 Zinc-cerium redox system

Zinc-cerium batteries are a type of redox flow battery first proposed by Plurion Inc. (UK) in 2000s. Negative side half cell contains zinc electrolyte, positive side half cell contains cerium electrolyte and electrolytes which are circulated while operation are stored in two separate reservoirs. Negative and positive half cell electrolyte compartments are separated by a Nafion cation exchange membrane. Due to the high standard electrode potentials of both cerium and zinc redox reactions in aqueous media the open-circuit cell voltage is significantly high as 2.43 V [7]. Compared to other developed flow battery systems, this system has the highest power density per electrode area and cell voltage. Also supporting electrolyte which is made up of Methanesulfonic acid is used. During charging zinc is electroplated at the negative electrode and redox reactions of Ce(III)/Ce(IV) occur at the positive electrode. Furthermore, this system is classified as a hybrid flow battery.

1.2.4 Polysulphide bromide battery (PSB)

A polysulphide bromide battery is a flow battery in which sodium polysulphide and sodium bromide are used to prepare electrolyte salt solution. The Sodium ions are allowed to pass through the membrane to maintain the electroneutrality of the cell. Even though this technology is used to be environmentally friendly, there is possibility that toxic bromine vapour might be released if any accident occurs[8]. There are engineering technical difficulties need to be solve for the commercial use.

1.2.5 Soluble lead-acid battery

This type of flow battery is based on the electrode chemical reactions of lead(II) in methanesulfonic acid solution. The Pb(II) is highly soluble in the aqueous acid electrolyte, therefore this system differs from conventional lead acid battery. It also differs from other redox flow batteries because there is no need of membrane or separator and it needs only a single electrolyte, therefore it considerably minimizes the cost and design complexity of the batteries [10]. During charging process due to electrode reactions soluble species convert into a solid phase, while discharging process dissolution takes place in the electrode. The process of deposition and dissolution of lead due to reaction should be fast which results in no overpotential.

If there is overpotential takes place then hydrogen evolution bubble formation may occur which results in reducing the capacity of the cell.

1.2.6 Vanadium-bromine redox system

Long ago the research on vanadium-bromide redox flow system was started, due to lack of technology development most of the researchers have recently shown interest. The vanadium bromide redox flow cell uses a Br/Br_3 couple in the positive half-cell and vanadium V(II)/vanadium V(III) couple in the negative half cell, using a mixture of hydrobromic acid, vanadium bromide and hydrochloric acid as the electrolyte in both half-cells. The two V/Br half-cell electrolytes are separated by an ion exchange membrane. The V/Br cell uses the same elements in both half-cell solutions, therefore there are no problems of cross contamination. At the positive half cell no electrochemical reaction takes place for the Vanadium-bromine redox system, i.e., the oxidation of V(IV) to V(V) does not occurs while cell charging. The V/Br redox system has all the advantages of the original vanadium redox flow cell, but the higher solubility of vanadium bromide has the potential to produce higher energy densities [11]. The possibility of using vanadium V(III)/V(IV) solutions and the excess bromide ions in the positive half-cell lead to increase in the energy densities approximately doubled.

1.2.7 All-vanadium redox flow battery (VRFB)

The all-vanadium redox flow battery first developed by Maria Skyllas-Kazacos and co-workers at the University of New South Wales, Australia. It has two half cells, encompasses electrolyte using vanadium redox couples, so there is no problem of self-discharge of vanadium ions through the membrane [9]. The vanadium is available in four different oxidation states, this property of vanadium utilizes to make a battery that has just one electroactive element instead of two. These flow batteries are more suitable for large stationary energy storage applications. A VRFB includes number of assembled power cells, each of which contains two half cells that are separated by proton exchange membrane or separator. The reduction and oxidation electrochemical reactions occurs in the porous electrodes from which the current is collected. The other VRFB components include pipes and pumps so that the electrolyte can flow from the external tanks to the stack. The electrolyte is prepared by dissolving

vanadium pentoxide into the dilute sulphuric acid solution. The VRFB electrolyte is reusable [12] and has an indefinite life span. According to Skyllas-Kazacos and co-researchers the VRFB system is not damaged by repeated total discharge or fluctuating power demand or charge rates as high as the maximum discharge rates. VRFB system can be charged to ensure that gassing side reactions is eliminated during the high charge rates associated with rapid charging cycles. The VRFB cells can be overdischarged and overcharged within the capacity of the electrolytes and can be cycled from any state of charge or discharge, without permanent damage to the electrolytes or cells [13].

1.3 Closure

In this chapter need of energy storage devices is discussed and different types of battery are introduced. Then the working principles of batteries are discussed in a nutshell. Furthermore, the working principle and operation of all-vanadium redox flow battery are discussed in detail.

Chapter 2

Review of Literature

2.1 Introduction

The research on batteries first started by Luigi Galvani, lecturer in anatomy at the University of Bologna in 1790. The study of the science and development of many types of batteries initiated by Alessandro Volta, professor of physics at Pavia University in 1800. From past 50 years the modelling of electrochemical processes has improved to analyze problems involving temperature variations, multiple reactions and physical property variations. The mathematical description of batteries plays a significant role in the design, control and monitoring of batteries. Modelling can minimize the design time and provide a fundamental understanding of the physical and chemical processes that occur in batteries [14]. Literature review on different modeling is described section wise below.

2.2 Experimental study

Sum et al. [3] studied the electrochemical behavior of the V(II) and V(III) reactant to investigate experimentally at glassy carbon electrodes using cyclic voltammetry. Sum et al. [15] also studied experimentally the V(IV) and V(V) electrochemical behavior of redox couple at glassy carbon and gold electrodes in sulphuric acid solutions using cyclic voltammetry and rotating disc voltammetry. They studied the suitability of redox couples V(IV) and V(V) for positive half cell of the redox flow battery.

Hwang et al. [16] studied the performance of the vanadium redox flow battery experimentally for the cross linked anion exchange membrane. Fabjan et al. [17] studied the vanadium redox flow battery performance by experimentally for photovoltaic applications. Experimental results shows that use of activation layers reduce the polarization, which are useful to improve performance of the cell by reducing the side reactions.

Experimental study has been done for the vanadium redox flow battery using cyclic voltammetry measurements for glassy carbon electrodes and the results suggest that the coulombic efficiency is more than 91% with negligible self discharge [18]. Experimental study was done for water transfer behavior across the membrane of the vanadium redox flow battery by Sukkar et al. [19]. The results show that the soc affects the water transfer and performance of the cell.

Zhao et al. [20] investigated the characteristics and performance of the 10 kW vanadium redox flow battery experimentally. Experimental study of the performance characteristics of non aqueous vanadium redox flow batteries has been done using tetrabutylammonium hexafluorophosphate and 1-ethyl-3-methyl imidazolium hexafluorophosphate ionic liquids as supporting electrolytes [21]. The coulombic efficiencies are measured as in the range of 53.31-57.44%. The performance of the VRFB was investigated [22] using asymmetric electrode configurations with acid treated and heat treated electrodes. The heat-treated electrodes in both half-cells are considered as the baseline case for comparison, as this configuration shows the better performance. Experiments were performed by Chen et al. [23] to determine the performances of VRFB for AEM (anion exchange membrane) and N212 membranes. It was found that AEM based membranes for VRFB achieved 100% coulombic efficiency at all current densities. The capacity fade of the VRFB was found for N212 membrane while it was absent for AEM membrane based VRFB.

Two VRFB cells were designed to measure the current density density distribution with an active area of 100 cm^2 [24]. In the first cell, the gold-plated current collector of the negative side is divided into 25 segments. In the other cell, the positive and negative graphite flow field plates are divided into 25 segments. The experimental results indicated that cell design significantly influenced the performance of cell. The accuracy of the measurement may be attributed to both the thickness of the flow field plates and the contact resistance. The second cell with divided graphite field plates showed a significant improvement in the measurement of the local current density.

Experiments [25] were conducted for VRFB to study the performance of VRFB for different membrane thicknesses with Nafion 117 and 212 membranes. It was found that with Nafion 117 the energy efficiency (EE) and charge efficiency (CE) of VRFB using Nafion 117 were higher than those of VRFB employing Nafion 212, while power efficiency was vice versa. Further more, vanadium crossover rate of VRFB using Nafion 212 was higher than that of VRFB using Nafion 117 membrane.

2.3 Lumped dynamic study

Li and Hikihara [26] first developed lumped dynamic model for the all-vanadium redox flow battery based on fluid flow, chemical reaction and electrical circuit. It was shown that dynamics of the battery are governed by concentration change of electrolysis solution. They also studied the frequency response characteristics of the battery. The model results were compared and validated with experimental data. Shah et al. [27] developed the analytical solution for the all-vanadium redox flow battery using the conservation equations of mass and charge combined with the effects of major resistances, electrochemical reactions and recirculation of the electrolyte through external reservoirs. They studied the cell performance analytically by varying the flow rate, concentration and temperature. Analytical results suggests that as the temperature increases, cell electric potential decreases and consequently the cell performance decreases. The model is able to relate important characteristics of performance such as the time to charge/discharge and the state of charge to key system properties. Analytical simulation results have demonstrated that the model is able to capture the performance in practical systems to a high degree of accuracy.

2.4 Two-dimensional numerical study

Numerical modeling can provide quantitative information and analysis to predict the battery behavior accurately. Solution to the governing equations is difficult because of coupling of the transport processes and the electrochemical reaction. Recently it is found that numerical modeling using computational fluid dynamics techniques can lead to remarkable capabilities and advantages in providing more quantitative information about the battery systems and their performance[28]. Shah et al. [29] developed two-dimensional transient numerical model for the vanadium redox flow

batteries. As per best of our knowledge, this is the first published work on numerical modeling of the vanadium redox flow battery. The governing equations are solved by COMSOL Multiphysics package. The study has been done for the effects of the variations in the concentration, electrolyte flow rate and electrode porosity on the performance of the cell. The model is validated with the experimental result and it shows better agreement. Bayanov and Vanhaelst [14] developed a two-dimensional numerical model based on the conservation of mass, momentum and charge with reaction equations. They studied the battery performance for various electrode collectors for different current density. The numerical simulation study has been done for two cases like carbon plates electrode collectors and steel plates electrode collectors. The results show that even though the resistance of the electrode collectors is same for steel plate give better voltage current characteristics than the carbon plate collectors. The charge and discharge time are higher for the carbon plate electrode collectors than the steel plate electrode collectors. The numerical simulation results validated with the experimental results which shows good agreement. You et al. [13] studied the two-dimensional stationary model for the vanadium redox flow battery based on the conservation laws coupled with electrochemical reactions. The equations of the continuity, momentum, species conservation, charge with the reaction equations are solved using the COMSOL Multiphysics package. They studied the performance of the cell by varying the electrode porosity, applied current density and local mass transfer coefficient. The results shows that the bulk reaction rate depends on the applied current density, if the applied current density increases two times the initial value then the transfer current density and overpotential increase almost double. The variation of the mass transfer coefficient only affects value of the overpotential. Also results show that if mass transfer coefficient decreases, it results in increased polarization and rate of side reactions. Chen et al. [28] did the numerical simulation of the electrolyte flow distribution for all vanadium redox flow battery by solving steady equations of continuity and momentum equation using the commercial CFD package ANSYS FLUENT. The numerical simulation results show that electrolyte has concentrated distribution at the central area of the flow field of the cell and disturbed flow and vortex flow of the electrolyte in the inlet and outlet regions. The higher flux of electrolyte in the battery leads to uniform distribution of electrolyte and minimizes the effect of flow irregularity on the battery. Vynnycky [12] has developed two-dimensional time dependent single phase isothermal numerical model for the operation of a single cell in a vanadium redox flow

battery. The model assumes that the membrane is fully humidified, only hydrogen ions can cross the membrane and the dilute solution approximation is valid. He also derived asymptotically reduced model, which decouples fluid mechanics from electrochemistry. This approach is proposed for accurate and computationally efficient vanadium redox flow battery models. The important advantage of using asymptotically reduced model is, it preserve geometrical resolution without losing the accuracy. The governing equations with suitable assumptions and boundary conditions are solved by using the COMSOL Multiphysics package. These mathematical models are useful in optimizing the vanadium redox flow battery.

Chen et al. [30] extended the above model by adding advection term in species conservation equations and proton concentrations in Nernst equation. This enhanced model is able to capture cell performance at different flow rates as evidenced by polarization curves. The optimal electrolyte flow rate can be determined by using power based round trip efficiencies. A quasi-steady state model was developed for VRFBs by Sharma et al. [31]. This model was more useful for rapid modeling, design and optimization of VRFB stacks. One more model was developed by Turker et al. [32] based on the experimental data. The overall system efficiency with soc was studied for VRFB unit and soc was estimated by including the energy losses at stacks during electrochemical conversion process and by the power consumption of the hydraulic circuits as well as the power conversion systems. By employing this model, optimal number of modules for certain power levels while charging and discharging operations were calculated for megawatt scale operations. Viscosity of the electrolyte dependent model was developed for the VRFB [33]. In reality the viscosity of the electrolyte varies during charging and discharging process as the concentrations of acid and vanadium ions in the electrolyte continuously change with the state of charge of VRFB. The results show that consideration of soc dependent electrolyte gives a more realistic simulation of the distributions of current density and overpotential in the electrodes. It results in more accurate estimations of system efficiency and pumping work of VRFBs. A model by Tian et al. [34] was proposed to reduce the pressure drop across the porous electrodes in VRFB. It was found that for lab-scale single electrode size, pressure drop can be minimized by introducing of channels in the flow cell and electrode designs. Also the proposed new design does not generate significant net power output loss.

A two-dimensional numerical model [35] was introduced by including the effects of electrode compression on voltage losses and hydraulics. The results show that reduc-

tion of the electrode thickness by compression reduces the porosity, the specific area resistance and hydraulic permeability, which results in increase in cell performance but also higher pressure drop. Also due to electrode compression reduces the ohmic losses leading to better performance. The VRFB model [36] based on the stack efficiency curves given by the manufacturer, the model includes mechanical model of the VRFB hydraulic circuit and pumps. Also the model takes into consideration of both the voltage and coulombic losses of the stack, therefore the performance of the model has a high degree of accuracy. Latha and Jayanthi [37] studied the electrolyte flow distribution for three sets of parallel, serpentine and interdigitated configurations for redox flow batteries. From the result it was showed that pressure drop in the interdigitated flow field is less than that in the serpentine for the same flow rate. Also interdigited flow fields show superior cell performance of RFBs. A model was developed by Rudolph et al. [38] to study the energy and efficiency losses during cyclic operation of the VRFB. It was observed that the capacity decrease is caused by the parasitic oxidation of V^{2+} ions in the negative half-cells and the internal resistance increase due to passivation of the negative graphite collector surface. The hydrodynamics of serpentine flow fields were studied for the RFB applications [39]. It was shown that considerable effect on the predicted pressure drop on the performance of the redox flow batteries. Rudolph et al. [40] developed model to study the distribution of the electrolyte in the electrode with different inlet configurations. This model was useful to achieve optimal electrolyte flow rate which results to obtain the uniform distribution of the electrolyte flow to each half-cell.

2.5 Three-dimensional numerical study

Ma et al. [41] developed three-dimensional isothermal model for negative half cell of the vanadium redox flow battery by solving the conservation equations of mass, momentum and charge along with a kinetic model for reaction involving vanadium species. The governing equations were solved numerically by using COMSOL Multiphysics package. They studied the distribution of velocity, overpotential, concentration and transfer current density. Qiu et al. [42] developed three-dimensional pore-scale model to study the performance of the VRFB with different electrode morphologies under various operating conditions. The results suggest that the cell voltage increases with increasing electrolyte flow rate due to decreasing concentra-

tion gradients of vanadium species within the porous electrode. The model also indicates that electrode structures with low porosity result in more uniform and lower absolute current density and overpotential fields at the expense of increased pressure drop.

Same model was extended by Qiu et al. Qiu12 [43] for VRFB based on XCT-reconstructed geometry of real carbon-felt electrode materials. Pore-scale model distinguishes between liquid electrolyte phase and solid electrode in the cell, so the model captures the effects of electrode geometry on cell performance. The cell performance was studied as a function of the electrolyte flow rate and external drawing current. Yin et al. [44] developed three-dimensional model of VRFB for interdigitated flow channel with single inlet and multi-inlet design configurations. For the multi-inlet design at low electrolyte flow rate the pressure of electrolyte drops significantly in the side inlet of porous electrode resulting in uneven distributions of electrolyte flow field and cell potential. For the higher electrolyte flow rate potential distribution of the multi-inlet cell becomes more uniform, therefore more efficient utilization of porous electrode than that of the single-inlet cell. One more 3D model was proposed by Xu et al. [45] to study the performance of VRFB for three different flow fields such as, no flow field, parallel and serpentine flow field designs. The VRFB with serpentine flow field gives better performance because of lowest overpotential due more uniform distribution of electrolyte over the electrode surface and the enhanced convective mass transport towards the membrane. Also round trip efficiency and energy efficiency was higher in the case of serpentine flow field.

2.6 Lumped and numerical study with thermal effect

Tang et al. [46] developed a thermal model for the vanadium redox flow battery by solving the equations based on the conservation of energy. In this model they studied the effect of heat transfer on the electrolyte temperature under different operating conditions. The simulations were carried out for stack including 19 cells and two cylindrical electrolyte tanks under varying air temperatures and operating conditions for a 2.5 kW/15 kWh. The simulation results predict the battery and electrolyte temperature at constant and varying environmental temperatures in the

presence of different charge and discharge currents. It is shown that increasing the current or reducing the flow rate leads to the increase of the electrolyte and stack temperature. By adjusting the thermal properties of the tank material and its surface area, heat transfer can be optimized.

Al-Fetlawi et al. [47] studied two-dimensional non-isothermal model by solving the equations of mass, charge, momentum and energy and combined with kinetic model for reaction including vanadium species. If the temperature is high, which is harmful to perfluorinated membranes, such as Nafion, it enhances corrosion of the plates and results in water loss. Therefore, thermal modeling is playing a vital role to enhance the performance of the cell. As per our best knowledge, this is the first paper on thermal modeling of the vanadium redox flow battery. In this paper the effects of temperature variations of the charge/discharge characteristics of the cell has been investigated. The numerical model includes the governing equations with suitable boundary conditions solved using the COMSOL Multiphysics package. While solving the energy equation heat generation due to heating by activation losses and effects of reaction and ohmic resistances were considered. Numerical simulation results suggest that without heat dissipation from the cell, the temperature will rise to unsatisfactory limits in a short duration. In order to overcome this problem of large temperature increase an effective cooling strategy is needed for operation in high temperature environment and under high loads. The non-uniform distribution of the reactant concentration leads to variation in potentials and transfer current densities and local maxima in temperature. Due to high flow rates the coulombic efficiency of the cell increases and the oxygen and hydrogen evolutions reduce. It is noted that from the results that the value of the applied current plays important role in heat generation during charge-discharge cycles, the applied current increases the coulombic efficiency of the cell decreases. The heat loss also plays role on the charge-discharge behavior and temperature distribution of the cell. The cell performance decreases with increase in magnitudes of the overpotentials in both the electrodes leads to gas evolution.

Thermal and hydraulic modeling [48] of VRFB is an important issue and temperature has significant impacts on the battery efficiency, the lifetime of material and the stability of the electrolytes. The model predicts the impact of electrolyte flow rate and temperature on the battery characteristics and efficiencies.

A electrical thermal-dependent model [49] for VRFB was developed to predict state of charge using extended Kalman filter (EKF) method. This model was able to pre-

dict soc accurately using stack terminal voltages and applied currents in the absence of an open flow cell for OCV measurement.

Wei et al. [50] developed dynamic thermal-hydraulic model for VRFB and study the effects of stack flow patterns on cell performance. Three stack flow patterns including flow without distribution channels and two cases of flow with distribution channels are compared to study their effects on battery performance. when comparing three flow patterns, it was found that serpentine-parallel pattern was preferable because it effectively controls the pressure drop, uniformity of flow rates and electrolyte temperature.

Zheng et al. [51] developed a three-dimensional numerical model for thermal analysis to gain a better understanding of thermal behavior in a VRFB. The results have indicated that the heat generation depends on applied current density. The over potential and reaction rate rise with an increased applied current density, resulting in the electrochemical reaction heat rises proportionally and the activation heat rises at a parabolic rate when the applied current density increases. This model is more useful to propose an effective control strategy, such as an optimal battery design, selecting appropriate materials, to eliminate any crisis of internal heat accumulation.

A complete dynamic electro-thermal model [52] of VRFB was developed incorporating forced cooling strategies. The model simulations are conducted under both water cooling and air cooling scenarios to verify the accuracy. From simulations it has been observed that increasing the electrolyte flow rate improves the coulombic efficiency, voltage efficiency and energy efficiency simultaneously but at the expense of higher pump power required. Oh et al. [53] proposed a three-dimensional transient thermal VRFB model to predict the charging and discharging performances. The 3D comprehensive model can be used to realistic multi cell stacks to determine the optimal design and operating conditions.

2.7 Lumped and numerical study with crossover

You et al.[54] have studied the self-discharge process in the vanadium redox flow battery. They simulated the self discharge process for state of charge as zero and 65%. The diffusion rate depends upon the partition coefficient, diffusion coefficient and concentration gradient of the vanadium ions in the battery. The numerical results show that the concentration of V(IV) decreases in the positive electrolyte,

increases in the negative electrolyte with time. Also the concentration gradient of V(IV) decreases in the membrane. Tang et al.[55] studied the effect of the self discharge process and side reactions on the performance loss for vanadium redox flow battery. The model was based on mass balances for each of the four vanadium ions in the vanadium flow battery electrolytes combined with the Nernst equation. The crossover of vanadium ions through the membrane can not be avoided as diffusion always takes place because of the concentration difference of vanadium ions exists in the positive and negative half cell electrolytes. This results in the self discharge reactions in each electrolyte consequently loss of capacity. Due to self discharge process an imbalance of vanadium ions takes place in the two half cells if the diffusion rates of the different vanadium ions are not equal. This leads to increasing of vanadium ions in one half cell and a corresponding decrease in the other, therefore there is a loss of cell capacity. During the charging process side reactions occur at both electrodes, leading to hydrogen evolution in negative electrode and oxygen evolution in positive electrode therefore there is a loss in coulombic efficiency. The oxygen evolution in the positive electrode was considered as negligible for the high state of charge (soc) and hydrogen evolution effects were considered for the state of charge above 90%. Badrinarayanan et al. [56] developed a lumped model for VRFB which involve effects of crossover of vanadium ions through membrane. The temperature dependence diffusion equation was solved, therefore effects of temperature on the performance were studied. The model was used to predict capacity decay for VRFB. The temperature effect on the change in concentration of Vanadium ions was investigated for three different membranes namely Selemion CMV, Nafion 115 and Selemion AMV. It was observed that the loss in capacity of the battery increases with the increase in temperature and the decay behavior was dependent on the type of membrane material used.

Agar et al. [57] proposed a two-dimensional transient model which included species transport mechanisms to predict capacity loss for s-Radel and Nafion 117 membranes of VRFB. It is observed that hydraulic and the electro-kinetic permeability of a membrane are equally as significant as vanadium diffusion characteristics while evaluating new membranes. Also the lifetime of the VRFB can be extended by reducing imbalances of species concentration between half cells while cycling process. Benjamin et al. [58] developed model which involves self discharge effects to calculate coulombic efficiency for VRFB using cutoff voltages and state of charge limit techniques. Analysis of the results recommend that soc limit provide a better way

to determine the coulombic efficiency of a VRFB, because unlike the cutoff voltage approach, soc limit accounts the change in the capacity of the device with number of cycles due to the crossover of species.

Knehr et al. [59] developed a two-dimensional unsteady isothermal model to study the species crossover through membrane for VRFB. The simulation results suggest that electro-osmotic convections in the membrane are important mechanism to affect species crossover. Also simulations indicate that one main approach to minimize the capacity loss of VRFB is to operate system at constant pressure condition through the utilization of asymmetric flow rates to minimize the effect of osmotic convection. A two-dimensional transient model [60] was developed to overcome capacity loss for VRFB by asymmetric current operation. Two membrane materials were tested namely, convection dominated and diffusion dominated membranes. Simulation results suggest that increasing the charging current density decreases the net convective crossover of the bulk electrolyte, which leads to a reduction in the overall crossover at the end of the cycle. Also it is shown that when both membranes are compared, a more significant improvement in capacity retention is observed for the diffusion dominated membrane because of the fact that diffusion has less time to influence the capacity during a single cycle as a result of increased charging current.

2.8 Lumped and numerical study with thermal effect and crossover

Tang et al. [61] developed lumped thermal model including the crossover effects for VRFB. The energy balance equations included the heat generation by the self-discharge reactions, whose reaction rate was coupled with diffusion term in mass balance equations. The mass balance equation includes the diffusion term which has coefficients to be accounted as a function of stack temperature. In this way self-discharge and heat transfer were modeled as a function of both concentrations and stack temperature. It is observed that the proposed model can be employed to determine the thermal effect of the selfdischarge reactions on charge discharge cycling and it can help in optimizing battery designs for different application. Won et al. [62] developed three-dimensional unsteady non-isothermal model which included vanadium crossover effects for VRFB. Numerical simulation results indicate that

loss of capacity of cell clearly shows difference in species distributions due to side reactions. Furthermore, result shows that due to vanadium ion crossover effect, more charging time and less discharging time have been achieved.

2.9 Numerical study considering the effect of hydrogen and oxygen evolution

Shah et al. [63] developed two-dimensional, isothermal, transient multi phase mixture models which included the effects of hydrogen evolution and bubble formation. The kinetics of the oxidation and reduction reaction are highly complex. There are number of effects due to oxygen and hydrogen evolution, which are presently not understood. The gas evolution reactions are parasitic, therefore consume a portion of the applied current from the cell. Due to gas evolution, bubbles formation takes place, which minimizes the liquid phase volume in the electrodes resulting in restricted flow of electrolyte, a reduced active surface area for reaction and reduced mass and charge transport coefficients. They studied the performance of the vanadium redox flow battery by vary the parameters like, effect of electrolyte flow rate, bubble diameter and applied current density. It is reported that the voltage and coulombic efficiency are lower for lower concentration and higher for higher concentration. Numerical results show that the higher the flow rate, more the uniform distribution of the reactant, which gives the higher the values of overpotentials and leads to lesser the hydrogen evolution in the negative electrode. Also the higher gas velocity removes the bubble at a faster rate which results in reduction of the gas volume fraction. It is also observed that the maximum gas volume fraction reached at higher current density. The increased volume fraction of the gas results in the faster hydrogen evolution.

Al-fetlawi et al. [64] have studied the non-isothermal, two-dimensional model including the multi phase mixture model to describe the oxygen evolution in the form of spherical gas bubbles. The effects of oxygen evolution are strongly felt at the end of charging process. While discharging process the presence of oxygen evolution reduces the time to discharge as a result of reducing the charge efficiency of the battery. Numerical results show that due to presence of oxygen evolution reaction, it consumes a part of the applied current density and minimizes the value of applied

current by a factor.

2.10 Motivation and Research Objectives

Commercialization of the various types of redox flow systems offers a series of challenges to researchers of this new technology, like scale-up and optimization (related to operating conditions and flow geometries), improvement in electrolyte stability, development of electrode materials resistant to oxidation and membrane fouling. Many of these challenges are not suitable for laboratory experiment alone, by virtue related to the financial costs and long time scales. In such cases it is beneficial to use modeling and simulation, therefore modeling and simulation helps us in optimization of the cell performance. After doing a detail literature survey we have found that there is much scope to do numerical simulation of all-vanadium redox flow battery. Based on the gap found in the literature the main specific objectives of this thesis are formulated below.

1. Development of analytical model for the VRFB and extend the model by including the mass transfer and crossover effects study the performance.

2. Analysis of VRFB system using the thermal model including the chemical power loss and pump power loss and study the system for different climatic conditions.

3. Development of two-dimensional, dynamic, isothermal model for VRFB system and study the performance for various parameters.

4. Study the effect of incorporation of concentration overpotential and ohmic losses into the two-dimensional model on coulombic, voltage and energy efficiencies.

5. Analysis of cell performance of three-dimensional VRFB system using both steady and unsteady isothermal numerical model and considering concentration overpotential and ohmic losses in to the model.

2.11 Thesis Overview

The work is presented in self contained chapters. The overall structure of this thesis is given below.

A thorough understanding of batteries, types of redox flow batteries and working principle are explained in chapter 1. A review of literature on numerical and experimental studies of VRFB and other batteries are presented in chapter 2. Chapter 3 presents the mathematical framework of the all-vanadium redox flow battery model and describes the formulation of both lumped and numerical model in detail. In chapter 4, the influence of various parameters are discussed using analytical model of the all-vanadium redox flow battery. The effects of crossover and mass transfer to study the capacity loss of the VRFB system are also discussed in this chapter. Chapter 5 discusses the dynamic thermal model for the VRFB system based on energy conservation including the chemical power loss, pump power loss and power loss due to cell internal resistance. In chapter 6 the dynamic two-dimensional, isothermal numerical model for the VRFB is discussed. The model considering the losses and without considering the losses is studied for various parameters to improve the performance of the cell. The effects of the variations in different parameters such as, flow rate, concentrations, electrode porosity and current density on performance of cell are discussed.

Chapters 7 and 8 discuss the three-dimensional numerical model for steady and unsteady conditions, respectively. Ohmic losses and concentration overpotential are included in the model which has shown significant contribution to predict performance accurately. The electrode properties and current density vary with state of charge and these parameters have significant impact on the coulombic, voltage and energy efficiencies. Finally, the main findings and suggestions for future work are summarized and shown in chapter 9.

2.12 Closure

Thorough literatures review on experimental, lumped and numerical studies for the VRFB system are discussed in this chapter. Based on the literature review the objectives of the present thesis are drawn. Then the thesis overview is presented at last.

Chapter 3

Model Development for All-Vanadium Redox Flow Battery

3.1 Introduction

The modeling of operation of vanadium redox flow battery is more attractive theoretical problem due to complex of partial differential equations of electrochemistry and fluid dynamics. A solution of this problem can help us optimizing cell configuration and parameters of redox flow battery and parameters of electrolytes. The redox flow batteries are employed as efficient new energy storage for all types of applications [9] like wind power plants and solar power plants. From last 10 years, all-vanadium redox flow battery (VRFB) is considered as the most appropriate for large scale energy storage system due to various advantageous such as long operation time, low cost and high energy efficiency. Using the only vanadium species in both half cells helps to overcome the problem of self discharge due to the transfer of ions through the membrane. The above features of the vanadium redox flow battery are more attractive for the application in electric vehicles. The main limitation of VRFB is that it has low energy density which limits many of these capabilities. To overcome this disadvantage, it is required to optimize the number of parameters of redox flow battery, for example, increasing the electrolyte flow rate at the inlet [29] optimizing the configuration of the VRFB. The operation of VRFB operation can be optimized on the basis of theoretical modeling and numerical simulations. These models include the system of equations which can be solved numerically.

The performance of the vanadium redox flow battery can be predicted by

1. Experimental investigations.
2. Theoretical calculations
   a. Analytical modeling of the vanadium redox flow battery.
   b. Numerical modeling of the vanadium redox flow battery.

Experimental investigation

Experimental measurements give the most reliable data about a physical process. The experimental measurements include full scale equipment, employed to determine how identical copies of equipment perform under the same conditions. Full scale experimental tests are in many cases most expensive and it is impossible. The alternative solution is to perform experimental measurements on small scale models, the outcome data has to be extrapolated to full scale models. It is very difficult to measure all the quantities using experiments alone, therefore numerical modeling is required to predict various quantities. In the case of vanadium redox flow battery, the variation in concentration, overpotential etc inside the cell can not possible to measure due to limitations in measuring instruments.

Theoretical calculation

Theoretical prediction involves developing mathematical model which involves a set of differential equations. Many practical phenomena of interest can be predicted using the methods of classical mathematics for solving these equations. A look at the classical text of fluid mechanics or electrochemistry or heat transfer leads to the conclusion that closed form solution can be obtained for a small fraction of the range of practical problems. The solution involves special functions, transcendental equations for eigen values, infinite series etc, so that numerical calculation may be difficult task. The development of numerical methods and the availability of high performance digital computers help us to develop mathematical model which can be solved for almost any practical problem [65].

3.2 Lumped model

3.2.1 Analytical model

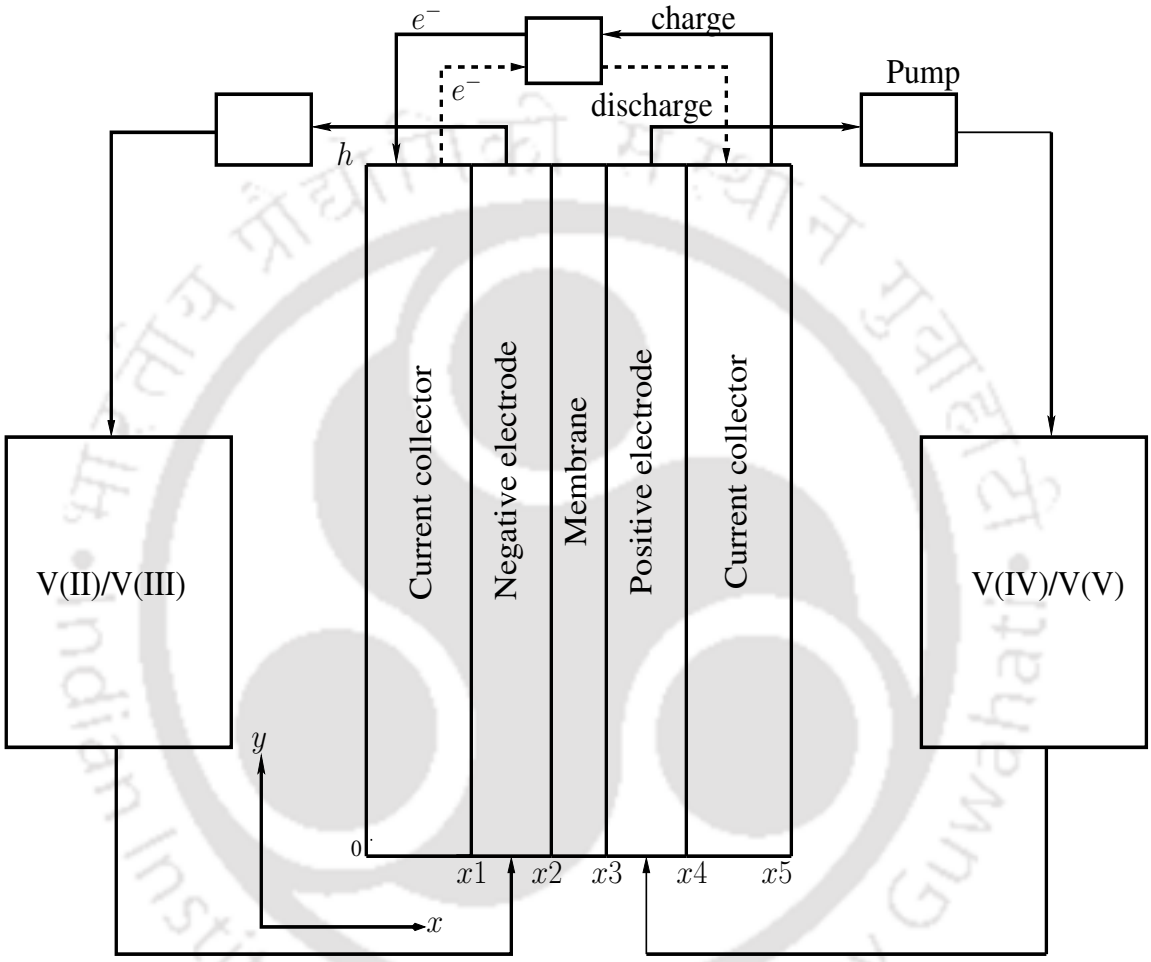

Figure 3.1: Schematic of the all-vanadium redox flow battery showing the components; porous electrodes, current collectors, reservoirs and membrane

The mathematical model for the all-vanadium redox flow battery is based on the principles of conservation of mass and charge. It also includes the electrochemical reactions, major resistances and recirculation of the electrolyte through external reservoirs [27]. The assumptions for developing the mathematical model are, the hydrogen and oxygen evolution in the cell are neglected and the self discharge effect is neglected. The kinetics of oxidation and reduction half cell reactions at the electrode are approximated as follows.

At the positive electrode:

$$VO^{2+} + H_2O - e^- \rightleftharpoons VO_2^+ + 2H^+ \tag{3.1}$$

At the negative electrode:

$$V^{3+} + e^- \rightleftharpoons V^{2+} \tag{3.2}$$

The recirculation of the electrolytes from reservoirs to the cell alters the concentrations of all species entering the electrodes. To model recirculation the concentration of species i in the appropriate reservoir (C_i^{res}) is introduced. The inlet/outlet area of the electrodes is given by $A_{in} = A_{out} = b_e w_e$, where b_e and w_e are the breadth and width of the electrode, respectively. The electrolyte density is assumed constant. From the conservation law of mass, the net change per unit time in the number of moles of species i in the electrode due to recirculation is approximately equal to $\varepsilon A_{in} u(C_i^{res} - C_i)$,where ε is the porosity of the electrode and u is the electrolyte flow velocity. Similarly, the net change in the reservoir concentration is equal to $-\varepsilon A_{in} u(C_i^{res} - C_i)$.

The mass balance of species i in the reservoir can be written as,

$$\frac{dC_i^{res}}{dt} = -\frac{\varepsilon A_{in} u}{V_r}(C_i^{res} - C_i) = -\frac{\varepsilon \nabla u}{h_e}(C_i^{res} - C_i) \tag{3.3}$$

εA_{in} is the actual area of the electrode, h_e is the height of the electrode, $V_e = b_e w_e h_e$, is the volume of the electrode, V_r is the volume of the reservoir and ∇ is the ratio of the volume of the electrode to the volume of the reservoir. If the mass of species i includes recirculation and electrochemical reaction, then the following equation can be written of the concentration of V(III) and V(IV),

$$\varepsilon V_e \frac{dC_i}{dt} = \varepsilon A_{in} u\,(C_i^{res} - C_i) - A_s \frac{j_{app}}{F} \tag{3.4}$$

Similarly, the equation for concentration of V(II) and V(V) can be written as,

$$\varepsilon V_e \frac{dC_i}{dt} = \varepsilon A_{in} u\,(C_i^{res} - C_i) + A_s \frac{j_{app}}{F} \tag{3.5}$$

where A_s is the active surface area for reaction, which can be taken as $A_s = SV_e$, where S is the specific surface area of the electrode. The variation of the vanadium

of the reservoir concentration, V(III) and V(IV) is given by,

$$C_i^{res} = (\varepsilon\nabla + 1)C_i^0 - \frac{\nabla S}{F} j_{app} t - \varepsilon\nabla C_i \tag{3.6}$$

Variation of the cell concentration of V(III) and V(IV) is given by,

$$C_i = C_i^0 + \frac{S j_{app}}{\varepsilon\tilde{\varepsilon}F}\left(\frac{\varepsilon\nabla + e^{-\tilde{\varepsilon}t}}{1+\varepsilon\nabla} - 1 - \frac{\varepsilon\nabla}{\tau}t\right) \tag{3.7}$$

Variation of the cell concentration of V(II) and V(V) is given by,

$$C_i = C_i^0 - \frac{S j_{app}}{\varepsilon\tilde{\varepsilon}F}\left(\frac{\varepsilon\nabla + e^{-\tilde{\varepsilon}t}}{1+\varepsilon\nabla} - 1 - \frac{\varepsilon\nabla}{\tau}t\right) \tag{3.8}$$

The variation of the vanadium of the reservoir concentration, V(II) and V(V) is given by,

$$C_i^{res} = (\varepsilon\nabla + 1)C_i^0 + \frac{\nabla S}{F} j_{app} t - \varepsilon\nabla C_i \tag{3.9}$$

where $\tau = \frac{h_e}{u}$ and $\tilde{\varepsilon} = \frac{1}{\tau}(\varepsilon\nabla+1)$. The ratio $\tau = \frac{h_e}{u}$ is a direct measure of the residence time for reaction. Water mass balance for negative electrode can be expressed as,

$$\varepsilon V_e \frac{dC_{H_2O}}{dt} = \varepsilon A_{in} u (C_{H_2O}^{res} - C_{H_2O}) + A_e n_d \frac{j_{app}}{F} \tag{3.10}$$

Water mass balance for positive electrode can be expressed as,

$$\varepsilon V_e \frac{dC_{H_2O}}{dt} = \varepsilon A_{in} u (C_{H_2O}^{res} - C_{H_2O}) - (A_e n_d + A_s)\frac{j_{app}}{F} \tag{3.11}$$

Proton mass balance for positive electrode during charging process can be expressed as,

$$\varepsilon V_e \frac{dC_{H^+}}{dt} = \varepsilon A_{in} u (C_{H^+}^{res} - C_{H^+}) + A_e \frac{j_{app}}{F} \tag{3.12}$$

The reservoir concentrations of H_2O for both electrodes can be expressed as,

$$\frac{dC_{H_2O}^{res}}{dt} = -\frac{\varepsilon\nabla}{\tau}(C_{H_2O}^{res} - C_{H_2O}) \tag{3.13}$$

The reservoir concentrations of protons H^+ for both electrodes can be expressed as,

$$\frac{dC_{H^+}^{res}}{dt} = -\frac{\varepsilon\nabla}{\tau}(C_{H^+}^{res} - C_{H^+}) \tag{3.14}$$

The variations of reservoir concentration of water in the positive electrode is given by,

$$C_{H_2O}^{res} = (\varepsilon\nabla + 1)C_{H_2O}^0 - \varepsilon\nabla C_{H_2O} - \frac{j_{app}}{F}\nabla t\left(S + \frac{n_d}{w_e}\right) \tag{3.15}$$

The variations of reservoir concentration of water in the negative electrode is given by,

$$C_{H_2O}^{res} = (\varepsilon\nabla + 1)C_{H_2O}^0 - \varepsilon\nabla C_{H_2O} + \frac{n_d}{w_e}\frac{J_{app}}{F}\nabla t \tag{3.16}$$

Variation of concentration of water at the positive electrode is given by,

$$C_{H_2O} = C_{H_2O}^0 - \frac{j_{app}}{\varepsilon\tilde{\varepsilon}F}\left(S + \frac{n_d}{w_e}\right)\left(\frac{\varepsilon\nabla + e^{-\tilde{\varepsilon}t}}{1 + \varepsilon\nabla} - 1 - \frac{\varepsilon\nabla}{\tau}t\right) \tag{3.17}$$

Variation of concentration of water at the negative electrode is given by,

$$C_{H_2O} = C_{H_2O}^0 - \frac{j_{app}}{\varepsilon\tilde{\varepsilon}F}\frac{n_d}{w_e}\left(\frac{\varepsilon\nabla + e^{-\tilde{\varepsilon}t}}{1 + \varepsilon\nabla} - 1 - \frac{\varepsilon\nabla}{\tau}t\right) \tag{3.18}$$

Variation of the concentration of protons at the positive electrode side reservoir can be expressed as,

$$C_{H^+}^{res} = (\varepsilon\nabla + 1)C_H^0 - \varepsilon\nabla C_H^+ + \frac{j_{app}}{F}\frac{\nabla}{w_e}t(2Sw_e - 1) \tag{3.19}$$

Variation of the concentration of the protons at the negative electrode is given by,

$$C_{H^+}^{res} = (\varepsilon\nabla + 1)C_H^0 - \varepsilon\nabla C_H^+ + \frac{j_{app}}{F}\frac{\nabla}{w_e}t \tag{3.20}$$

Variation of the concentration of the protons at the positive electrode is given by,

$$C_{H^+} = C_H^0 + \frac{j_{app}}{\varepsilon\tilde{\varepsilon}w_eF}(2Sw_e - 1)\left(\frac{\varepsilon\nabla + e^{-\tilde{\varepsilon}t}}{1 + \varepsilon\nabla} - 1 - \frac{\varepsilon\nabla}{\tau}t\right) \tag{3.21}$$

Variation of the concentration of the protons at the negative electrode is given by,

$$C_{H^+} = C_H^0 + \frac{j_{app}}{\varepsilon\tilde{\varepsilon}w_e F}\left(\frac{\varepsilon\nabla + e^{-\tilde{\varepsilon}t}}{1+\varepsilon\nabla} - 1 - \frac{\varepsilon\nabla}{\tau}t\right) \tag{3.22}$$

For a given applied current density j_{app} the cell potential difference E_{cell} is calculated using the following formula.

$$E_{Cell} = E_{Cell}^{rev} - \sum_k (IR)_k + \sum_k |\eta| = E_{Cell}^{rev} - (IR)_m - (IR)_e - (IR)_c - \eta_a \tag{3.23}$$

where, E_{Cell}^{rev} is the reversible outlet concentration voltage, η_a is the activation overpotential contributed from the both electrodes, $(IR)_m$ is the ohmic drop from the membrane, $(IR)_e$ is the ohmic drop related with electrolyte and $(IR)_c$ is the ohmic drop from the current collector. The outlet concentrations voltage is approximated by using Nernst's equation,

$$\begin{aligned} E_{Cell}^{rev} &= (E_2^0 - E_2^0) + \frac{RT}{F}\ln\left(\frac{C_{V(II)}C_{V(V)}[H^+]^2}{C_{V(III)}C_{V(IV)}}\right) \\ E_{Cell}^{rev} &= E^0 + \frac{RT}{F}\ln\left(\frac{C_{V(II)}C_{V(V)}}{C_{V(III)}C_{V(IV)}}\right) + \frac{4.6RT}{F}\log_{10}[H^+] \end{aligned} \tag{3.24}$$

The ohmic losses due to current collector, membrane and the electrolyte are given by,

$$(IR)_c = j_{app}\frac{w_c}{\sigma_c}(IR)_m = j_{app}\frac{w_m}{\sigma_m}(IR)_e = j_{app}\frac{w_e}{\varepsilon^{3/2}\sigma_e} \tag{3.25}$$

σ_c, σ_m and σ_e are the conductivities and w_c, w_e and w_m are the widths of the current collector, electrolyte and membrane, respectively. The Bruggeman correction can be used to calculate the effective conductivity of the electrolyte. Conductivity of Nafion membrane is approximated by the following empirical relation,

$$\sigma_m = (0.5139\lambda - 0.326)\exp\left(1268\left[\frac{1}{303} - \frac{1}{T}\right]\right) \tag{3.26}$$

where λ is the membrane water content. Since the membrane is in constant contact with the liquid electrolyte on both sides, it is reasonable to assume that it is fully saturated. The overpotentials related with the electrode reactions can be calculated using the Butler-Volmer equation as follows. For negative electrode during charging

process,

$$\eta_1 = -\frac{2RT}{F}\sinh\left(\frac{j_{app}}{2Fk_1\sqrt{C_{V(III)}C_{V(IV)}}}\right) \tag{3.27}$$

For positive electrode during charging process,

$$\eta_2 = \frac{2RT}{F}\sinh\left(\frac{j_{app}}{2Fk_2\sqrt{C_{V(IV)}C_{V(V)}}}\right) \tag{3.28}$$

where k_1 and k_2 are the reaction rate constants related with the reactions at the positive and negative electrodes, respectively. The reaction constants are dependent on temperature and these are expressed as follows. Reaction rate constant k_1 at the positive electrode is given by,

$$k_1 = k_{1,ref}\exp\left(-\frac{FE_1^0(T_{ref})}{R}\left[\frac{1}{T_{ref}}-\frac{1}{T}\right]\right) \tag{3.29}$$

Reaction rate constant k_2 at the negative electrode is given by,

$$k_2 = k_{2,ref}\exp\left(-\frac{FE_2^0(T_{ref})}{R}\left[\frac{1}{T_{ref}}-\frac{1}{T}\right]\right) \tag{3.30}$$

The state of charge (soc) of a battery which can be calculated using the method based on the open-circuit voltage is given by,

$$\begin{aligned} soc(t) &= -\tfrac{E_{min}}{E_{max}-E_{min}} + \tfrac{E^0}{E_{max}-E_{min}} + \tfrac{2RT}{F(E_{max}-E_{min})} \\ &\times \ln\left(\tfrac{C^0_{V(III)}+\zeta(t)}{C^0_{V(II)}-\zeta(t)}\right) + \tfrac{4.6RT}{F(E_{max}-E_{min})}\left(\log_{10}(C_{H^+}+[\tfrac{2Sw_e-1}{Sw_e}]\zeta(t)) - 3\right) \end{aligned} \tag{3.31}$$

$$\zeta(t) = -\frac{Sj_{app}}{\varepsilon\tilde{\varepsilon}F}\left(\frac{\varepsilon\nabla + e^{-\tilde{\varepsilon}t}}{1+\varepsilon\nabla} - 1 - \frac{\varepsilon\nabla}{\tau}t\right) \tag{3.32}$$

3.2.2 Lumped model considering mass transfer and crossover

There is crossover of vanadium ions across membrane of VRFB after many cycles which results in capacity loss of the cell. There are different membrane materials which show different diffusion behavior and it results in variation in the cell potential response. The diffusion coefficients of the membrane is temperature dependent,

therefore concentration profile vary with temperature. The model is considered the effects of crossover of vanadium ions through membrane and mass transfer.
The following main electrochemical reactions are taking place at each electrode.
At the negative electrode

$$V^{3+} + e^{-} \rightleftharpoons V_2^{+} \tag{3.33}$$

At the positive electrode

$$VO^{2+} + H_2O - e^{-} \rightleftharpoons VO_2^{+} + 2H^{+} \tag{3.34}$$

The following are the self-discharge reactions occurred at each of the electrode.
At negative electrode

$$V^{2+} + VO^{2+} + 2H^{+} \longrightarrow 2V^{3+} + H_2O \tag{3.35}$$

$$2V^{2+} + VO_2^{+} + 4H^{+} \longrightarrow 3V^{3+} + 2H_2O \tag{3.36}$$

$$V^{3+} + VO_2^{+} \longrightarrow 2VO^{2+} \tag{3.37}$$

At positive electrode

$$2VO^{2+} + V^{2+} + 2H^{+} \longrightarrow 3VO^{2+} + H_2O \tag{3.38}$$

$$VO_2^{+} + V^{3+} \longrightarrow 2VO^{2+} \tag{3.39}$$

$$VO^{2+} + V^{2+} + 2H^{+} \longrightarrow 2V^{3+} + H_2O \tag{3.40}$$

After many cycles, concentration imbalance takes place in the battery due to difference in diffusion rates of vanadium ions. Vanadium crossover occurs between two half cells through membrane which results in loss of performance of cell [55]. Water crossover affects on the overall concentration of vanadium in both half of cell. Here water crossover is neglected and this can be overcome by approximating the effective diffusion coefficient of vanadium species.
The following are the assumptions considered for simplifying the equation.
1. Apart from oxidation-reduction reactions there will be hydrogen and oxygen gas evolving reactions under normal conditions [63, 64].
2. Vanadium ions are diffused through the membrane and react instantaneously;

therefore side reactions are considered.

3. Water crossover is neglected due to difficulty in predicting the electro-osmatic drag and osmosis by lumped model.

Model equations

The equations are based on law of conservation of mole for vanadium species in the electrodes and reservoir volumes of each half cell. Due to diffusion in the membrane, the concentration of vanadium changes in the porous electrode by recirculation of electrolytes between the reservoir and electrode and externally applied current. The model contains total eight unknowns of concentrations, four for positive and negative porous electrodes and four for concentrations in the external reservoirs. Therefore, the mass balance of species i in the reservoir can be written as,

$$\frac{dC_i^{res}}{dt} = \frac{Q}{V_{res}}(C_i - C_i^{res}) \tag{3.41}$$

where C_i^{res} and C_i are the respective concentrations in the reservoir and cell of species $i \in [2, 3, 4, 5]$ corresponding to V^{2+}, V^{3+}, VO_2^+ and VO^{2+}, respectively, V_{res} is the volume of electrolyte in the reservoir, Q is the electrolyte flow rate.

The mass balance for species includes electrochemical reaction, recirculation and diffusion of species through membrane and these are expressed as,

$$\frac{dC_2}{dt} = \frac{Q}{\varepsilon V_e}(C_2^{res} - C_2) + \frac{A_m j}{\varepsilon V_e F} - \frac{A_m}{w_m}(D_2 c_2 + 2D_5 c_5 + D_4 c_4) \tag{3.42}$$

$$\frac{dC_3}{dt} = \frac{Q}{\varepsilon V_e}(C_3^{res} - C_3) - \frac{A_m j}{\varepsilon V_e F} - \frac{A_m}{w_m}(D_3 c_3 - 3D_5 c_5 - 2D_4 c_4) \tag{3.43}$$

$$\frac{dC_4}{dt} = \frac{Q}{\varepsilon V_e}(C_4^{res} - C_4) - \frac{A_m j}{\varepsilon V_e F} - \frac{A_m}{w_m}(D_4 c_4 - 3D_2 c_2 - 2D_3 c_3) \tag{3.44}$$

$$\frac{dC_5}{dt} = \frac{Q}{\varepsilon V_e}(C_5^{res} - C_5) + \frac{A_m j}{\varepsilon V_e F} - \frac{A_m}{w_m}(D_5 c_5 + 2D_2 c_2 + D_3 c_3) \tag{3.45}$$

where V_e is volume of the electrode, A_m is the contact area of the membrane, j is the applied current density, ϵ is the porosity of the electrode, w_m is the width of the membrane, and D_2, D_3, D_4 and D_5 are the diffusion coefficients of membrane corresponding to respective vanadium species.

The diffusion coefficients depend on temperature and these are approximated using

Ahrrenius law given by,

$$D = D_0 e^{\frac{E_a}{R}\left(\frac{1}{298}-\frac{1}{T}\right)} \tag{3.46}$$

where D_0 is the diffusion of each vanadium species at temperature 298 K, E_a is the activation energy. The value of E_a is 1.663×10^4J/mol taken from literature [66] based on experimental data.

The open circuit voltage is calculated from the Nernst equation given by,

$$E_{OC} = (E^0_{pos} - E^0_{neg}) + \frac{RT}{F} \ln\left(\frac{c_2 c_5 c^2_{H+}}{c_3 c_4}\right) \tag{3.47}$$

where E^0_{neg} and E^0_{pos} are the standard cell potentials for the reactions for negative and positive electrodes, F is the Faraday constant, T is the cell temperature, R is the gas constant and c_{H+} is the concentration of protons in the positive half cell. Due to complex ionic equilibria it is very difficult to model accurately the dynamics of proton concentration. However, the small changes in proton concentration will not affect on cell voltage significantly, therefore proton concentration is assumed to be constant, the value is taken to be 4 M for simulations.

The cell voltage E_{cell} is determined by deducting the voltage losses due to ohmic resistance, and activation overpotential to the open circuit voltage, which is given by

$$E_{Cell} = E_{OC} - \sum E_{ohm} - \sum E_{act} \tag{3.48}$$

Ohmic losses associated with current collector, membrane and electrolyte can be calculated by,

$$E_c = j_{app}\frac{w_c}{\sigma_c} \tag{3.49}$$

$$E_m = j_{app}\frac{w_m}{\sigma_m} \tag{3.50}$$

$$E_e = j_{app}\frac{w_e}{\varepsilon^{3/2}\sigma_e} \tag{3.51}$$

where, σ_c, σ_m, and σ_e are the conductivities and w_c, w_e and w_m are the widths of the current collector, electrode, and membrane, respectively. The effective conductivity of electrolyte $\epsilon^{3/2}\sigma_e$, is obtained by using a Bruggeman correction. For Nafion 115 membrane conductivity can be calculated using the following empirical relationship

given by [67],

$$\sigma_m = (0.5139\lambda - 0.326) \exp\left(1268\left[\frac{1}{303} - \frac{1}{T}\right]\right) \tag{3.52}$$

The membrane conductivity depends on membrane water content λ and temperature of cell. The membrane is assumed to be fully saturated ($\lambda = 22$) since, there is constant contact with liquid electrolytes on each side of the cell.

To derive the electrochemical reaction it requires overpotential which is calculated from the current-overpotential equation at a given current density assuming equal charge coefficients ($\alpha = 0.5$) [68]

$$\frac{j}{j_0} = \left(1 - \frac{j}{j_{1,c}}\right) exp\left(-\frac{F\eta}{2RT}\right) - \left(1 - \frac{j}{j_{1,a}}\right) exp\left(\frac{F\eta}{2RT}\right) \tag{3.53}$$

Here, η is the overpotential and j_0 is the exchange current density which can be expressed as,

For negative electrode

$$j_0 = F k_{neg} \sqrt{c_2 c_3} \tag{3.54}$$

For positive electrode

$$j_0 = F k_{pos} \sqrt{c_4 c_5} \tag{3.55}$$

Reaction rate constant at the positive electrode k_{pos} and the negative electrode k_{neg} can be calculated by using Arrhenius law,

$$k_{pos} = k_{pos,ref} \exp\left(-\frac{F E^0_{pos}(T_{ref})}{R}\left[\frac{1}{T_{ref}} - \frac{1}{T}\right]\right) \tag{3.56}$$

$$k_{neg} = k_{neg,ref} \exp\left(\frac{F E^0_{neg}(T_{ref})}{R}\left[\frac{1}{T_{ref}} - \frac{1}{T}\right]\right) \tag{3.57}$$

Here, $k_{neg,ref}$ and $k_{pos,ref}$ are reaction rate constants at 293 K (reference temperature). The anodic and cathodic currents, $j_{l,a}$ and $j_{l,c}$, consider the rate at which the consumed species can be brought to the electrode surface from the bulk electrolyte solution and are associated to the bulk concentration and mass transfer coefficient given by,

For negative electrode

$$j_{1,a} = -Fm_3c_3 \tag{3.58}$$

$$j_{1,c} = Fm_2c_2 \tag{3.59}$$

For positive electrode

$$j_{1,a} = -Fm_4c_4 \tag{3.60}$$

$$j_{1,c} = Fm_5c_5 \tag{3.61}$$

Where m_2, m_3, m_4, and m_5 are the mass transfer coefficients. It is assumed that mass transfer is same for each vanadium species and it is denoted by m_v. The mass transfer coefficient depends on electrolyte flow velocity v and it can be calculated by the following empirical equation [69]

$$m_v = 1.6 \times 10^{-4} v^{0.4} \tag{3.62}$$

Numerical methods are required to solve the nonlinear overpotential Eq. (3.53). If the current density is very small compared to the limiting current density, the concentration of consumed species in the bulk solution and at the electrode surface are approximately equal, then Eq. (3.53) reduces to the ButlerVolmer equation [68]

$$\frac{j}{j_0} = exp\left(-\frac{F\eta}{2RT}\right) - exp\left(\frac{F\eta}{2RT}\right) \tag{3.63}$$

Above equation can be inverted to calculate the overpotential at each electrode.
For negative electrode

$$\eta = \frac{2RT}{F} \sinh^{-1}\left(\frac{j}{2Fk_{neg}\sqrt{c_2c_3}}\right) \tag{3.64}$$

For positive electrode

$$\eta = \frac{2RT}{F} \sinh^{-1}\left(\frac{j}{2Fk_{pos}\sqrt{c_4c_5}}\right) \tag{3.65}$$

If the mass transfer effects are not important then Butler-Volmer equation is computationally most efficient method of approximating the overpotential. Yu and Chen

[69] first time proposed new model by introducing mass transfer coefficient into the overpotential equation of the lumped model and it gives significant increase in overpotential, which is important in predicting the cell potential variation accurately. This model gives closed form piecewise equations to approximate current-overpotential equation over the entire range up to the limiting current.

If the current density is small with respect to limiting current density the Butler-Volmer equation is accurate in predicting the overpotential. If the current density is high the Butler-Volmer equation is less accurate in predicting the overpotential because it fails to capture the mass transfer effects which contributes to overpotential. Yu and Chen [69] proposed new approximations called mass transfer-limited (MTL) approximations to calculate overpotential by adding the mass transfer effects into the overpotential equation.

At high positive current densities overpotential approximations can be found by neglecting cathodic component (right side) of Eq. (3.53). This can be proved if the current density approaches $j_{1,a}$ at large negative overpotentials. Therefore, MTL approximations to calculate overpotential for an anodic reaction can be expressed as

$$\frac{j}{j_0} = -\left(1 - \frac{j}{j_{1,a}}\right) exp\left(\frac{F\eta}{2RT}\right) \tag{3.66}$$

$$\eta = \frac{2RT}{F}\left[ln\left(\frac{j_{1,a} - j}{j}\right) + ln\left(\frac{j_{1,a}}{j_0}\right)\right] \tag{3.67}$$

Similarly the MTL approximations to calculate overpotential for an cathodic reaction can be expressed as

$$\frac{j}{j_0} = \left(1 - \frac{j}{j_{1,c}}\right) exp\left(-\frac{F\eta}{2RT}\right) \tag{3.68}$$

$$\eta = \frac{2RT}{F}\left[ln\left(\frac{j_{1,c} - j}{j}\right) + ln\left(\frac{j_0}{j_{1,c}}\right)\right] \tag{3.69}$$

It is found that if the Butler-Volmer equation and MTL approximations under predicts the overpotential then larger of the two approximations should be considered for simulation [69]. In all of our simulations MTL approximations are used to calculate overpotentials.

3.2.3 Thermal model

Thermal model is based on the conservation of energy. There are three unknown variables, so three energy balance equations have to solved. Two energy balance equations for electrolyte reservoir and one energy balance equation for stack are solved to calculate the stack and electrolyte reservoir temperatures. The assumptions to simplify the energy balance equations are as follows,

1. No heat transfer takes place in the battery stack and pipes.
2. The heat transfer occurs between the surrounding air and the electrolyte tanks.
3. The electrolyte volume in the cells and tanks remains constant.
4. The electrolytes are mixed perfectly in the tanks and the cells.

$$\rho C_p V_s \frac{dT_s}{dt} = \rho Q_+ C_p (T_+ - T_s) + \rho Q_- C_p (T_- - T_s) + P_{Rc} + P_{ch} \tag{3.70}$$

$$\rho C_p V_+ \frac{dT_+}{dt} = \rho Q_+ C_p (T_s - T_+) + U_+ A_+ (T_{air} - T_+) + P_{pump+} \tag{3.71}$$

$$\rho C_p V_- \frac{dT_-}{dt} = \rho Q_- C_p (T_s - T_-) + U_- A_- (T_{air} - T_-) + P_{pump-} \tag{3.72}$$

The overall stack resistance will vary for both charging and discharging process. Therefore, Eq. (3.70) for discharging process can be written as,

$$\rho C_p V_s \frac{dT_s}{dt} = \rho Q_+ C_p (T_+ - T_s) + \rho Q_- C_p (T_- - T_s) + P_{Rd} + P_{ch} \tag{3.73}$$

Where, T_s = stack electrolyte temperature, $^\circ C$
T = temperature of the negative electrolyte in the tank $^\circ C$
T_+ = temperature of the positive electrolyte in the tank $^\circ C$
T_{air} = surrounding air temperature $^\circ C$
C_p = specific heat of the electrolyte J/gK
ρ = electrolyte density, g/m^3
Q_b = outlet flow rate of the battery stack, m^3/s
Q = outlet flow rate of the negative electrolyte in the tank, m^3/s
Q_+ = outlet flow rate of the positive electrolyte in the tank,m^3/s
A_- = surface area of the tank at negative side, m^2
A_+ = surface area of the tank at positive side, m^2
V_s = volume of the battery stack, m^3

V_-= volume of the negative electrolyte in the tank, m^3
V_+ = volume of the positive electrolyte in the tank, m^3
U = overall heat transfer coefficient of the tank at negative side, W/m^2K
U_+ = overall heat transfer coefficient of the tank at positive side, W/m^2K
I = charging or discharging current in A
P_{Rc} = power loss due to internal resistance during charging process in W
P_{Rd} = power loss due to internal resistance while discharging process in W
P_{ch} = power loss due to chemical reactions in W
R_c = overall stack resistance in charging Ω
R_d = overall stack resistance in discharging Ω
P_{pump+} = frictional and form power losses at the positive half cell in W
P_{pump-} = frictional and form power losses at the negative half cell in W
S_f = entropy of different species

3.3 Numerical model

The model is based on the conservation laws including fundamental modes of transport and kinetic model for reactions and the vanadium species will be used to predict the performance of the cell. The processes in the redox flow batteries are described by the equations of fluid mechanics, heat transfer, electrodynamics and electrochemistry. The flow of electrolyte through the porous electrodes and diffusion of ions across the membrane can be modeled by the conservation laws of mass, momentum and energy. The distribution of electric potential in redox flow batteries can be calculated by solving of Poisson equations. The electrochemical interaction of species in the cell is obtained by the Nernst equation and by the ButlerVolmer law. Combination of these processes makes the solution of equations more complicated. The following assumptions are considered in the numerical model

1. The dilute solution approximation is used for simplification and the flow is considered as laminar and incompressible.
2. Physical properties of electrode and membrane are homogeneous and isotropic.
3. The transport of the charged species takes place by convection and diffusion and migration terms are neglected for simplification.
4. There is no crossover of vanadium species across the membrane because there is no leakage of charge or reactant through the external surfaces of the cell.

The kinetics related with oxidation and reduction reaction of vanadium species are highly complex. The following simplified set of half-reactions can be used:
At the negative electrode:

$$V^{3+} + e^- \rightleftharpoons V_2^+ \tag{3.74}$$

At the positive electrode:

$$VO^{2+} + H_2O - e^- \rightleftharpoons VO_2^+ + 2H^+ \tag{3.75}$$

There are several side reactions occur in the cell, such as,
Hydrogen evolution reaction:

$$2H_2O + 2e^- \rightleftharpoons H_2 + 2OH^- \tag{3.76}$$

Oxygen evolution reaction:

$$2H_2O \rightleftharpoons O_2 + 4e^- + 4H^+ \tag{3.77}$$

$$VO^{2+} + 2H_2O \rightleftharpoons HVO_3 + 3H^+ + e^-$$

3.3.1 Governing equations

The performance of the vanadium redox flow battery can be predicted by solving the conservation equations of mass, momentum, energy, species and charge along with the reaction equations. The transport of charged species takes place by convection, diffusion and migration and it contributes to the current and affects the performance. Therefore, inclusion of all three transport mechanisms is important. The governing equations of the battery system involve highly nonlinear terms and coefficients in a complex system of partial differential equations that couple the electrochemical phenomena and fluid dynamics. In order to formulate a problem, certain assumptions have to be made to simplify the governing equations. In general assumptions mainly depend on the number of species accounted and their relative concentrations. The model is of the all-vanadium redox flow battery as shown in Fig. 3.1 . The main components of the battery are, porous electrodes, membrane, reservoirs and current collectors.

Equations in the porous carbon electrode

The concentration of species i involves $V(II), V(III), V(IV), V(V), H_2O, H^+, HSO_4^-$, in the electrolyte. A volume averaged mass balance in the porous regions can be expressed as,

$$\frac{\partial}{\partial t}(\epsilon C_i) + \nabla \cdot \overrightarrow{N_i} = -S_i \tag{3.78}$$

where ϵ is porosity, and S_i is the source term for species i. For the concentration fluxes $\overrightarrow{N_i}$, modified Nernst-Planck equations can be used in which transport of a charged species is assumed to occur by convection, electrokinetic effects and hydrodynamic dispersion (osmosis and electro-phoresis). The total flux $\overrightarrow{N_i}$ is given by,

$$\overrightarrow{N_i} = -D_i^{eff}\nabla C_i - \frac{Z_i C_i D_i^{eff}}{RT} F \nabla \phi + \overrightarrow{v} C_i \tag{3.79}$$

where $\overrightarrow{v}$ is the superficial electrolyte velocity, ϕ is the ionic potential and D_i^{eff} and z_i are the effective diffusion coefficient and valence for species i, respectively.
The effective diffusion coefficient is calculated using the Bruggemann correction,

$$D_i^{eff} = \epsilon^{\frac{3}{2}} D_i$$

The velocity $\overrightarrow{v}$ of the electrolyte in the porous medium can be calculated by using Darcy's law,

$$\overrightarrow{v} = -\frac{d_f^2}{k\mu} \frac{\epsilon^3}{(1-\epsilon)^2} \nabla p \tag{3.80}$$

where p is the electrolyte pressure, d_f is a mean fiber diameter, μ is the dynamic viscosity of the liquid and K is the Kozeny-Carman constant for a fibrous medium. In the above equation inertial permeability term is neglected. Variations in density associated with variations in dissolved vanadium content of the electrolyte is very small. There is no significant variations in vanadium content, so inertial permeability in Darcy's law is not considered. In keeping with the incompressibility and dilute solution approximation assumption, density and viscosity of the liquid are assumed constant.
The electrolyte is accounted as electrically neutral, therefore it is governed by the following equation,

$$\sum_i z_i C_i = 0 \tag{3.81}$$

Conservation of charge equation:
The charge entering the electrolyte $\overrightarrow{i_e}$ is balanced by the charge leaving the solid phase $\overrightarrow{i_s}$, which can be expressed as,

$$\nabla \cdot \overrightarrow{i_e} + \nabla \cdot \overrightarrow{i_s} = 0 \tag{3.82}$$

The total current transferred from the solid phase to the electrolyte,

$$\nabla \cdot \overrightarrow{i} = \nabla \cdot \overrightarrow{i_e} = -\nabla \cdot \overrightarrow{i_s}$$

Also the total current transferred is equal to the net rate of electrochemical reaction multiplied by Faraday's constant given by,

$$\overrightarrow{i} = z_i F \overrightarrow{N_i}$$

The total current density in the electrolyte satisfies the electroneutrality condition:

$$\overrightarrow{i} = \sum_i \overrightarrow{i_i} = -k^{eff} \nabla \phi - F \sum_i z_i D_i^{eff} \nabla C_i \tag{3.83}$$

The effective conductivity k^{eff}, is given by

$$k^{eff} = \frac{F^2}{RT} \sum_i z_i^2 D_i^{eff} C_i \tag{3.84}$$

where R is the molar gas constant and T is temperature.
Darcy's law gives the relationship between velocity and pressure gradient for porous electrode. The continuity equation can be written as,

$$\nabla \cdot \overrightarrow{v} = 0 \tag{3.85}$$

In the above equation the electrolyte is assumed as incompressible fluid. Combining Eqs. (3.80) and (3.85), we can get,

$$-\frac{d_f^2}{k\mu} \frac{\epsilon^3}{(1-\epsilon)^2} \nabla^2 p = 0 \tag{3.86}$$

The electronic potential in the porous electrode can be calculated from the Ohm's law,

$$\sigma_s^{eff}\nabla^2\psi = -\nabla \cdot \overrightarrow{i} \tag{3.87}$$

The effective conductivity of the porous carbon electrode can be determined by using Bruggemann correction given by,

$$\sigma_s^{eff} = (1-\epsilon)^{3/2}\sigma_s$$

where, σ_s^{eff} is the effective conductivity of the porous carbon electrode obtained from the value for the solid material.

Equations in the membrane

For the transport processes in the proton conducting membrane, we can use the formulation of Bernadi and Verbrugge [70]. The model of Bernadi and Verbrugge is the most appropriate if the membrane is close to fully saturated. This model formulation permits a straightforward coupling between the porous electrode and membrane equations.

The concentration of water dissolved in the membrane C_{H_2O} satisfies continuity equation,

$$\frac{\partial C_{H_2O}}{\partial t} - \nabla \cdot (D_w^{eff}\nabla C_{H_2O}) + \nabla \cdot (\overrightarrow{v} C_{H_2O}) \tag{3.88}$$

where, D_w^{eff} is the effective diffusion coefficient for water and $\overrightarrow{v}$ is the electrolyte velocity. The driving forces for the flow are pressure and potential gradients.

The velocity can be calculated using the Schloegl's equation [29],

$$\overrightarrow{v} = -\frac{k_\phi}{\mu_{H_2O}} F C_{H^+} \nabla\phi - \frac{k_p}{\mu_{H_2O}}\nabla p \tag{3.89}$$

where, k_ϕ is electrokinetic permeability, k_p is hydraulic permeability, μ_{H_2O} is water viscosity and C_{H^+} is proton concentration.

If the electrolyte is assumed as incompressible, the continuity equation for the liquid in the membrane is given by,

$$\nabla \cdot \overrightarrow{v} = 0 \tag{3.90}$$

Substituting the above equation into gradient of Schloegl's equation, the pressure p can be calculated.

From the electroneutrality condition the proton concentration satisfies the following condition.

$$C_H^+ = -z_f C_f$$

where C_f is the fixed charge site concentration in the membrane and z_f is the fixed site charge. The value of C_{H^+} is taken as constant.
The equation for current conservation can be written as,

$$0 = \nabla \cdot \overrightarrow{i} = \nabla \cdot \overrightarrow{N}_{H^+} = -\frac{F^2}{RT} D_H{}^{eff} C_H^+ \nabla^2 \phi \tag{3.91}$$

Using the Laplace's equation for the ionic potential the pressure equation becomes,

$$-\frac{k_p}{\mu_{H_2O}} \nabla^2 p = 0 \tag{3.92}$$

Current collectors

The only equation for the current collectors is the electronic potential equation. The effect of temperature variations is neglected (in this equation), and it is given by Ohm's law.

$$\sigma_{coll} \nabla^2 \psi = 0 \tag{3.93}$$

Where σ_{coll} is the electronic conductivity of the collectors, which is approximated a constant value.

Reaction kinetics

The reversible reactions occur on the solid surfaces of the porous carbon electrode can be expressed by using the Butler-Volmer law. It is used here because the precise multi step reaction mechanism is not known and it is expected that the basic reversible redox features can be captured easily with this form.
The transfer current densities for the negative and positive electrode can be written as,

$$\nabla \cdot \overrightarrow{i} = \epsilon A F k_1 (C_{III}^s)_{-,1}^{\alpha} (C_{II}^s)^{\alpha_{+,1}} \left[\exp\left(\frac{\alpha_{+,1} F \eta_1}{RT} RT \right) - \exp\left(-\frac{\alpha_{-,1} F \eta_1}{RT} \right) \right]$$

$$\nabla \cdot \overrightarrow{i} = \epsilon A F k_2 (C_{III}^s)_{-,2}^{\alpha} (C_{II}^s)^{\alpha_{+,2}} \left[\exp\left(\frac{\alpha_{+,2} F \eta_2}{RT} \right) - \exp\left(-\frac{\alpha_{-,2} F \eta_2}{RT} \right) \right] \tag{3.94}$$

Where, k_1 and k_2 are the standard rate constants for reactions Eqs. 3.1 and 3.2 respectively. A is the specific active surface area of the electrode(solid-liquid interface), $\alpha_{+,k}$ and $\alpha_{-,k}$ are the anodic and cathodic transfer coefficients respectively and η_1 and η_2 are the overpotentials in the negative and positive electrode respectively. where the subscript $k = 1, 2$ refers to reaction Eqs. 3.1 and 3.2, respectively. The overpotentials are defined as,

$$\eta_k = \phi_s - \phi_e - E_{0,k} \tag{3.95}$$

Where $E_{0,k} = 1, 2$ are the open circuit potentials for reactions (1) and (2) respectively, which are calculated from the Nernst equations given by,

$$E_{0,1} = E'_{0,1} + \frac{RT}{F} \log_{10}\left(\frac{C_{II}}{C_{III}}\right)$$

$$E_{0,2} = E'_{0,2} + \frac{RT}{F} \log_{10}\left(\frac{C_{IV}}{C_V}\right) \tag{3.96}$$

Where $E_{0,1}$ and $E_{0,2}$ are the equilibrium potentials . In the above equations variation of proton concentration is neglected since the value is very low during charge/discharge cycles.

The quantities C_i^s are vanadium species concentrations at the solid liquid interfaces in the porous regions, which are different from the bulk values due to additional transport resistance. They can be related to the bulk values, C_i, by approximately balancing the rate of reaction with the rate of diffusion of reactant to (or from) the electrode surface at steady state. Therefore, it is convenient to re-write the Butler-Volmer terms in a form that shows linear dependence on the surface concentrations. For the positive electrode during charge, the balance is,

$$C_{IV} - C_{IV}^s = \frac{\epsilon k_1}{\gamma_{IV}} \left\{ C_{IV}^s \exp\left(\frac{F\left(\phi_s - \phi_e - E'_{0,2}\right)}{2RT}\right) - C_V^s \exp\left(-\frac{F\left(\phi_s - \phi_e - E'_{0,2}\right)}{2RT}\right)\right\} \tag{3.97}$$

$$C_V - C_V^s = -\frac{\epsilon k_2}{\gamma_V} \left\{ C_V^s \exp\left(\frac{F\left(\phi_s - \phi_e - E'_{0,1}\right)}{2RT}\right) - C_V^s \exp\left(-\frac{F\left(\phi_s - \phi_e - E'_{0,1}\right)}{2RT}\right)\right\} \tag{3.98}$$

Where $\gamma_{IV} = D_{IV}/d$ and $\gamma_V = D_V/d$. δ is the average inter fibre distance in the porous carbon electrode and D_i is the diffusion coefficient for species i in solution.

Solving these simultaneous equations for C_{IV}^s and C_V^s gives,

$$C_{IV}^s = \frac{C_{IV} + \epsilon k_2 e^{-\frac{F\left(\phi_s - \phi_e - E'_{0,2}\right)}{2RT}} \left(C_{IV}/\gamma_V + C_V/\gamma_{IV}\right)}{1 + \epsilon k_2 \left(e^{-\frac{F\left(\phi_s - \phi_e - E'_{0,2}\right)}{2RT}}/\gamma_V + e^{\frac{F\left(\phi_s - \phi_e - E'_{0,2}\right)}{2RT}}/\gamma_{IV}\right)} \tag{3.99}$$

$$C_V^s = \frac{C_V + \epsilon k_2 e^{-\frac{F\left(\phi_s - \phi_e - E'_{0,2}\right)}{2RT}} \left(C_{IV}/\gamma_V + C_V/\gamma_{IV}\right)}{1 + \epsilon k_2 \left(e^{-\frac{F\left(\phi_s - \phi_e - E'_{0,2}\right)}{2RT}}/\gamma_V + e^{\frac{F\left(\phi_s - \phi_e - E'_{0,2}\right)}{2RT}}/\gamma_{IV}\right)} \tag{3.100}$$

Above equations are used in the reaction rates to eliminate the surface concentrations in favour of the bulk values. Similar expressions apply to the species at the negative electrode.

3.3.2 Inlet conditions and pump approximations

The movements of the electrolyte solution across the pump and electrode vary the concentrations at the inlet boundaries with time. From the conservation of volume, the volumetric flow at the outlet boundary is $w = v_{in}\epsilon A$, with cross-sectional area $A = L_t L_w$, where L_w is the electrode width and L_t is the electrode thickness . The variation of the outlet concentrations can be found out from the calculated average concentration at the outflow boundaries. Which is given by,

$$C_i^{out} = \frac{1}{L_t} \int_{y=h} C_i dx \tag{3.101}$$

The inlet concentrations are calculated in the following manner, which assumes that instantaneous mixing and negligible reaction in the reservoir of volume V and also assumed that the volume in the pipes is negligible. The change in number of moles of species i in the reservoir in a time ∇t is equal to the difference between the number of moles of species i added to the reservoir and the number of moles of species i leaving the reservoir.

$$\nabla n = C_i^{out} w - C_i^{in} w \tag{3.102}$$

where C_i^{in} and C_i^{out} are the electrodes inlet and outlet concentrations of species i, respectively. The change in concentration of species i in the reservoir is given by,

$$\frac{\nabla C_i^{in}}{\nabla t} = \frac{\nabla n}{V} \tag{3.103}$$

$$\text{The limit}, \nabla t \to 0, \tag{3.104}$$

$$\frac{dC_i^{in}}{dt} = \frac{w}{V}(C_i^{out} - C_i^{in})$$

$$C_i^{in}(0) = C_i^0$$

where C_i^0 is the initial concentration of species i. The total volume V_T of electrolyte on each side of the battery is the sum of the reservoir and the electrode volumes. Here h is the height of the porous carbon electrode.

3.3.3 Initial and Boundary conditions

From Figure 3.1 at the interfaces between the porous carbon electrode and membrane regions the species fluxes (excluding water and protons) and electron flux are considered to be very small hence can be neglected. At all external boundaries except at the inlets and outlets the same conditions applies to the species fluxes.

$$\overrightarrow{N} \cdot \overrightarrow{n} = 0 \begin{cases} x = x1, x = x4, & \\ x = x2,\ x = x3, & \text{(except water/protons)} \\ y = 0,\ y = h, & \text{(except inlet/outlet)} \end{cases} \tag{3.105}$$

$$\nabla \phi_s \cdot \overrightarrow{n} = 0 \begin{cases} x = x2, x = x3, \\ y = 0,\ y = h, \end{cases} \tag{3.106}$$

The proton flux at the interfaces between porous carbon electrode and the current collectors is zero, similarly at all external boundaries in the membrane.

$$-\nabla \cdot (\sigma_e \nabla \phi_e + FA \sum_i z_i D_i \nabla C_i) \cdot \overrightarrow{n} = 0, \text{at } x = x1, \text{and } x = x4 \tag{3.107}$$

$$-\nabla\phi_e \cdot \overrightarrow{n} = 0, \text{ at } y = 0, \text{and}, y = h, \text{membrane}$$

At all boundaries of the domain except at the inlets and outlets, integration of the pressure equation a Neumann condition can be used.

$$\nabla p \cdot \overrightarrow{n} = 0, (\text{except inlets/outlets}) \tag{3.108}$$

At the inlets, the reactants and water enter with a prescribed bulk velocity and concentrations that depend on the pump flow rate,

$$C_i = C_i^{in}(t); \quad v_y = v_{in} \qquad (\text{inlets}) \tag{3.109}$$

At the outlets electrolyte pressure is prescribed and all diffusive fluxes are set to zero (fully developed flow condition),

$$\nabla C_i \cdot \overrightarrow{n} = 0; p = p_{out} \text{ (outlets)} \tag{3.110}$$

Along the current collector/electrode interfaces a no slip condition is applied on the liquid velocity,

$$\overrightarrow{u} = 0; x = x1; x = x4 \tag{3.111}$$

The boundary conditions on the electronic potential depend on whether the battery is operated in galvanostatic or potentiostatic mode. For the present galvanostatic case the current is assumed to enter or leave uniformly through the current collectors, manifested through the following flux conditions (while charge):

$$-\sigma_{coll}\ \phi_s \cdot \vec{n} = \left\{ \begin{array}{ll} -\frac{I_{app}}{A} & x = 0 \\ -\frac{I_{app}}{A} & x = 5 \end{array} \right\} \tag{3.112}$$

where I_{app} is the current and A is the projected area to which the current is applied. For discharge conditions the signs are reversed.
The initial conditions for the concentrations and potentials is given by,

$$C_i(t = 0) = C_i^0; \phi_s(t = 0) = E_{0,+}(t = 0); \phi_s(t = 0) = 0; \text{at positive electrode} \tag{3.113}$$

$$C_i(t=0) = C_i^0; \phi_s(t=0) = E_{0,-}(t=0); \phi_s(t=0) = 0; \text{at negative electrode} \tag{3.114}$$

3.3.4 Numerical model considering losses

The numerical model adding concentration overpotential and ohmic losses proposed by Shah et al. [29] can predict the performance more accurately. Due to these overpotentials, there is considerable amount of voltage drop taking place, therefore significant amount of variation in efficiencies can be observed. Concentration overpotential of an electrode is a result of formation of a diffusion layer adjacent to the electrode surface, where there is a gradient of the ion concentration. Ohmic losses include losses associated with current collector, membrane and the electrolyte.

Overpotential

There are three processes leading to overpotential due to electrochemical reactions, including activation overpotential, concentration overpotential and Ohmic losses due to resistance in the cell.

$$\eta = \eta_{act} + \eta_{con} + (IR)_c + (IR)_m + (IR)_e \tag{3.115}$$

Activation overpotential

Activation overpotential can be expressed by Butler-Volmer equation given by,

$$i = i_0 \left[\exp\left(\frac{\alpha_{a,+} F \eta_+}{RT} \right) - \exp\left(-\frac{\alpha_{c,+} F \eta_+}{RT} \right) \right] \tag{3.116}$$

Concentration overpotential

Concentration overpotential can be described by the Nernst equation given by,

$$\eta_{con} = \frac{RT}{F} ln \frac{C_0}{C_b} \tag{3.117}$$

where C_0 is the reactant concentration at the electrode surface and C_b is the bulk concentration in the solution.

Ohmic losses

The ohmic losses associated with current collector, membrane and the electrolyte is given by [27],

$$(IR)_c = j_{app}\frac{w_c}{\sigma_c}, \qquad (IR)_m = j_{app}\frac{w_m}{\sigma_m}, \qquad (IR)_e = j_{app}\frac{w_e}{\varepsilon^{3/2}\sigma_e}$$

σ_c, σ_m and σ_e are the conductivities and w_c, w_e and w_m are the widths of the current collector, the electrolyte and membrane, respectively.

Cell voltage

The cell voltage for charge and discharge is given by [27],

$$E_{Cell} = E_0 + \frac{RT}{F}\ln\left(\frac{C_{V(II)}C_{V(V)}[H^+]^2}{C_{V(III)}C_{V(IV)}}\right) - \sum_k (IR)_k - \sum_k \mid \eta_a \mid - \sum_k \mid \eta_{con} \mid \tag{3.118}$$

Coulombic efficiency (CE)

Coulombic efficiency is the ratio of the charge withdrawn from the system during the discharge Q_d to the charge supplied during the charge Q_c, which is given by,

$$CE = \frac{Q_d}{Q_c} = \frac{\int_{t_c}^{t_d} I_d\, dt}{\int_0^{t_c} I_c\, dt} \tag{3.119}$$

where I_d is the discharging current and I_c is the charging current.

Voltage efficiency (VE)

The voltage efficiency is the ratio of the integral of the stack voltage V_d during discharge to that of the stack voltage V_c during charge.

$$VE = \frac{\int_{t_c}^{t_d} V_d\, dt}{\int_0^{t_c} V_c\, dt} \tag{3.120}$$

Energy efficiency (EE)

Energy efficiency is the product of voltage efficiency (VE) and the coulombic efficiency (CE).

$$EE = VE \times CE \tag{3.121}$$

3.4 Closure

The governing equations for lumped and numerical model of all-vanadium redox flow battery are presented. The lumped model based equations are solved using inhouse code. The numerical model based on the conservation equations of mass, momentum, species and charge with reaction equations are solved using commercial software COMSOL multiphysics [71]. The numerical model encompasses various losses taking place during charging and discharging reaction process. The coulombic, voltage and energy efficiencies related to VRFB are also presented.

Chapter 4

A Lumped Dynamic Model to Evaluate Performance of the All-Vanadium Redox Flow Battery

4.1 Introduction

All-vanadium redox flow battery (VRFB) is one of the promising rechargeable battery since it is able to withstand average loads, high energy efficiency and high power output. The battery exhibits the excellent transient behaviour and sustains sudden voltage drop. The dynamics of the battery is governed by the conservation equations of mass and charge. The lumped dynamic model includes electrochemical reactions, major resistances, and recirculation of electrolyte through external reservoirs. The mathematical model is capable to predict the performance of the battery.

Li and Hikihara [26] developed the transient model of the redox flow battery based on chemical reactions. Shah et al. [27] developed a dynamic analytical model for the vanadium redox flow battery, which can provide accurate, rapid solution. Numerical models of the redox flow battery incorporate the fundamental modes of transport, the electrochemical kinetics and heat losses. It is not feasible to incorporate this level of detail in control/monitoring tools. Therefore, there is need to develop control oriented models that can capture the performance accurately. This lumped dynamic model involves control oriented model for the vanadium redox flow battery

system.

After using VRFB for many cycles the performance reduces due to ion diffusion of vanadium ions pass through membrane. Therefore, a of lot research is going on to improve performance and maintain the capacity for long term cycling. It was found that no membrane gives 100 % performance [56], there will be vanadium ions diffusion through membrane from negative half cell to positive half cell and vice versa. Due to diffusion of vanadium ions, the vanadium concentration of one half cell increases and the other half cell vanadium concentration decreases, which results in performance loss of the cell. Due to self discharge reactions, capacity of the cell decreases and this can be restored by remixing the vanadium ions to both half cells periodically. Also there is oxygen and hydrogen evolution side reactions taking place inside the cell, which results in capacity loss, to restore the capacity it requires electrochemical rebalance. Several researchers proposed few approaches to overcome the performance loss for different operating conditions of the cell. Studies have shown that crossover of vanadium and water through membrane reduce the coulombic efficiency and capacity.

The present simulation is based on model developed by Shah et al. [29], Yu and Chen [69], with and without including the effects of mass transfer and crossover of vanadium ions through membrane. The effects of temperature on diffusion coefficients and effects of porosity on concentration for different membrane materials using this model have not been studied so far. The lumped dynamic model has simple ODEs based on some assumptions, therefore these are easy to solve and it requires less computational time without losing accuracy. Also this model is useful in the comparative study of various parameters at the same conditions.

4.2 Problem Description

Figure 4.1 shows the schematic of VRFB. Due to reduction and oxidation reaction in the cell the variation in concentration of vanadium species takes place, therefore the performance of the cell varies. The performance of the cell is studied for two cases,

i) Without considering the crossover and mass transfer effect in the model : Effects of concentration, electrode porosity, electrolyte flow rate, applied current density and temperature.

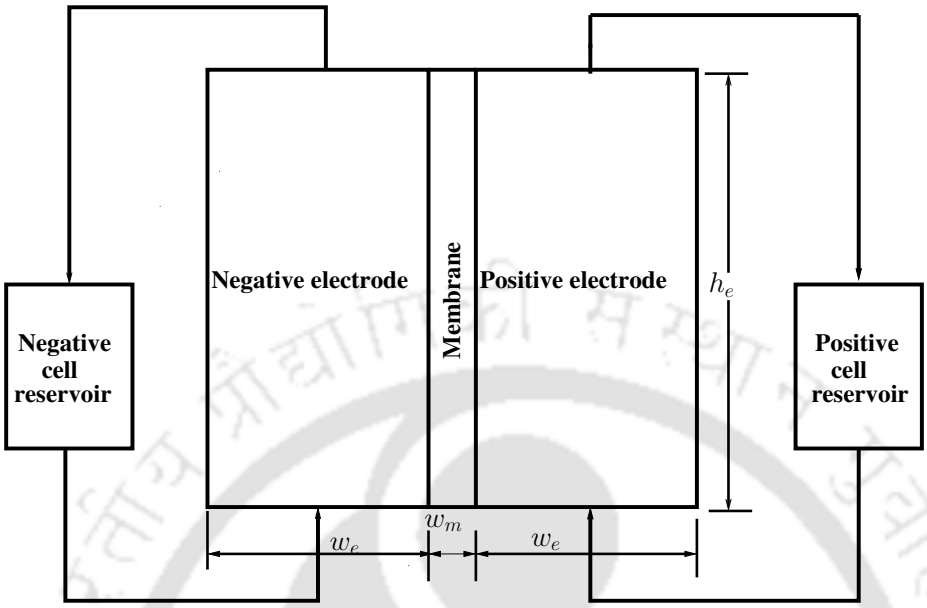

Figure 4.1: Schematic of the all-vanadium redox flow battery showing the components, current collectors, porous electrodes, membrane and reservoirs.

ii) Accounting the effects of mass transfer and crossover in the model : Effects of temperature on diffusion coefficients and reaction rate constants, effects of temperature and porosity on the cell potential response is studied for different membrane materials.

4.3 Results and Discussion

The governing equations for lumped model as shown in Section 3.2 are solved in this study. The structural dimensions of the VRFB are based on the experimental setup taken from Ref. [27]. The full detail of the derivation calculation of cell and reservoir concentration are shown in Appendix A. The default parameters related to structural dimensions and initial conditions are given in Table B.1-B.4 in Appendix B. Figure 4.2 shows the comparison between simulated and experimental cell potential difference. The cell temperature was *297 K*, the vanadium concentration was *1200 mol/m*^{3} , the flow rate was $1\times10^{-6} m^3/s$ and the current density was *1000 A/m*^{2}. The model results are validated with the available experimental result of Shah et al. [27] and it shows good agreement. Figure 4.3 shows cell concentration variation inside the negative half of the cell. The cell temperature was *300 K*, the

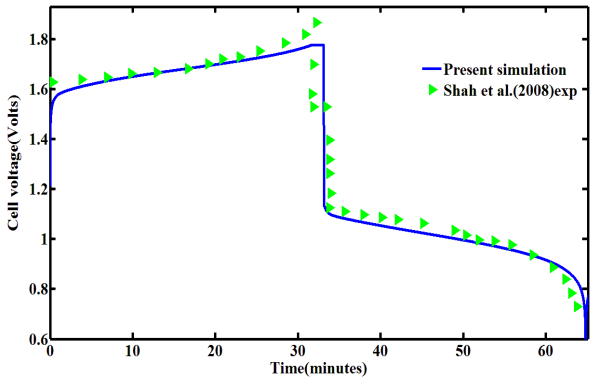

Figure 4.2: Comparison between simulated and experimental cell potential difference. The cell temperature was *297 K*, the vanadium concentration was *1200 mol/m*^{3} , the flow rate was $1\times10^{-6}m^3/s$ and the current density was *1000 A/m*^{2}.

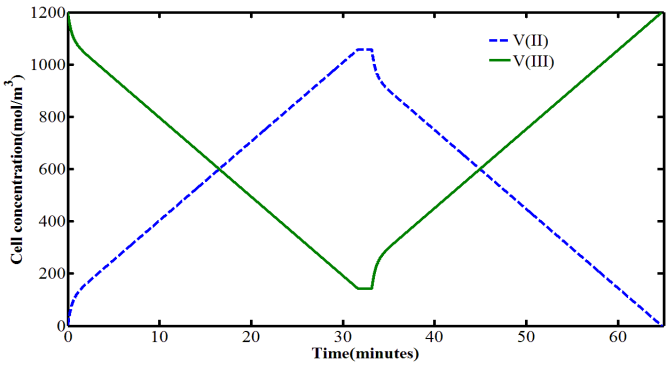

Figure 4.3: Cell concentration V(II) and V(III) variation with time during the full charge-discharge cycle. The cell temperature was *300 K*, the vanadium concentration was *1200 mol/m*^{3} , the flow rate was $1\times10^{-6}m^3/s$ and the current density was *1000 A/m*^{2}.

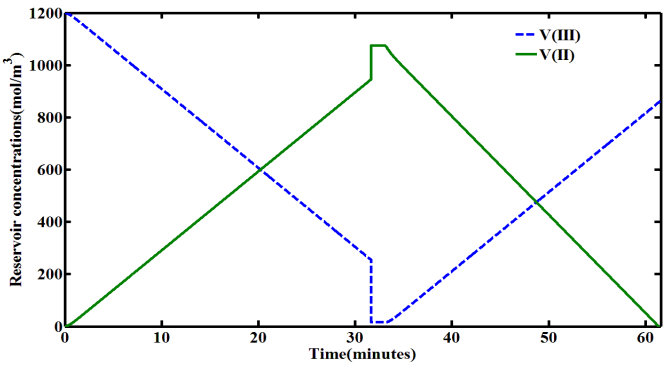

Figure 4.4: Reservoir concentration V(II) and V(III) variation with time during the full charge-discharge cycle. The cell temperature was *300 K*, the vanadium concentration was *1200 mol/m*^{3} , the flow rate was $1\times10^{-6}m^3/s$ and the current density was *1000 A/m*^{2}

vanadium concentration was *1200 mol/m*^{3}, the flow rate of 1×10^{-6} m^3/s and the current density of *750 A/m*^{2}. The concentration of vanadium V(III) decreases during charging from maximum i.e. *1200 mol/m*^{3} to minimum value. While discharging process the vanadium V(III) concentration increases from minimum to maximum value. This is due to the fact that during charging of the cell vanadium V(III) ions reduces to vanadium V(II) ions. Similarly, while discharging the cell vanadium V(II) ions reduces to V(III), this phenomena can be seen in Fig. 4.3. For V(II) concentration increases linearly from zero to maximum value during charging process. While discharging the cell vanadium V(II) concentration decreases linearly from maximum to zero. This phenomena is due to the oxidation and reduction reaction of vanadium ions in the process of charging and discharging. Figure 4.4 shows the variation of the vanadium concentration of the negative electrode side reservoir, the vanadium V(III) concentration decreases linearly, before charging process completion (short duration) concentration drops suddenly to minimum, then concentration increases linearly during discharging the cell. Similarly, the reservoir concentration of vanadium V(II) increases linearly from zero to below maximum value before completion of charging process (small duration) the concentration suddenly increases to maximum value, then decreases linearly during discharging process.

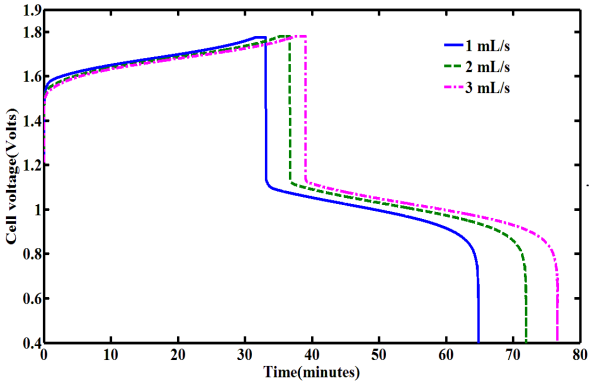

Figure 4.5: Model simulated results obtained cell potential difference, E_{cell} at flow rates, $\omega = 1\ mLs^{-1}$, $\omega = 2\ mLs^{-1}$ and $\omega = 3\ mLs^{-1}$. In all cases the vanadium concentration was *1200 mol* m^{-3} , the temperature was *297 K* and the current density was *1000 A* m^{-2}

4.3.1 Effects of flow rate

Electrolyte flow rate is very important parameter in the operation of vanadium redox flow battery. If the electrolyte flow rate is very high, it leads to risk of leakage or may not give good performance for the extra power required. On the other hand low electrolyte flow rate leads to insufficient circulation of electrolyte and stagnant regions are formed in the electrode. The effects of flow rate variations are shown in Fig. 4.5. In all the simulations the total vanadium concentrations for each electrode/reservoir *1200 mol* m^{-3} has been taken. Results suggest that electrolyte flow rate increases the potential difference of the cell increases which leads to better performance of the cell. The reason behind the improvement in the performance is that concentration in the electrode is more evenly distributed for higher flow rate.

4.3.2 Effects of applied current densities

Simulated cell potential difference, E_{cell} curves while charge/discharge at three different applied current densities are shown in Fig. 4.6. In these calculations, $C^0_{V(III)} = C^0_{V(IV)} = 1200\ \text{mol m}^{-3}$ and flow rate ω*=1 mL* s^{-1}. As the current density increases, the cell voltage decreases and it gives lesser performance of the cell. The reason behind that as the current density increases there is possibility of gas evolution inside the cell which leads to decrease in performance of the cell.

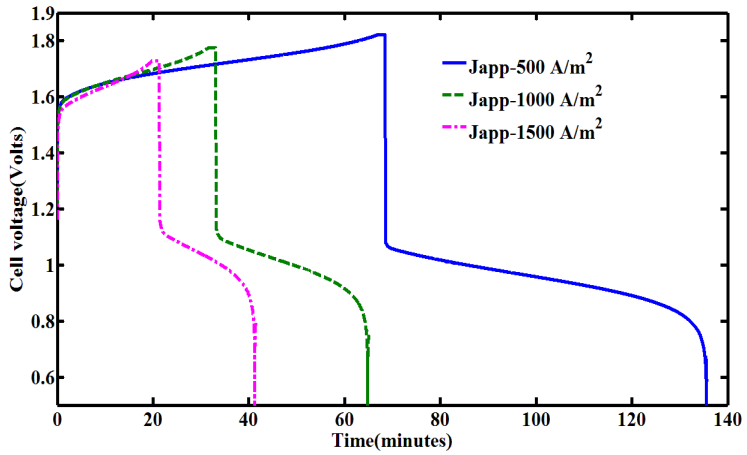

Figure 4.6: Comparison of the model simulated charge/discharge curves at three different applied current densities. In all the cases the temperature was *300 K,* the vanadium concentration was *1200 mol* m^{-3} and the flow rate was $1\times10^{-6}m^3/s$

4.3.3 Effects of vanadium concentrations

Figure 4.7 shows simulation results of three different concentrations of vanadium. In all cases the temperature was *300 K,* the current density was *1000 A* m^{-2} and flow rate was 1×10^{-6} m^3 s^{-1}. As the concentration increases cell terminal voltage and charge time increases which gives better performance.

4.3.4 Effects of electrode porosity

Simulated potential difference, E_{cell} curves during charge/discharge at three different electrode porosity values are shown in Fig. 4.8. The total volume of electrolyte was kept same in all cases. In all the simulations vanadium concentration was *1200 mol* m^{-3} , the current density was *1000 A* m^{-2} and the electrolyte flow rate was $1\times10^{-6}m^3/s$ and the temperature was *300 K*. There are several effects associated with increase in porosity such as, increased permeability, decreased bulk conductivity, increased bulk diffusion coefficients and higher the electrolyte volume in the electrode. As the porosity of the electrode decreases, cell voltage and charging time increase and this results in better performance of the cell. The polarization is greater at higher porosity, therefore side reactions rate is increased during charging.

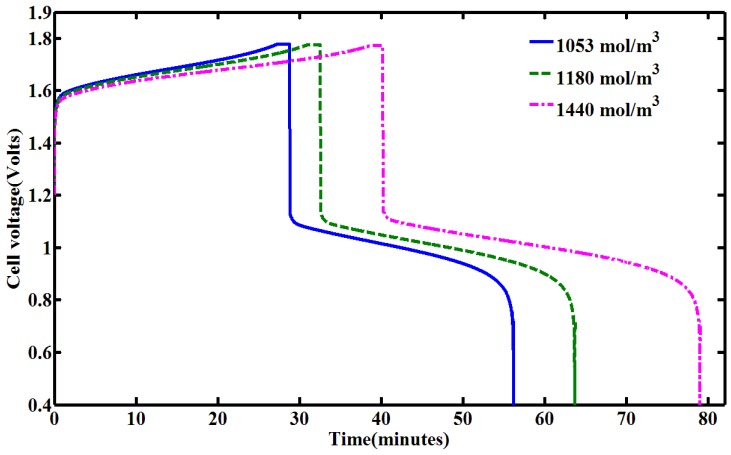

Figure 4.7: Model simulated results obtained cell potential difference, E_{cell} at three different vanadium concentrations. In all cases the flow rate was $1{\times}10^{-6}\ m^3\ s^{-1}$, the temperature was $300\ K$ and the current density was $1000\ A\ m^{-2}$

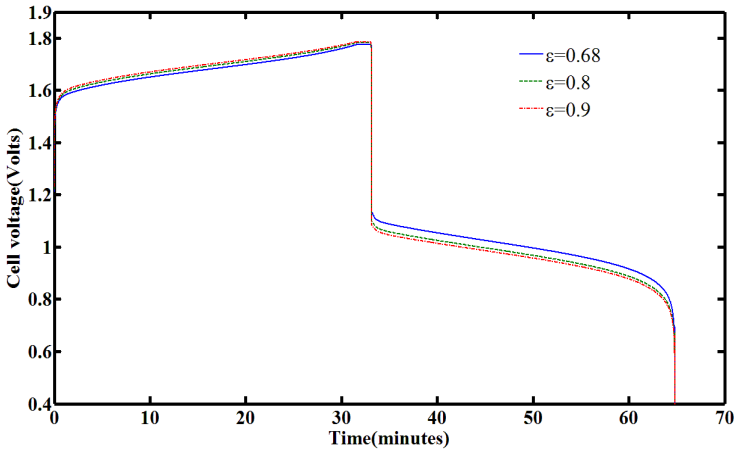

Figure 4.8: Comparison of the model simulated cell voltage curves for three electrode porosity values. In all the cases the temperature was $300\ K$, the vanadium concentration was $1200\ mol\ m^{-3}$, the flow rate was $1{\times}10^{-6}m^3/s$ and the current density was $1000\ A\ m^{-2}$

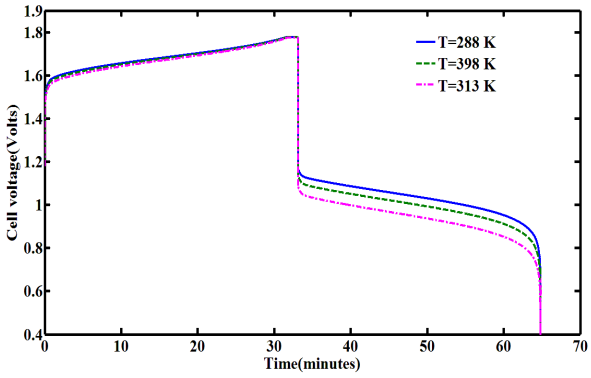

Figure 4.9: Model simulated results obtained cell potential difference, E_{cell} at three different operating temperatures. In all cases the vanadium concentration was *1200* $mol\ m^{-3}$, the flow rate was $1\times10^{-6}\ m^3\ s^{-1}$ and the current density was *1000* $A\ m^{-2}$

4.3.5 Effects of operating temperatures

Figure 4.9 shows the comparison of cell potential difference, E_{cell} at three operating temperatures T_0=*288, 298* and *313 K*. In all simulations the flow rate was 1×10^{-6} $m^3\ s^{-1}$, vanadium concentration was *1200* $mol\ m^{-3}$ and the current density was *1000* $A\ m^{-2}$. Simulation result shows that as the temperature increases, the cell voltage decreases while charging and increases during discharging. If the temperature increases, the reaction rate constants increases which leads to decreases in the magnitudes of overpotentials. Therefore, higher operating temperature gives lesser performance.

4.4 Results accounting the effects of mass transfer and crossover effects

4.4.1 Effects of temperature on diffusion coefficients and reaction rate constants

Figure 4.10 shows variation of diffusion coefficients with temperature for Selemion AMV, Selemion CMV and Nafion 115 membranes. The variation of diffusion coefficients with temperature is based on the model of Arrhenius. Here the assumption is that the activation energy is same for all vanadium species. It is observed that

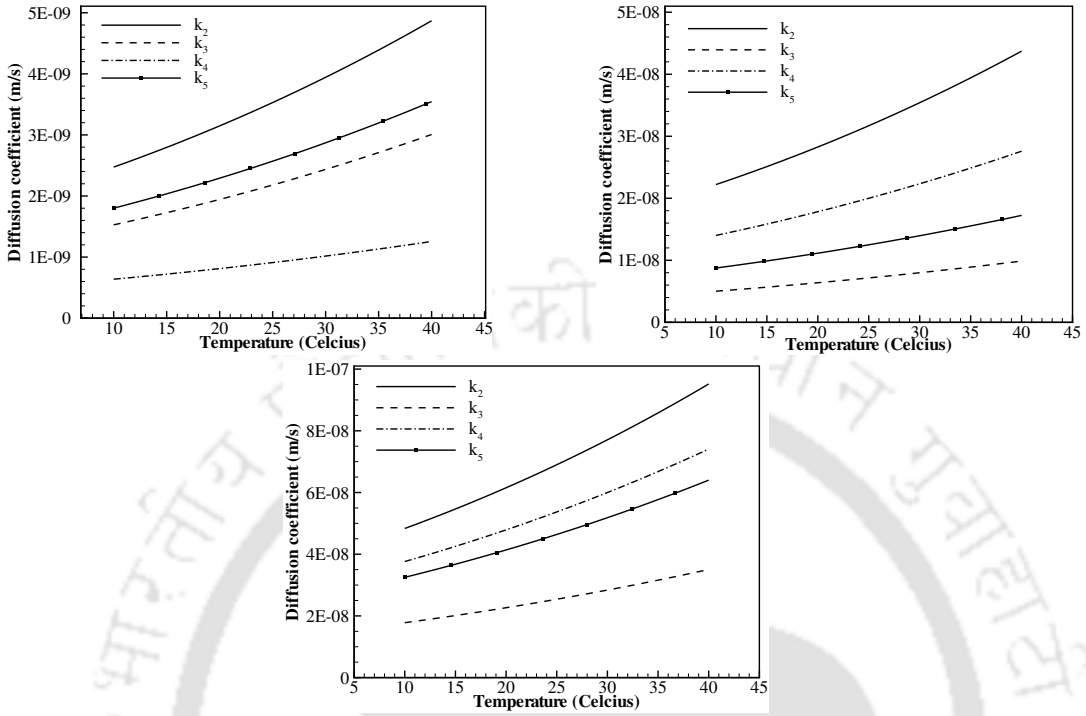

Figure 4.10: Variation of membrane diffusion coefficients at different temperatures (a) Selemion AMV (b) Selemion CMV (c) Nafion 115.

diffusion coefficients increase with temperature, therefore change in concentration of vanadium ions takes place in both half of the cell.

The reaction rate constants also depend on temperature for both negative and positive electrode. Variation of reaction rate constant with temperature for negative and positive electrode is shown in Figs. 4.11(a) and (b), respectively. The temperature dependent variation is based on Arrhenius model. It is understood from Figure 4.11 that for negative electrode if temperature increases, reaction rate constant decreases, for positive electrode if temperature increases, reaction rate constant increases. The reaction rate constants are useful in predicting the overpotentials accurately.

4.4.2 Cell potential response for Butler-Volmer and MTL approximations

Figure 4.12 shows cell potential variation with time and comparison for Butler-Volmer and MTL approximations. It is observed higher cell voltage variation for MTL approximations in comparison with Butler-Volmer equation approximations.

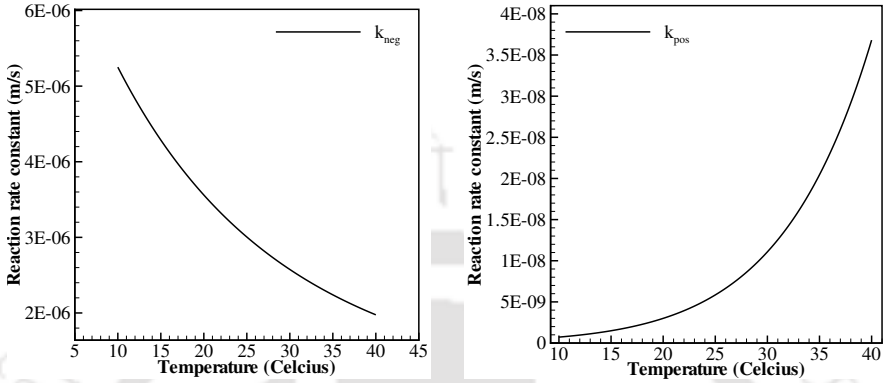

(a) (b)

Figure 4.11: Reaction rate constant at different temperatures (a) Negative electrode (b) Positive electrode.

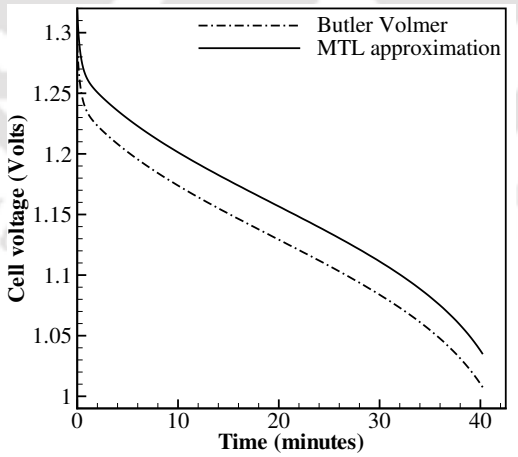

Figure 4.12: A comparison of Butler-Volmer equation and MTL approximation to the cell voltage. The flow rate was $1 \times 10^{-6}\ m^3/s$ and the soc were set to 80%.

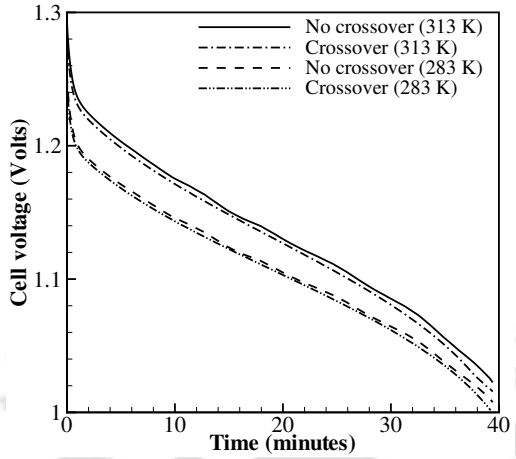

Figure 4.13: Simulated discharge cell potential response with and without crossover at 283 K and 313 K. The flow rate and current density were set to 1 mL/s and 1000 A/m^2. The initial soc were set to 80%

Also it is understood that there is small difference in cell voltage between two approximations, because of adding the mass transfer term in the overpotential equation. Considering the effects of mass transfer lead to prediction of overpotential accurately. Yu and Chen [69] showed that Butler-Volmer approximation predicts overpotential accurately for small current densities in comparison with the limiting current density. In present simulations value of current densities are high in comparison with limiting current density, therefore, MTL approximations are used.

4.4.3 Cell voltage response due to crossover effects

Figure 4.13 shows the comparison of cell voltage variation response with and without crossover for discharging conditions. The flow rate and current density were set to 1×10^{-6} m^3/s and 1000 A/m^2, respectively. The difference in cell potential between two cases is less for higher soc but increases considerably for lower soc. After discharging process, the differences in cell potential are 6 and 6.86 mV at 283 K and 313 K, respectively. The difference is considerably higher for higher temperature due to increase in diffusion coefficients with temperature and it results in increase of self discharge rate. Using the cell for long term, capacity of cell decreases due to crossover and this can be overcome by electrolyte rebalancing [9]. It is observed that voltage efficiency increases with temperature because of lower activation overpotential.

4.4.4 Concentration response due to temperature

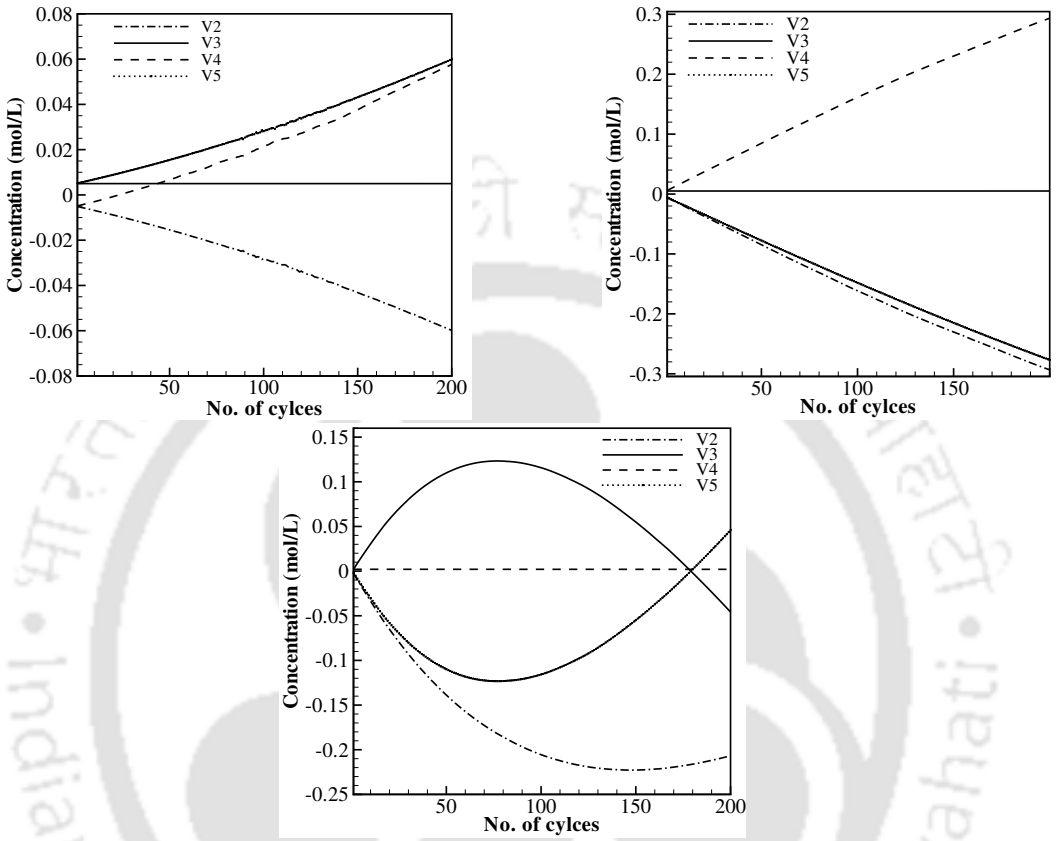

Figure 4.14: Variation in diffusion trend due to temperature at 1.7 V (a) for AMV membrane (b) for CMV membrane (c) for Nafion 115 membrane.

Three different membranes such as, Selemion AMV, Selemion CMV and Nafion 115, are considered for temperature dependence solution. The upper voltage limit is assumed to be 1.7 V and lower voltage limit is 0.95 V. The vanadium species concentration for V^{2+}, V^{3+}, V^{4+} and V^{+5} are analyzed at 1.7 V and temperatures ranging from 10° C to 40° C. The vanadium ion concentration variation with number of cycle trends are consistent with those diffusion model of Badrinarayanan et al. [56]. Four different vanadium ion concentrations are plotted by calculating the difference in diffusion between 10° C and 40° C as shown in Figs. 4.14 (a),(b) and (c) for three membranes (Selemion AMV, Selemion CMV and Nafion 115). The Figure 4.15 describe the difference in vanadium concentration change between 40° C and 10° C.

The variation of concentration difference with number of cycles between 40° C and

10° C shown in Fig. 4.14 for 200 charging/discharging cycles. From Fig. 4.14 (a) for Selemion AMV membrane based cell, the difference in diffusion does not reduce with number of cycles but it increases with number of charging/discharging cycles. It is understood that relative difference varies linearly with number of cycles and the difference increases with the number of charging/discharging cycles. The temperature dependence characteristics curves of Selemion AMV looks similar to that of Selemion CMV (Fig. 4.14 (b)), but the diffusion of vanadium ion species is different. Figure 4.14(c) shows the concentration difference with number of cycles between 40° C and 10° C for Nafion 115 membrane. It is observed that difference in diffusion increases upto 77 cycles then decreases as the number of charging/discharging cycles progresses. The diffusion of Selemion AMV and Selemion CMV does not vary linearly as it depends on the diffusion coefficient of the membrane.

4.4.5 Concentration response due to porosity

The variation in concentration depends on the porosity of the electrode as seen from Eqs.3.42 to 3.45. If the porosity of the electrode varies, there is variation in the concentration which leads to changes in difference in diffusion of vanadium ions. Here three different membranes such as, Selemion AMV, Selemion CMV and Nafion 115, are also considered for porosity dependence solution. The upper cell potential limit is assumed to be 1.7 V and lower cell potential limit is 0.95 V. The vanadium species concentration for V^{2+}, V^{3+}, V^{4+} and V^{+5} are analyzed at 1.7 V at porosity values ranging from 0.6 to 0.8.

Figure 4.15 (a) shows difference in diffusion variation for Selemion AMV membrane based cell, the diffusion difference increases with number of charging/discharging cycles. It is observed that for both Selemion AMV membrane and Selemion CMV membrane (from Fig. 4.15 (b)) relative difference of diffusion of concentration varies linearly with the number of cycles. The porosity dependence characteristics curves of Selemion AMV looks similar to that of Selemion CMV (Fig. 4.15 (b)).

Figure 4.15 (c) shows the concentration difference with number of cycles between 0.6 and 0.8 for Nafion 115 membrane. It is understood that difference in diffusion increases up to 77 cycles then decreases as the number of charging/discharging cycles increases. Also, it is observed that for current diffusion coefficient values of Nafion 115 membrane the diffusion trend is not linear compared to the other membranes (Selemion AMV membrane and Selemion CMV membrane). The

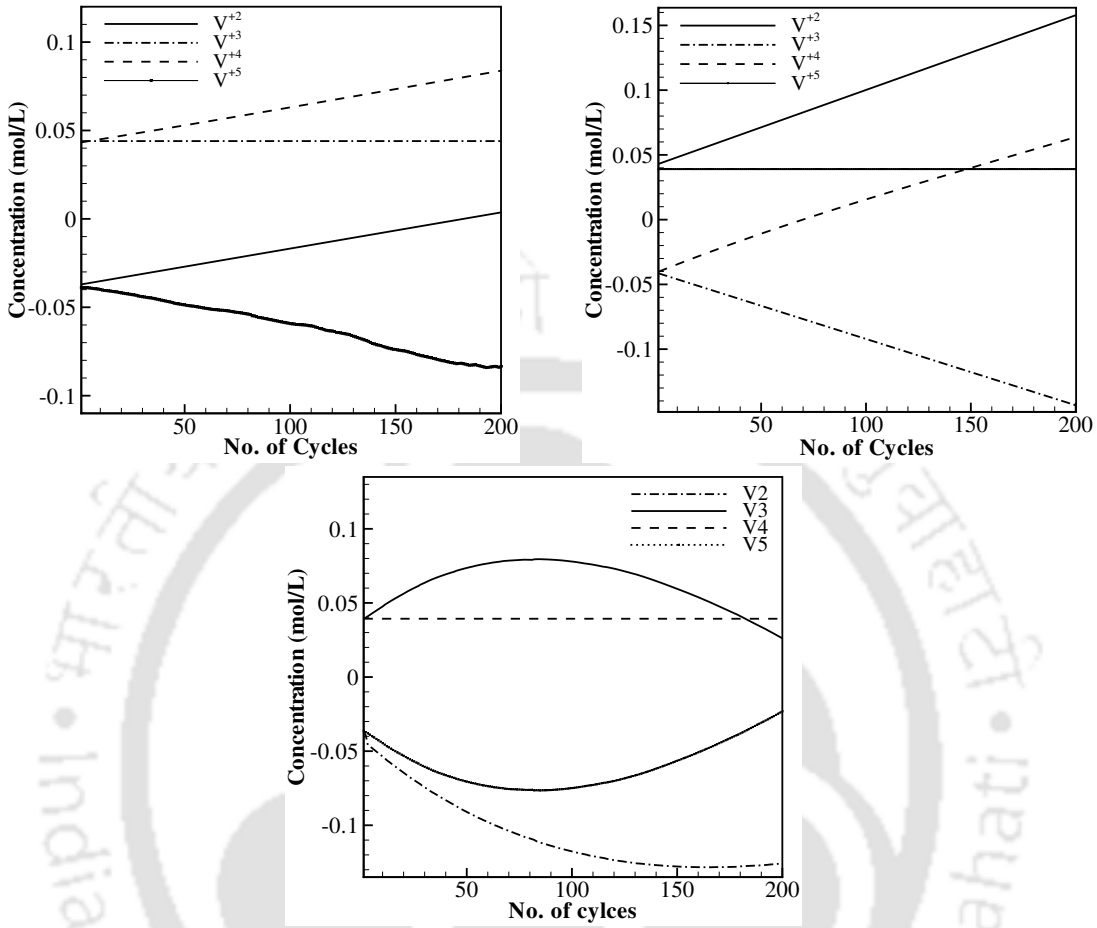

Figure 4.15: Difference in diffusion trend due to porosity at 1.7 V (a) for Selemion AMV membrane (b) for Selemion CMV membrane (c) for Nafion 115 membrane.

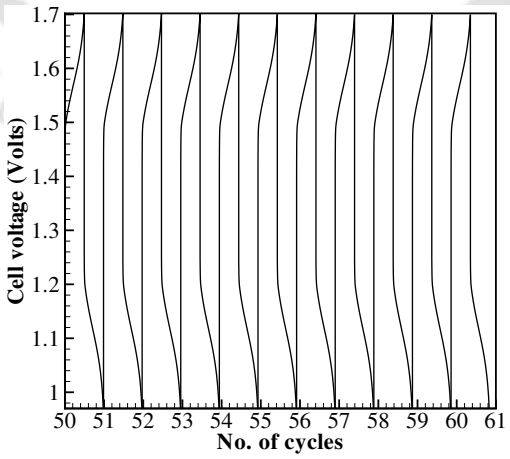

Figure 4.16: Cell potential difference plot for different cycles for Nafion 115 membrane for 11 cycles.

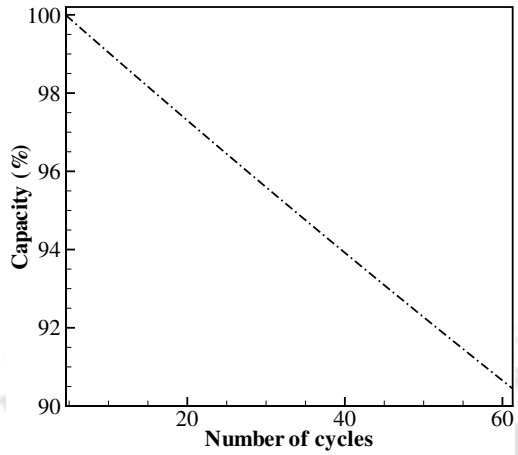

Figure 4.17: Capacity versus number of cycles for Nafion 115 membrane for 60 cycles. The flow rate and current density were set to 1 mL/s and 1000 A/m^2 respectively.

cell voltage variation for 11 cycles (starting from 50 to 61) is shown in Fig. 4.16 for Nafion 115 membrane. It is understood that capacity of the cell decreases with charging/discharging cycles due to the effect of vanadium ions crossover through the membrane. Figure 4.17 shows the capacity loss of the cell variation with number of cycles for Nafion 115 membrane. It is observed that the capacity of the cell linearly decreases to 90.5% after 60 cycles. The capacity decay is mainly due to the effect of crossover of vanadium ions through the membrane.

4.5 Closure

A lumped dynamic model based on the approaches established by Shah et al. [27] has been implemented to predict the effects of flow rate, applied current density, concentration, porosity temperature on the performance of an all-vanadium redox flow battery. The cell performance can be increased by increasing the concentration of the vanadium ions, the flow rate and the temperature inside the cell. The model results are validated with the available experimental results which show better agreement.

Also model is considered the effects of crossover of vanadium ions through membrane and mass transfer. The model is predicting the capacity loss for different membrane materials. The simulation results show that reaction rate constants diffusion coefficients are depending on temperature which affects on the cell performance. The

results show that for Selemion AMV and Selemion CMV membranes capacity loss increses linearly at different temperatures and porosity with increase in number of cycles. In the case of Nafion 115 membrane the capacity decay increases up to 77 cycles then it is stabilized.

Chapter 5

A Thermal Modeling and Simulation of the All-Vanadium Redox Flow Battery

5.1 Introduction

With the development of non-conventional energy technologies, it reduces the usage of conventional energy in electrical energy production and it also leads to reduction in greenhouse gas emission. The energy storage system is the alternative solution to overcome this disadvantage [1, 9]. Redox flow batteries are the better option due to many interesting features such as, they are inexpensive, high reliability, long life, low maintenance costs and low operation costs [1]. Therefore, there is a need to optimize the battery performance at lesser cost. The all-vanadium redox flow battery is most developed compared to other redox flow batteries. The all-vanadium redox flow batteries are initially proposed and commercialized by Skyllas-Kazacos and Co-researchers in 1980s [15, 55, 56, 72, 73]. The surrounding temperature which is different in different places, will vary between -5 to 45$^{\circ}C$. If the temperature goes below 5$^{\circ}C$ precipitation of V^{2+}/V^{3+} in the negative electrolyte occurs. Similarly, if the temperature goes above 40$^{\circ}C$ thermal precipitation of V^{5+} takes place. If this precipitation phenomenon is not controlled, there could be blockage in electrolyte channels and it may lead to reduction in battery performance. Therefore, the tem-

perature of battery is a most important parameter need to be accounted for the efficient and safe operation of the VRFB. Shah and Co-researchers [47] developed a temperature dependent numerical model to predict the cell temperature under different operating conditions. Tang et al. [46] developed thermal model for VRFB based on energy equation which is able to predict the stack and reservoir temperature with time.

The objective of this study is to develop a lumped thermal model based on the law of conservation of energy and to employ the model to determine the VRFB temperature variation with time and surrounding air temperature. The present model also includes the internal resistance, pump power loss and chemical power loss. By incorporating these losses into the model, it can predict the results of temperature variation with time accurately. Tang et al. [46] model did not considered the pump power loss and chemical power loss. This model is providing more detailed information of the electrolyte temperature in the reservoir and stack temperature which is usable in the design of VRFBs for the installation in different locations of the world. Also thermal model for dynamic conditions is more useful in the advanced model development based battery temperature controller to ensure safe, efficient operation of the cell within operational limits.

5.2 Problem Description

VRFB includes four major components as shown in Fig. 5.1: i) two porous electrodes that act as active sites for redox reactions, ii) two current collectors iii) liquid electrolytes that include different vanadium ions dissolved in sulphuric acid solution, and iv) a proton exchange membrane that prevent the diffusion of the vanadium ions from both the positive and the negative half-cells. External reservoirs are connected to porous electrodes through pipe to continuous supply of the electrolyte using the pump. The dimensions shown in the figure are given in Appendix B. Figure 5.1 also shows heat flow diagram showing heat sources, sinks. The reactions taking place in the porous electrodes lead to heat generation. And heat is rejected to the surroundings from the external reservoirs. The temperature of the stack and the reservoir is studied for two cases,

1. Maintain surrounding air at constant temperature.
2. Vary the surrounding air temperature with time.

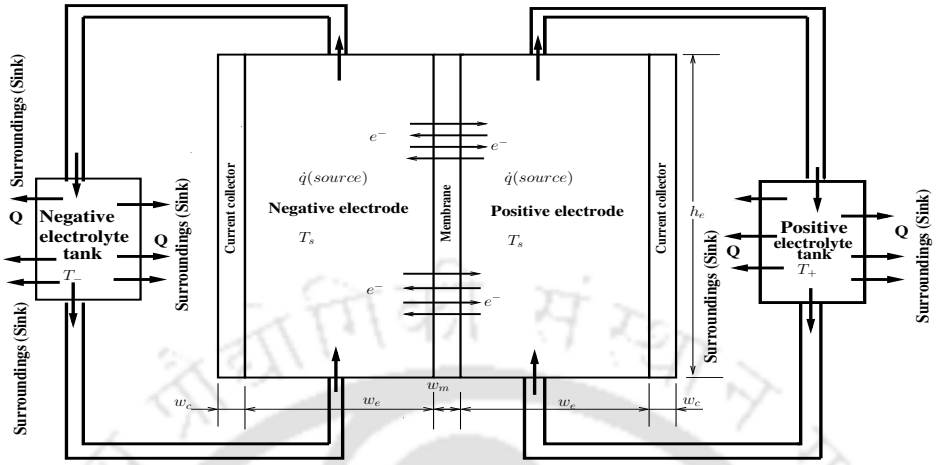

Figure 5.1: Schematic of the VRFB system, includes heat flow diagram indicating heat sources, sinks and heat transfer to the surroundings.

5.2.1 Parameters

A VRFB system consists of 19 cells are used in the simulation. The size of the individual cells are assumed to be same. The external reservoir tank with the shape of cylinder has a volume of 200 L. Both external reservoirs have the same dimensions and the outlet flow rates of the both reservoirs are assumed to be equal. The default parameters used in the simulation are summarized in Table B.13 and other details are specified below.

The prepared electrolyte solution contains 4.4 M sulfate which encompasses 2 M Vanadium. The electrolyte density was taken as 1354 kg/m^3, the specific heat of the electrolyte was taken to be that of 4.4 M sulfate. The battery cells are made up of polyethylene low-density material. The electrode area and membrane area are taken as 1500 cm^2 each. The average cell area resistances are taken as 2.9 Ωcm^2 for charging and 3.13 Ωcm^2 for discharging. From the Faradays law of electrolysis, it is assumed that the flow rates of all the half cells are equal with a value of twice the maximum theoretical flow rate, which is given by,

$$Q = \frac{2 \times I}{F \times z \times SOC \times c} \tag{5.1}$$

where I is the maximum applied current during charge-discharge cycle. In this model, the tanks and battery stack are assumed to be fully filled with the respective electrolyte solutions and there are no ion diffusion and side reactions taking place

during operation. From Faradays law of electrolysis the charging and discharging times are investigated from the equations given below.
The charging time is given by,

$$t_c = \frac{c \times V_s \times z \times F}{I_c \times eff} \tag{5.2}$$

The discharging time is given by,

$$t_d = \frac{eff \times c \times V_s \times z \times F}{I_d} \tag{5.3}$$

In reality, the charging time is much higher than the theoretical value from calculation but the discharging time is shorter due to the side reactions.
Two cylindrical external tanks are made up of polypropylene material. It is assumed that tank is exposed to outside air and therefore free convection from both inner and outer isothermal surfaces takes place. So heat transfer occurs by two convection resistances and one conduction resistance. The heat transfer by conduction can be calculated by Fouriers law based on the conductivity of polypropylene material, while the heat transfer by convection is determined by Newtons law of cooling. In the present simulation, the convective heat transfer coefficients for the air side are taken to be 3.5 W/m^2K (cylinder wall) and 5.3 W/m^2K (top and bottom plate) respectively . The procedure and equations to determine convective heat transfer coefficients are taken from Tang et al. [46] paper. After the calculation the electrolyte side heat transfer coefficients are taken as 270.1 W/m^2K (cylinder wall) and 405.2 W/m^2K (top and bottom plate). The overall heat transfer coefficient for the cylindrical tank can be divided into two parts which can be calculated as given below.
The overall heat transfer coefficient for the cylindrical wall of the tank based on the inside area is,

$$U_1 = \frac{1}{(1/h_{11}) + (r/k)ln(r + \theta/r) + (r/r + \theta)(1/h_{21})} \tag{5.4}$$

The overall heat transfer coefficient for the bottom or top circular wall of the tank is,

$$U_2 = \frac{1}{(1/h_{12}) + (\theta/k) + (1/h_{22})} \tag{5.5}$$

where A_1 $(2 \times \pi \times r \times H)$ is the inside area of the cylindrical wall and A_2 $(\pi \times r^2)$ is the area of the bottom or top circular wall.
The overall heat transfer across the cylindrical external tank can be calculated by,

$$UA = U_1 A_1 + 2U_2 A_2 \tag{5.6}$$

5.3 Results and Discussion

The governing equations discussed in Section 3.8 of Chapter 3 are solved using Matlab. The value of default parameters used in the simulations is given in Table B.13 of Appendix B. The full detail of the calculation of convective heat transfer coefficients are shown in Appendix C. The temporal variation of battery temperature was simulated under different air temperatures and charging and discharging currents. The charging and discharging time was calculated by Eqs. 5.2 and 5.3. In the present calculations it was assumed that the battery always started charging from maximum temperature i.e. highest temperature reached of the day, therefore the initial temperature of the electrolyte in both the tanks and the stack were equal to the maximum air temperature. The calculation of the temperature variation inside the battery stack can give detailed information of the battery operating status under varied operating conditions which are more useful in the optimizing battery temperature control for different locations of the world.

5.3.0.1 Case 1: maintain surrounding air temperature constant

Initially the present simulation result of battery stack temperature variation with time is validated with the numerical results of Tang et al. [46] as shown in Fig. 5.2 and it shows good agreement with literature. Figures 5.2-5.4 show the variation of battery stack and tank temperatures for the VRFB with three sets of charging and discharging currents. From Fig. 5.2 it is observed that at temperature reaches steady state and oscillates at $26.4°C$. Also it is indicating that stack and tank temperatures decrease during charge while increasing during discharge process after steady state reached. This is due to the very small cell resistance during the discharge process that results from the faster reaction kinetics of the V(V) reduction process compared with the V(IV) to V(V) oxidation reaction. This results in heat generation by the stack resistances. This heat generation phenomena can be observe in Fig. 5.3, where

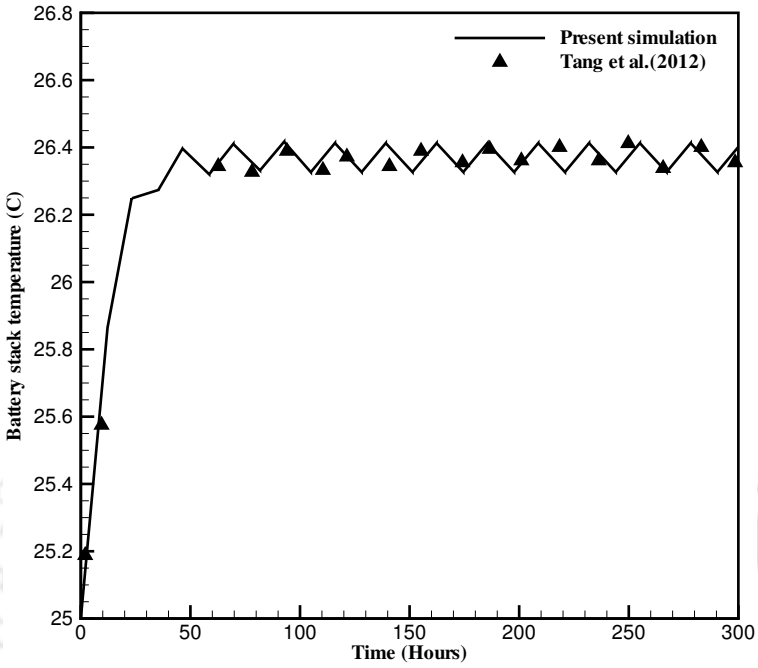

Figure 5.2: Comparison of present simulation result with literature result of battery stack temperature variation for validation. The charging and discharging current were set to 30 A and air temperature was 25°C.

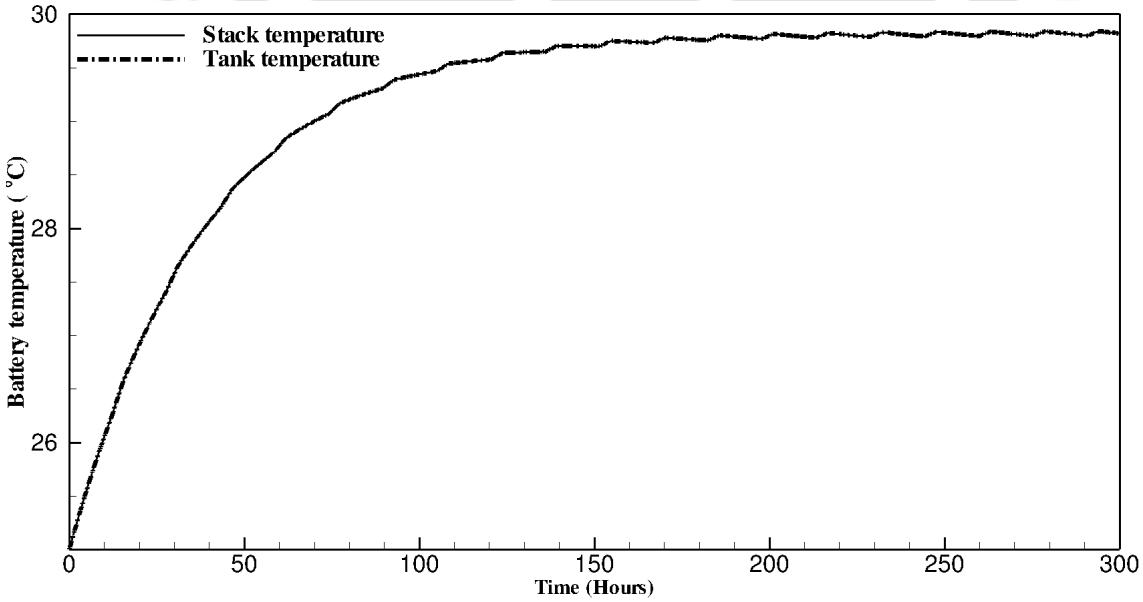

Figure 5.3: Variation of battery temperature with charging current 30 A and discharging current 100 A under a constant air temperature of 25°C. Flow rate was set to be 246.2 cm^3/s.

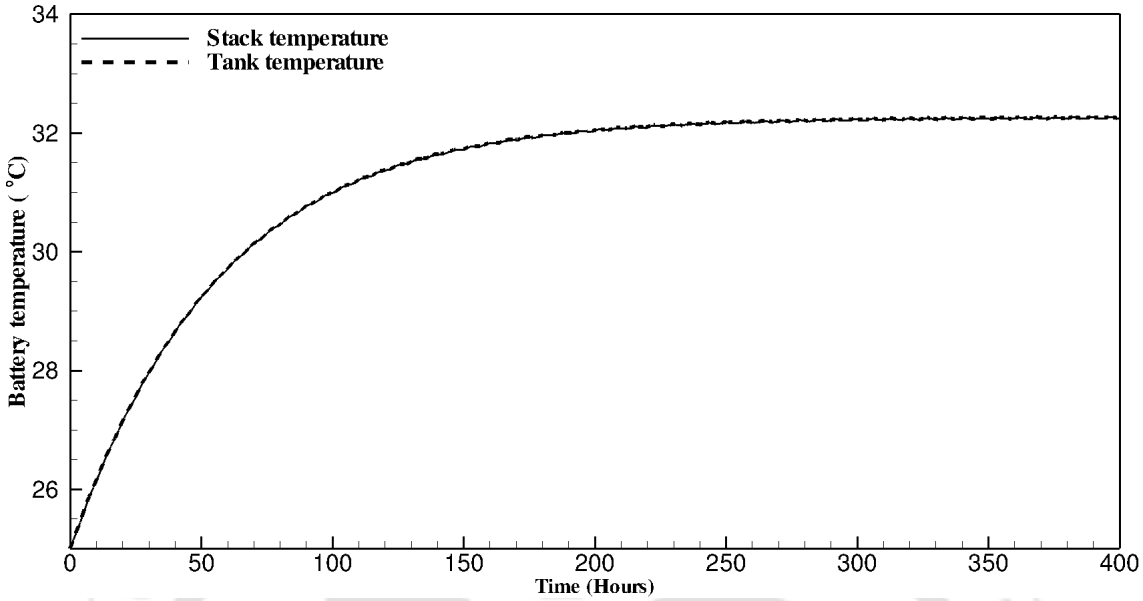

Figure 5.4: Simulated battery temperature variation with 100 A charging and discharging current under a constant air temperature of 25°C. Flow rate was set to be 246.2 cm^3/s.

a discharging current 100 A was used which leads to increase in heat generation rate between charging and discharging process. Also it is noted that stack temperature is always higher than the tank temperature due to the assumption of no heat transfer from stack to the surrounding air. Figure 5.4 shows the battery stack and tank temperature variation in the case of 100 A charging and discharging current. Due to increase in charging current both the stack and tank temperature reach 32°C. Also it is observed from the simulation results that the variation of fluctuation of the battery temperature during chargedischarge cycling is very small and can not see in Fig. 5.4 as in Fig. 5.2, this is due to magnitude of heat generation does not vary from the stack resistances.

5.3.1 Case 2: varying surrounding air temperature

There are three sets of air temperature profiles used in the simulation which representing a hot climate, a warm climate and a cold climate to determine the battery stack temperature under different climatic conditions. Further, the surrounding atmospheric air temperature was assumed to have the form of sine-squared function

which is given by,

$$T_{air} = B \cdot sin^2(\omega t + \phi) + C \tag{5.7}$$

Where,

$B + C$ = maximum temperature

C = minimum temperature

ω =angular frequency rad/s

ϕ = phase, rad

t = time, s

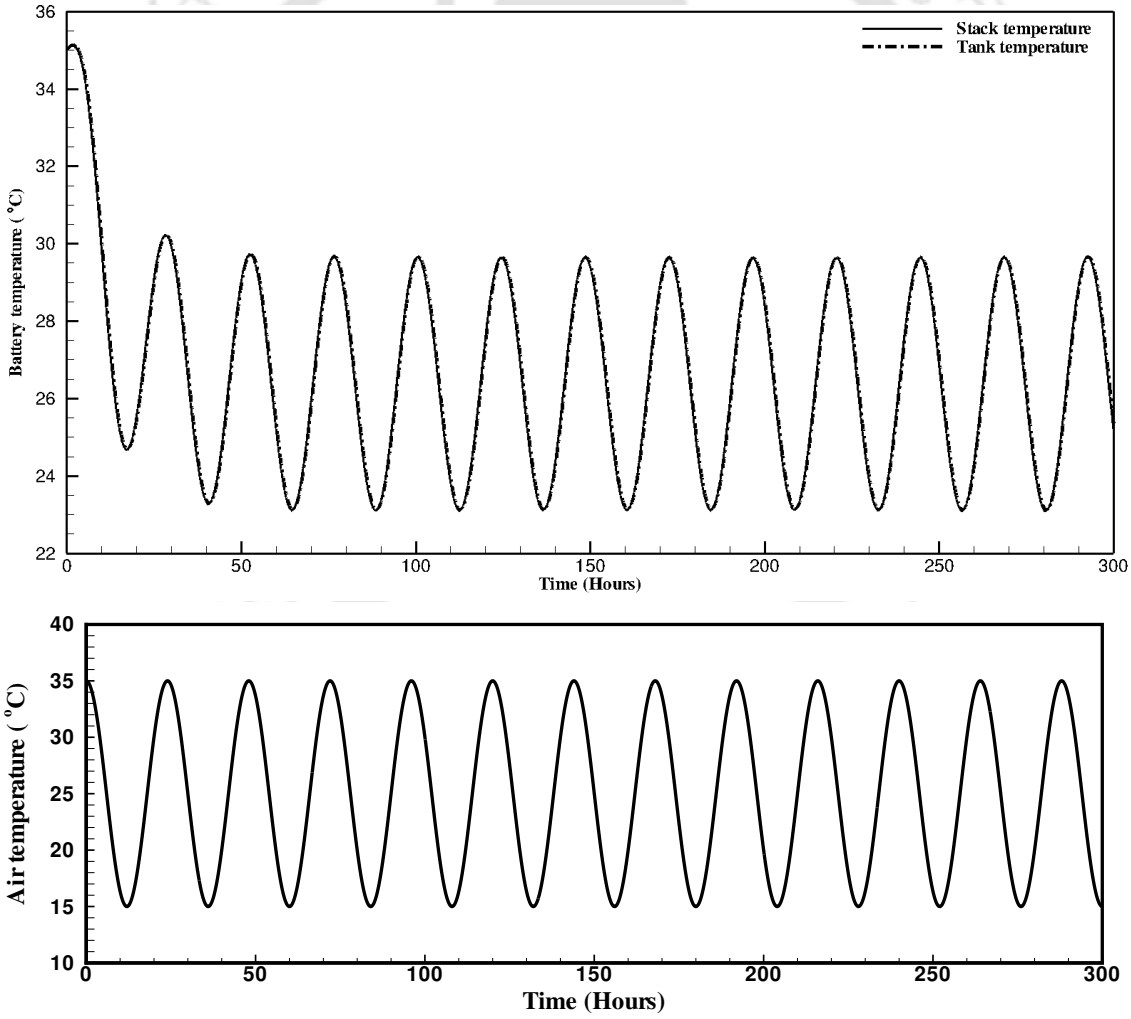

Figure 5.5: Simulated battery temperature variation with 30 A charging and discharging currents under a varying air temperature range from $15°C$ to $35°C$.

5.3.1.1 Summer (medium temperature) climate scenario

Simulation of temperature for summer conditions, a daily temperature ranging from $15°C$ to $35°C$ was used in the thermal model based on Eq. (5.7). The charging and discharging current of 30 A is used in the simulation, initially temperature of the battery decreases and finally fluctuates around the point of equilibrium of $24°C$ with the same air temperature frequency . Due to relatively small applied current, lesser the heat generation is produced from the stack resistance which makes little variation of battery temperature compared with the surrounding air temperature as shown in Fig. 5.5. If the discharge current is increased to 100 A, it is observed

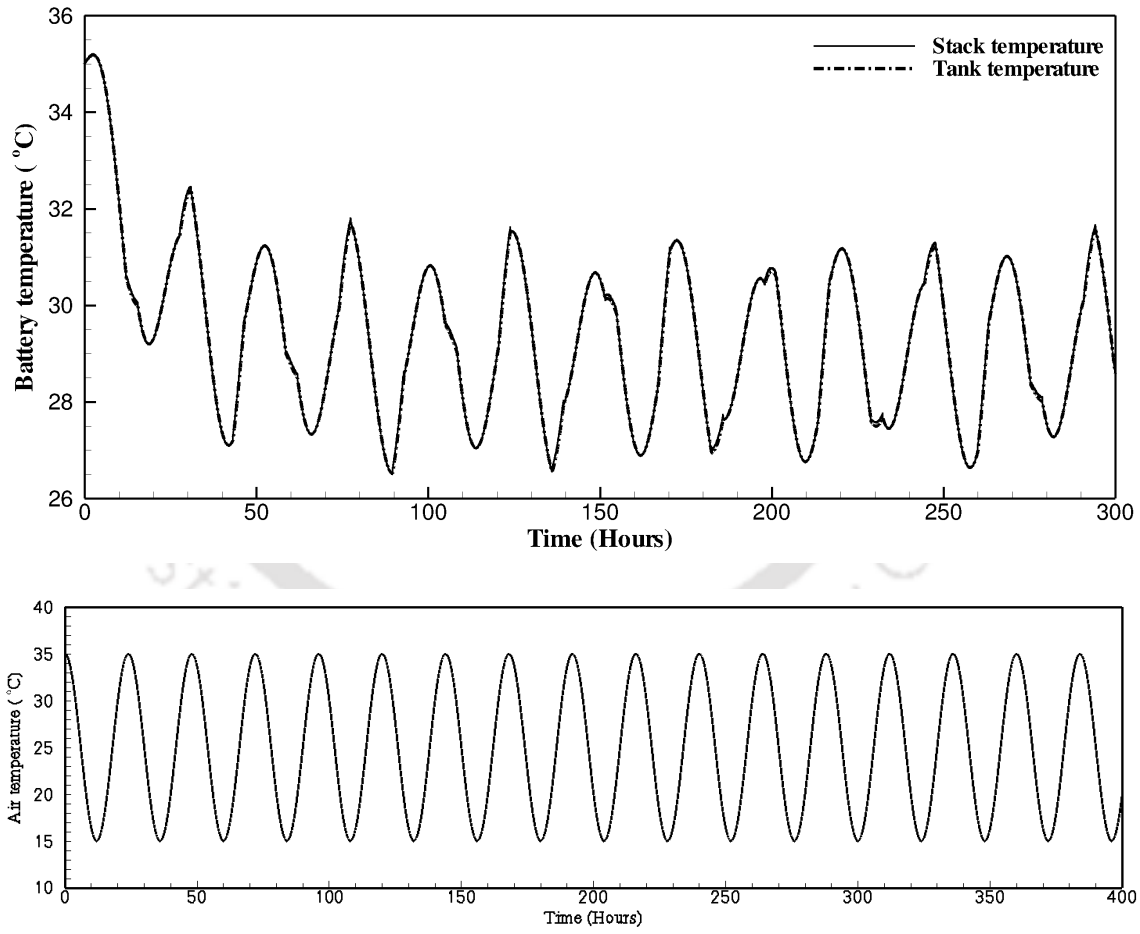

Figure 5.6: Simulated battery temperature variation with charging current 30 A and discharging current 100 A under a varying air temperature range from $15°C$ to $35°C$. Flow rate was set to be 246.2 cm^3/s.

that irregular fluctuation in the temperature of both tanks and stack shown in

Fig. 5.6, where the average of the electrolyte temperature temperature $29°C$. In both the cases the electrolyte temperature is above $5°C$ and below $40°C$. There is no precipitation to be expected to takes place during this operating condition. Also it is noted that temperature of the battery generally follow the air temperature with a large heat transfer capability by tanks, instead it is effected at chargedischarge points, by the heat difference between charge and discharge. If the charging current increased to 100 A, it is observed that from Fig. 5.7 the heat transfer increased from charging which is the driving force to increase the electrolyte temperature to $41.8°C$, thereby allowing the battery into the thermal precipitation region for the positive electrolyte solution. Also is noted that battery temperature also varies sinusoidally

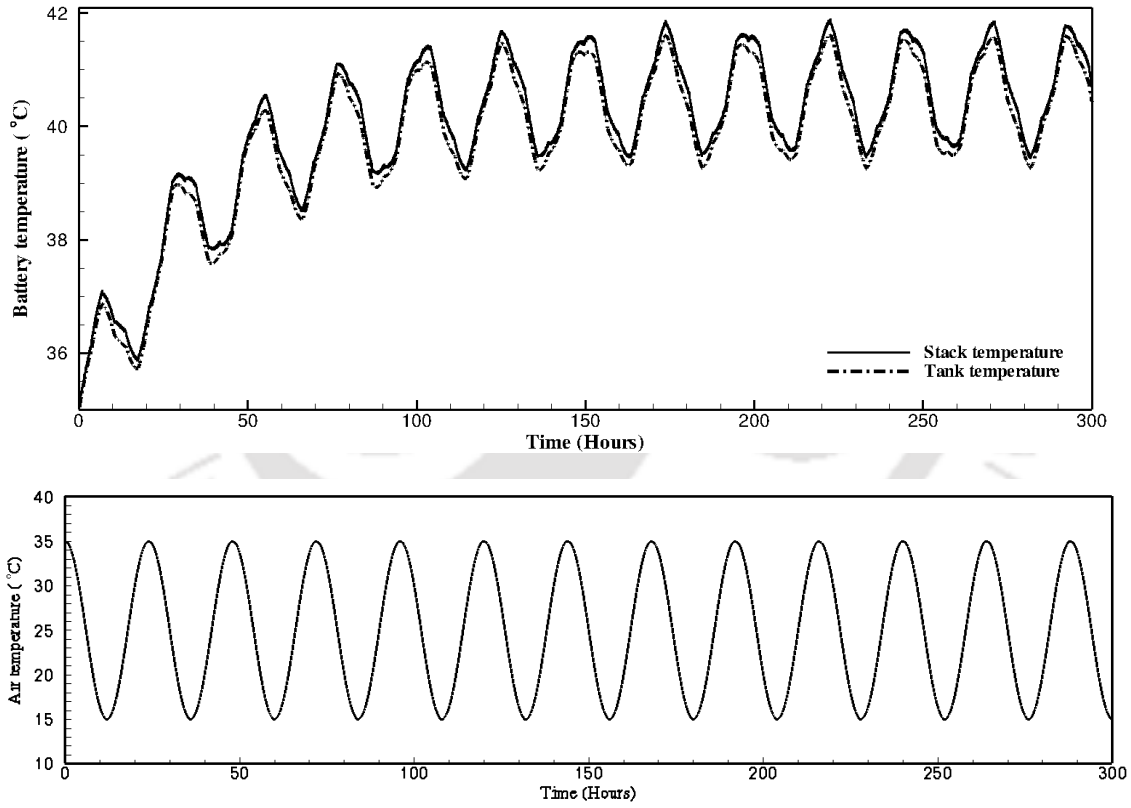

Figure 5.7: Variation of battery temperature with both 100 A charging current and discharging currents under a varying air temperature range from $15°C$ to $35°C$. Flow rate was set to be 246.2 cm^3/s.

shown in Fig. 5.7, this being attributed to small discrepancy in the heat generated between charge and discharge. Generally, the smaller difference in heat generation during charge and discharge, more closer the prediction of the battery temperature

with the surrounding air temperature. From Figures 5.5-5.7 it is understood that surrounding daily air temperature has high effect on the battery temperature, which interact and determine the final steady state temperature of the electrolyte tanks and battery stack.

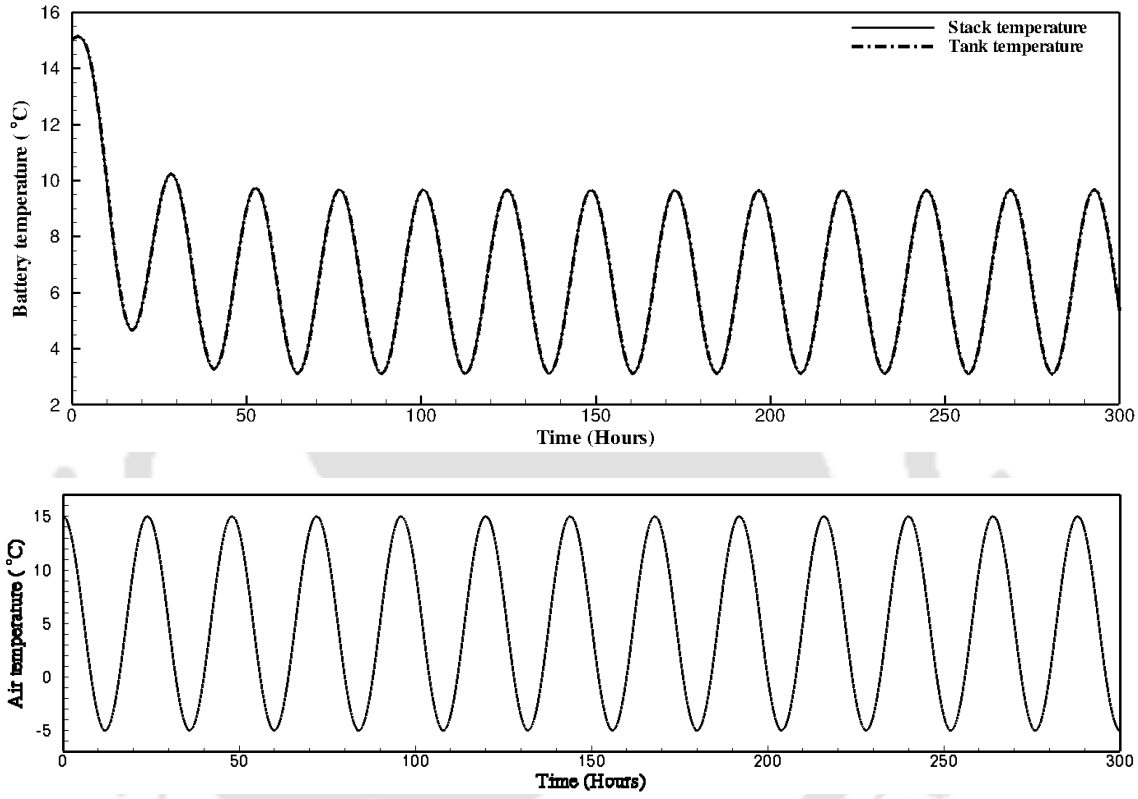

Figure 5.8: Battery temperature variation with both 30 A charging current and discharging currents under a varying air temperature range from $-5°C$ to $15°C$. Flow rate was set to be 246.2 cm^3/s.

5.3.1.2 Winter climate scenario

To simulate a winter climate temperature profile, a daily surrounding air temperature of $-5°C$ to $15°C$ was employed. Both charging and discharging current were set to be 30 A. Figure 5.8 shows the stack and electrolyte tank temperature variation, and same trend is observed as seen in Figs. 5.6 and 5.7. The difference is overall $20°C$ shift in the temperature. The frequencies of air and heat are same therefore variation of battery temperature will shift up or down depending on the air temperature range. It is seen from Fig.5.8 stack temperature would drop below $4°C$

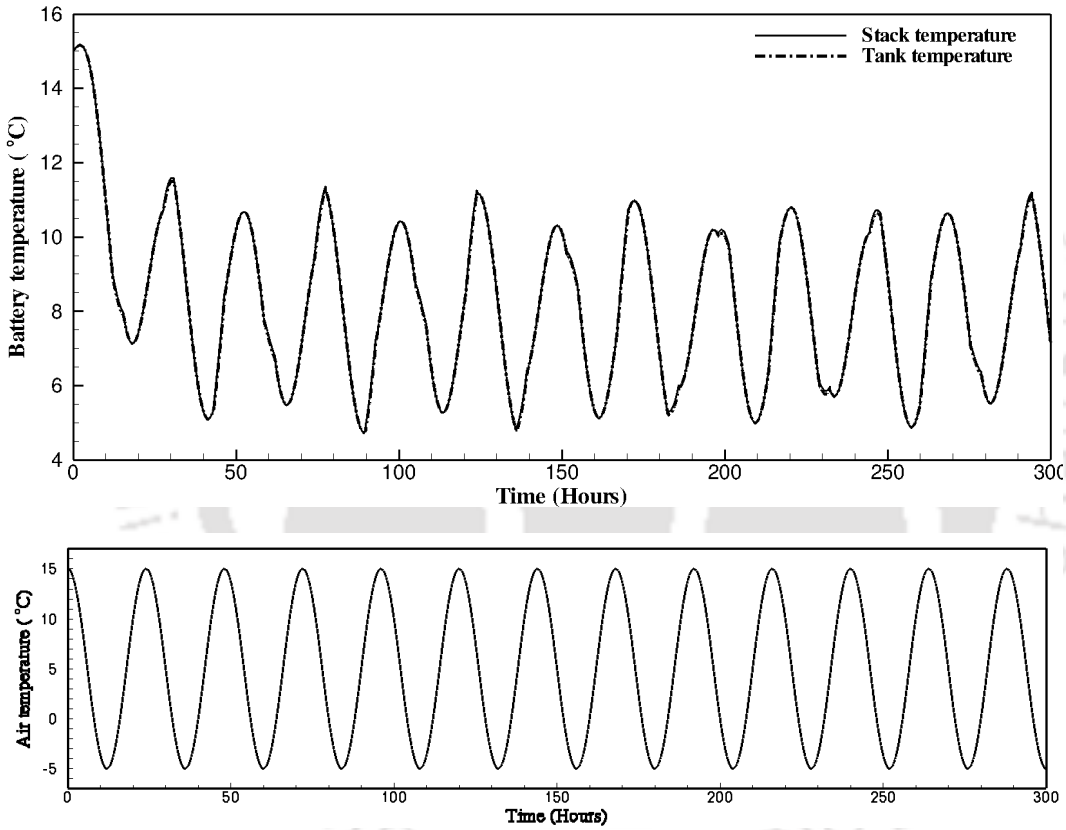

Figure 5.9: Simulated battery temperature variation with charging current 30 A and discharging current 100 A under a varying air temperature range from $-5°C$ to $15°C$. Flow rate was set to be 246.2 cm^3/s.

for the case of 30 A charging and discharging currents. In this case vanadium ions precipitation taking place in the negative electrolyte were allowed to stand at near either 0% or 100% state of charge at the low temperatures. If the discharging current is increased to 100 A, it allows the temperature of the battery to be maintained above $5°C$ at all times shown in Fig. 5.9. The heat energy plays a very important role and it increases due to excessive drop in electrolyte temperature. Therefore, it leads to precipitation of V^{2+}/V^{3+} . Due to precipitation, electrolyte will become supersaturated in either the V^{2+} or V^{3+} ions. It is observed that at intermediate states of charge, both ions would be present at concentrations significantly below their saturation level, therefore precipitation would not be predicted.

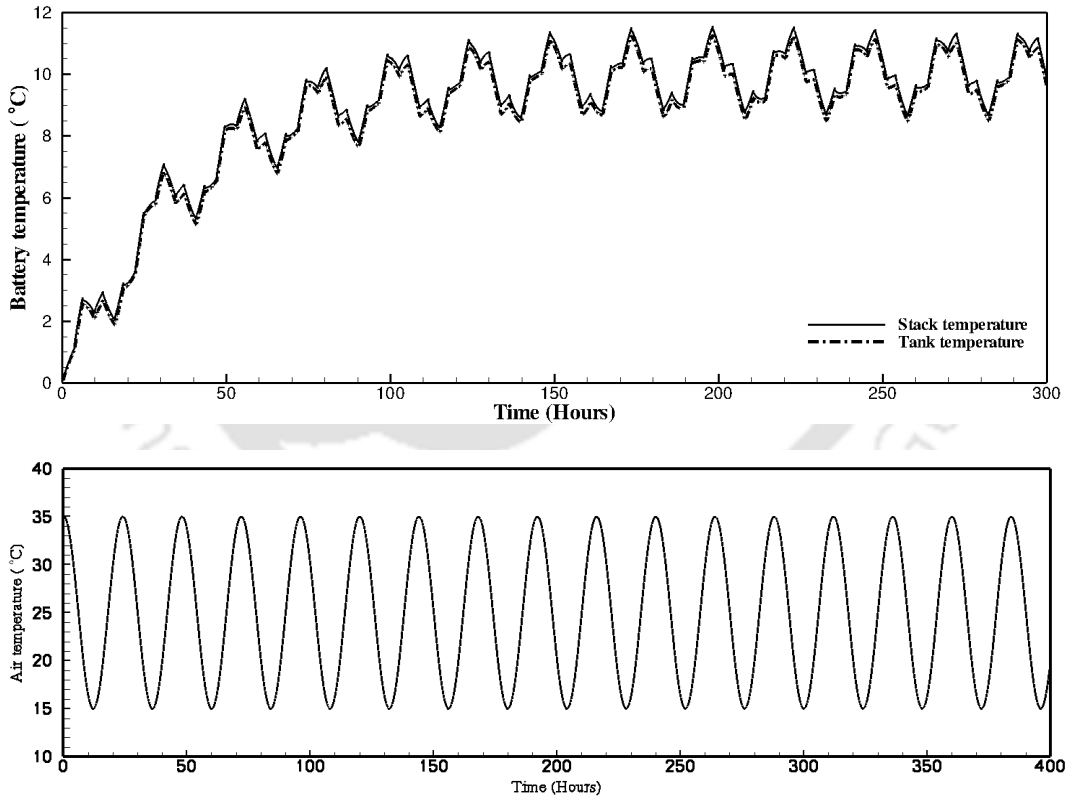

Figure 5.10: Simulated battery temperature variation with charging current 100 A and discharging current 130 A under a varying air temperature range from $-20°C$ to $0°C$. Flow rate was set to be 320 cm^3/s.

5.3.1.3 Cold winter climate scenario

To determine the VRFB temperature variation during a general winter scenario in a cold climate, a daily surrounding air temperature range of $-20°C$ to $0°C$ was used in the simulation. From previous case results it is understood that the temperature of electrolyte is not able to exceed the maximum temperature of $0°C$ with charging current of 30 A and 100 A or even smaller values of current. Therefore, charging current of 100 A and discharge current of 130 A are used in this case as shown in Fig. 5.10. From the Fig. 5.10 it is observed that the stack temperature could be increased above $5°C$ after approximately 23 h during charging/discharging cycling, oscillation around $9°C$ therefore the influence of precipitation of V^{2+}/V^{3+} could be eliminated. In reality it is not desirable to store or prepare the electrolyte in the fully charged or discharged state at such a low temperature which results in loss of the capacity of the VRFB. Therefore, under cold climate conditions it is necessary that the electrolyte temperature can be maintained using heating devices, to overcome the problem of precipitation.

5.4 Closure

A thermal model for the VRFB has developed based on energy conservation to determine the battery temperature with time under different operating temperature conditions. Simulation results shown that the stack and electrolyte tank temperature at both constant and varying air temperatures is able to predict the oscillations of the battery temperature with different charge and discharge currents. From the results it is understood that increasing the current or decreasing the flow rate will increase the stack and electrolyte in the tank temperature. This model can be used as a thermal control system which is useful to control the electrolyte temperature in the optimal range for different climate scenario.

Chapter 6

2D Unsteady Numerical Modelling and Efficiencies Analysis of All-Vanadium Redox Flow Battery

6.1 Introduction

Flow batteries have been highly influenced from industry and academia due to their more flexibility in upgrade and more economical related with scale-up. Flow batteries are used as electrical energy storage systems in associated with non conventional energy sources such as wind and solar energy. There are many challenges to be overcome for the commercial applications of the vanadium redox flow battery such as, optimization and scale-up which involves flow geometries assemblage and operation conditions. Modeling and simulation are most economical methods for solving these problems, which can minimize the time and costs associated with laboratory based experiments. The whole detailed information into the fundamental processes inside the vanadium redox flow battery can be attained by modeling and simulation, which is more useful for optimizing the design and operating condition.

In this chapter we study a two dimensional, isothermal, dynamic model based on the conservation laws which include the fundamental modes of transport and kinetic model for reactions involving the vanadium species to predict the performance of the cell. The processes in the redox flow batteries are described by the equations of

electrodynamics, electrochemistry, fluid mechanics and heat transfer. The diffusion of ions through the membrane and electrolyte flow across the porous electrodes can be modeled by the conservation laws of mass, momentum. By solving the Poisson equations, the distribution of electric potential in redox flow batteries can be calculated. The electrochemical interaction of species in the cell is obtained by the Nernst equation and Butler Volmer law. Combination of these processes makes the solution of equations more complicated. Shah et al. [29] developed comprehensive distributed numerical model, based on two-dimensional isothermal conditions, which is able to capture time dependent and spatial distributions of electrolyte concentrations, current density, overpotential in the porous electrodes. This model had been further enhanced by taking into consideration effects of temperature variation inside the cell [47]. Same model is further modified by considering the effects of oxygen and hydrogen [64, 63] evolution side reactions. Based on Shah et al.[29] model, two-dimensional steady state model had been studied [13]. Above distributed models have not considered the ohmic losses associated with electrolyte, membrane, current collector. In this chapter concentration overpotential and ohmic drop are included into the numerical model. However, the prediction of cell potential may not be accurate without considering ohmic drop and concentration overpotential between the half cells.

As per the literature review till date, coulombic, voltage and energy efficiency analysis by considering concentration overpotential and ohmic losses have not been attempted till now and the effects of change in concentration, electrolyte flow rate, electrode porosity and applied current are studied. Including these models, it helps in accurately predicting the performance of the VRFB.

6.2 Problem Definition

The geometry considered in this study is shown in Fig. 6.1. The main components of the battery are electrodes, membrane, current collectors and reservoirs. The model is based on the fundamental laws of mass, momentum, charge conservation, along with a kinetic model for reaction involving soluble vanadium species. The model also incorporates concentration overpotential and ohmic losses for the all-vanadium redox flow battery. The structural dimensions of the VRFB cell has taken as, 8 $cm \times 8\ cm \times 4\ mm$. Referring to Fig. 6.2(a), the line $x1$ denotes the

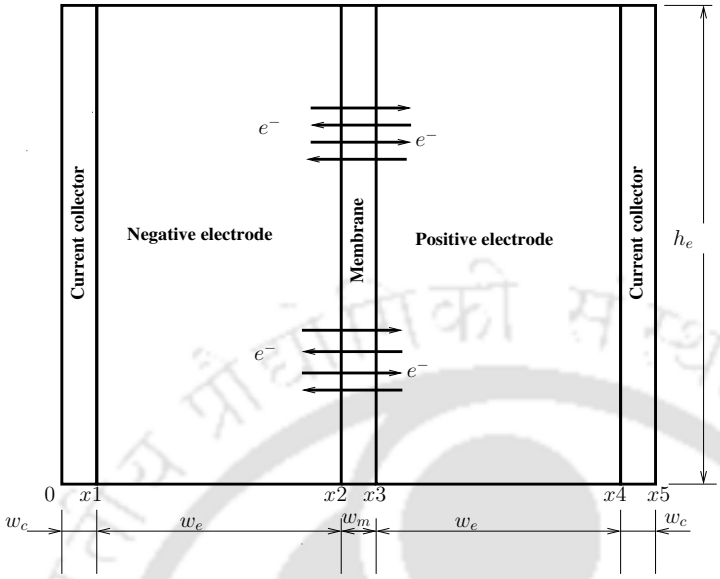

Figure 6.1: Schematic of the all-vanadium redox flow battery showing the components, porous electrodes, membrane, current collectors and reservoirs.

current electrode/current-collector interface and $x2 = 0.004\ m$ denotes the membrane/electrode interface. The dimensions in x and y direction denotes in meters. Due to reduction and oxidation reactions in the cell, the variation in concentration of vanadium species is taking place, therefore the performance of the cell changes. The assumptions considered during modeling are,

1. The dilute solution approximation is used for simplification and the flow is considered as laminar and incompressible.
2. The transport of the charged species takes place by convection and diffusion and migration terms are neglected for simplification.
3. Physical properties of electrode and membrane are homogeneous and isotropic.
4. There is no diffusion of vanadium species through the membrane because there is no leakage of reactant or charge through the external surfaces of the cell.

The performance of the cell is studied for two cases,

i) Without considering the losses in the model: Effects of concentration, electrolyte flow rate, electrode porosity and applied current density.

ii) Considering the losses in the model: Effects of electrolyte flow rate, concentration, electrode porosity and applied current density.

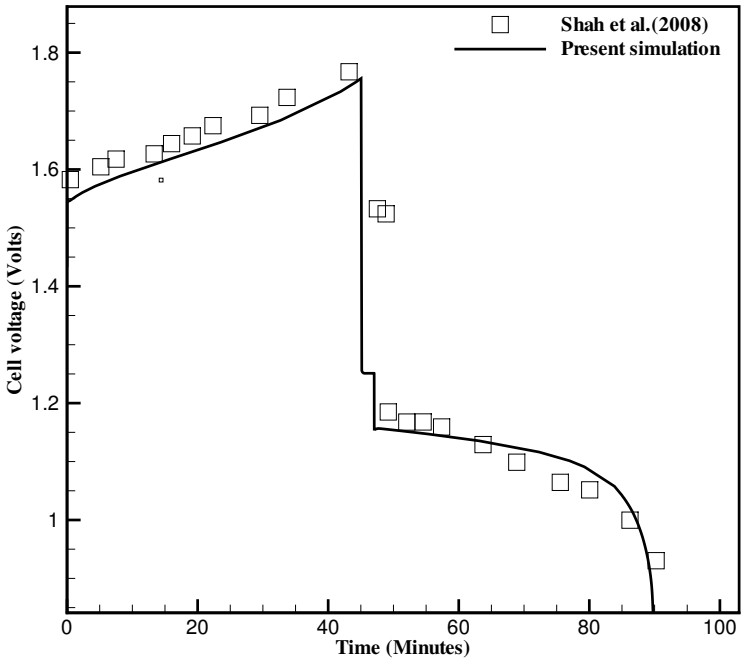

Figure 6.2: A comparison of simulated and experimental charge-discharge curves for $C_3^0 = 1440\ mol/m^3$, The other parameter values are given in Table B.5-B.7.

6.3 Numerical details

The present model is solved using commercial package COMSOL Multiphysics, which is a finite element method solver. The total number of elements in all the simulations is taken as 8874. The relative error or tolerance is set to 1×10^{-6}. The governing equations including initial and boundary conditions have been already discussed in Sections 3.9 to 3.14. The actual dimensions of the battery and other default parameters are given in Tables B.5-B.7 in appendix B.

6.4 Results and discussion

Figure 6.2 shows a comparison of the simulation result with the experimental result of Shah et al.[29] for validation. In this case concentration was $C_{III}^0 = C_{IV}^0 = 1440\ mol/m^3$, the model result shows good agreement with the experimental result. In this calculations, the charge time is approximately 2714 s, $T = 300\ K$, $C_3^0 = C_4^0 = 1080\ mol/m^3, \omega = 1\ mL/s$ and $j_{app} = 1000\ A/m^2$. The other parameter values are given in Table B.5-B.7.

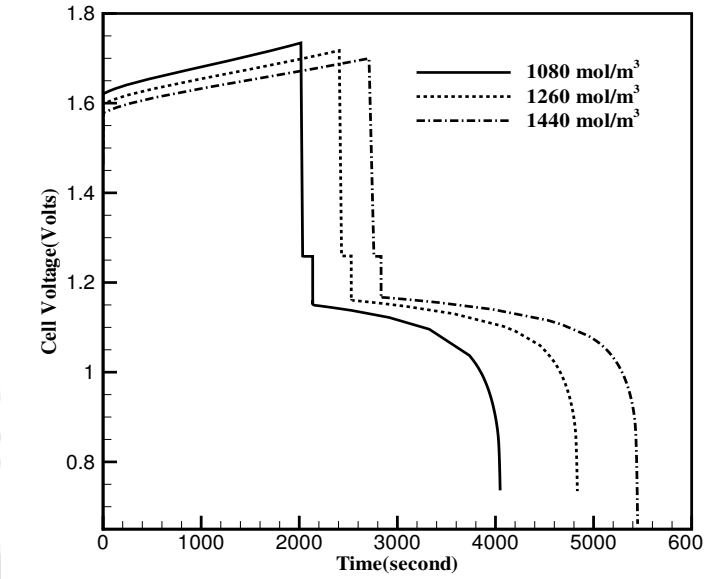

Figure 6.3: A comparison of simulated charge-discharge curves for $C_3^0 = 1080\ mol/m^3$, $C_3^0 = 1260\ mol/m^3$ and $C_3^0 = 1440\ mol/m^3$. The other parameter values are given in Table B.5-B.7

6.4.1 Concentration effects

Figure 6.3 shows cell voltage variations with time for three different concentrations, $C_{III}^0 = C_{IV}^0 = 1080\ mol/m^3$, $C_{III}^0 = C_{IV}^0 = 1260\ mol/m^3$ and $C_{III}^0 = C_{IV}^0 = 1440\ mol/m^3$. The results show an increased coulombic efficiency for increased concentration. In the calculations, the charge times are, approximately, 2010s, 2410s and 2703 s for the cases $C_{III}^0 = 1080\ mol/m^3$, $C_{III}^0 = C_{IV}^0 = 1260\ mol/m^3$ and $C_{III}^0 = 1440\ mol/m^3$, respectively. Faraday's law states that the concentration change in V(III) for a spatially homogeneous system of volume V_T, ΔC, is related to the time of charging, t_c, and the current, I, as follows where $1 - C/C_0$ is a normalized concentration change, related to an initial concentration C_0, and n is the number of moles. The time to reach a given SOC (or $1 - C/C_0$) for a given current and volume is therefore directly proportional to the initial concentration.

$$-\frac{It_c}{F} = \Delta n = V_T \Delta C = -V_T C_0 \left(1 - \frac{C}{C_0}\right) \tag{6.1}$$

If we use average concentration C_{av} as the concentration C in the above equation, the estimated concentration change in V(III) for the case $C^0_{III} = 1080\ mol/m^3$ is $\Delta n = It/F = 0.209\ mol$. The normalized concentration change is therefore $1 - C/C_0 = \Delta n/(V_T C_0) = 0.794$, which is exactly equal to the simulated value of 0.794. Moreover, the ratio of charge times for the two cases in Fig. 6.3 can be estimated as $1.44/1.08 = 1.33$, which is approximately equal to the value of $2703/2010 = 1.3447$ found by the calculations.

Figure 6.4 shows contour plots of the V(III) and V(IV) concentration at times while charge and discharge for the case $C^0_3 = 1440\ mol/m^3$. In these plots, the dimension in x-axis is shown from $x1$ to $x4$ as shown in Fig. 6.1. The inlet surface is denoted by the line $y = 0$ and the outlet by, $y = 8$ cm. While charging (Fig. 6.4(a)) the reduction of V(III) increases with the height above the inlet surface. The magnitude of variation of concentration in this direction is calculated by the rate at which the electrolyte is passed through the electrode through the pump, i.e. the electrolyte volumetric flow rate ω, and, as we predict, the highest concentration takes place along the inlet surface. Since minimum concentration V(III) lies at the intersection of the upper surface ($y = 0.08$ m) and the electrode/current-collector interface ($x1$). These effects are reflected in the V(II) concentration during discharge, the evolution of which can be deduced form the V(III) profiles shown on the bottom row. It is observed that similar trend in the positive electrode, where the minimum concentration of V(IV) takes place at the intersection of the outlet and current collector (during charge) shown in Fig. 6.4(a).

6.4.2 Effects of inlet flow rate

A vital parameter to control the operation of a VRFB is the electrolyte flow rate. If the electrolyte flow rate is too low, the electrolyte is not circulated uniformly therefore stagnant regions will be formed in the electrode. There is a risk of leakage leading to reduction in performance for the extra power required if the electrolyte flow rate is too high. Figure 6.5 shows the comparison of simulated results at three volumetric flow rates in the case of $C^0_{III} = 1080\ mol/m^3$. From the simulation result for $\omega = 3\ mL/s$, it is understood that the gain in coulombic efficiency decreases with increased flow rate therefore there is optimum flow rate in which the performance is maximum. Figure 6.6 shows contours of the V(III) and V(IV) concentration in the negative and positive electrode at the end of the discharge period at t = 2034 s for

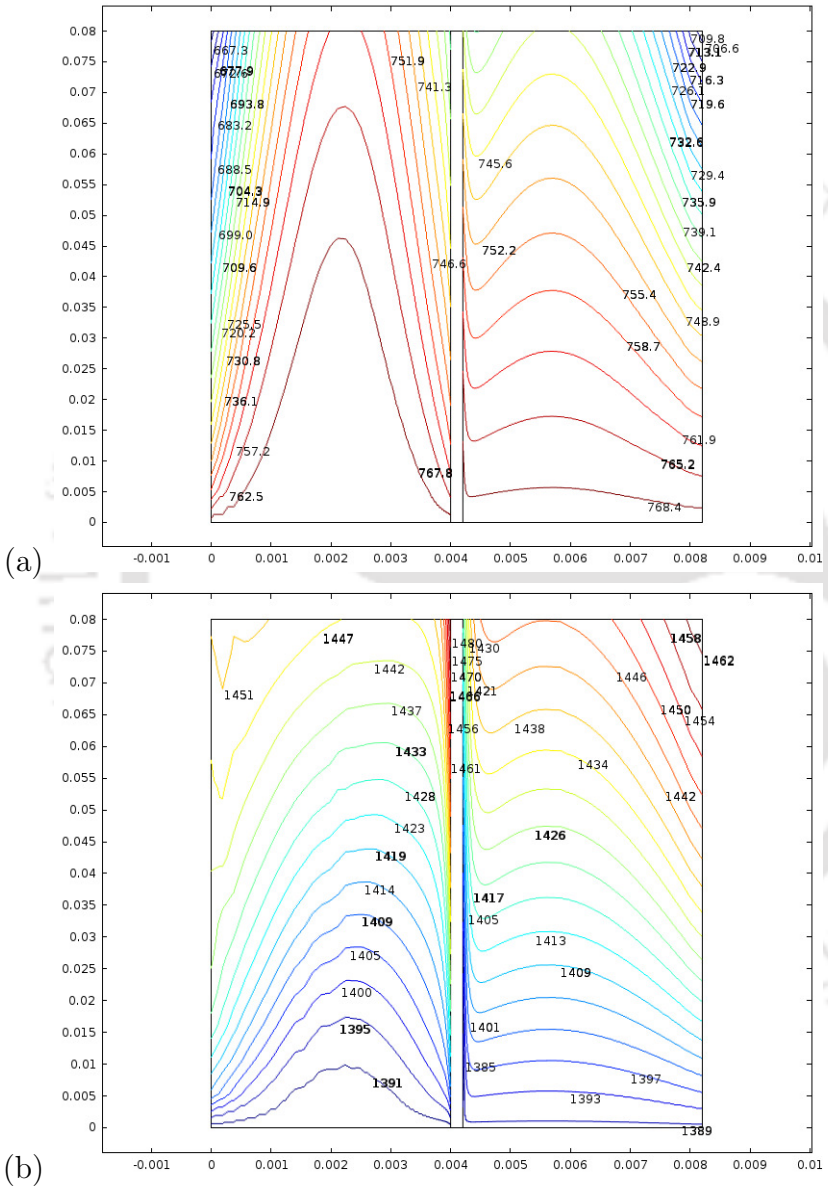

Figure 6.4: Contours of the V(III) and V(IV) concentration while charge (a) and during discharge (b) corresponding to the cycle $C_3^0 = 1440\ mol/m^3$ shown in Fig. 6.3.

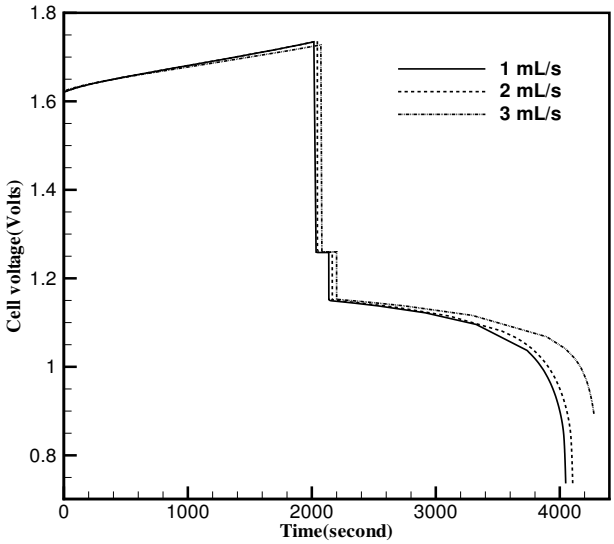

Figure 6.5: A comparison of simulated charge-discharge curves for three volumetric flow rates with initial concentration of $C_3^0 = 1080\ mol/m^3$. The charge times are *2010 s* for $\omega = 1\ mL/s$, 2034 *s*for $\omega = 2\ mL/s$ and 2058 *s* for $\omega = 3\ mL/s$. The other parameter values are given in Table B.5-B.7.

$\omega = 2\ mL/s$. If we compare concentration contour for $\omega = 1\ mL/s$ (Fig. 6.4) and $\omega = 2\ mL/s$ (Fig. 6.6), it is understood that the concentration in the electrode is more uniformly distributed at the higher flow rate for $\omega = 2\ mL/s$. This is because a higher flow rate minimizes the contact time for reaction in the electrode, which results in little longer time for the exit solution to reach the required state of charge. So coulombic efficiency increases with increase in flow rate and it decreases oxygen and hydrogen gas evolution rate.

6.4.3 Effects of electrode porosity

Factors to be considered for selecting the electrode material are electrical conductivity, specific surface area, resistance to corrosion and porosity. Figure 6.7 shows charge-discharge curves for three different values of electrode porosity. The total volume of electrolyte was equal in all cases. The difference in the curves can be observed in Fig. 6.7 even for small difference in porosity. If we compare Fig. 6.8 and Fig. 6.9, it is evident that the bulk reaction rate is going from $\varepsilon = 0.8$ to $\varepsilon = 0.6$, therefore it increases the time taken to reach an equivalent state of charge as well

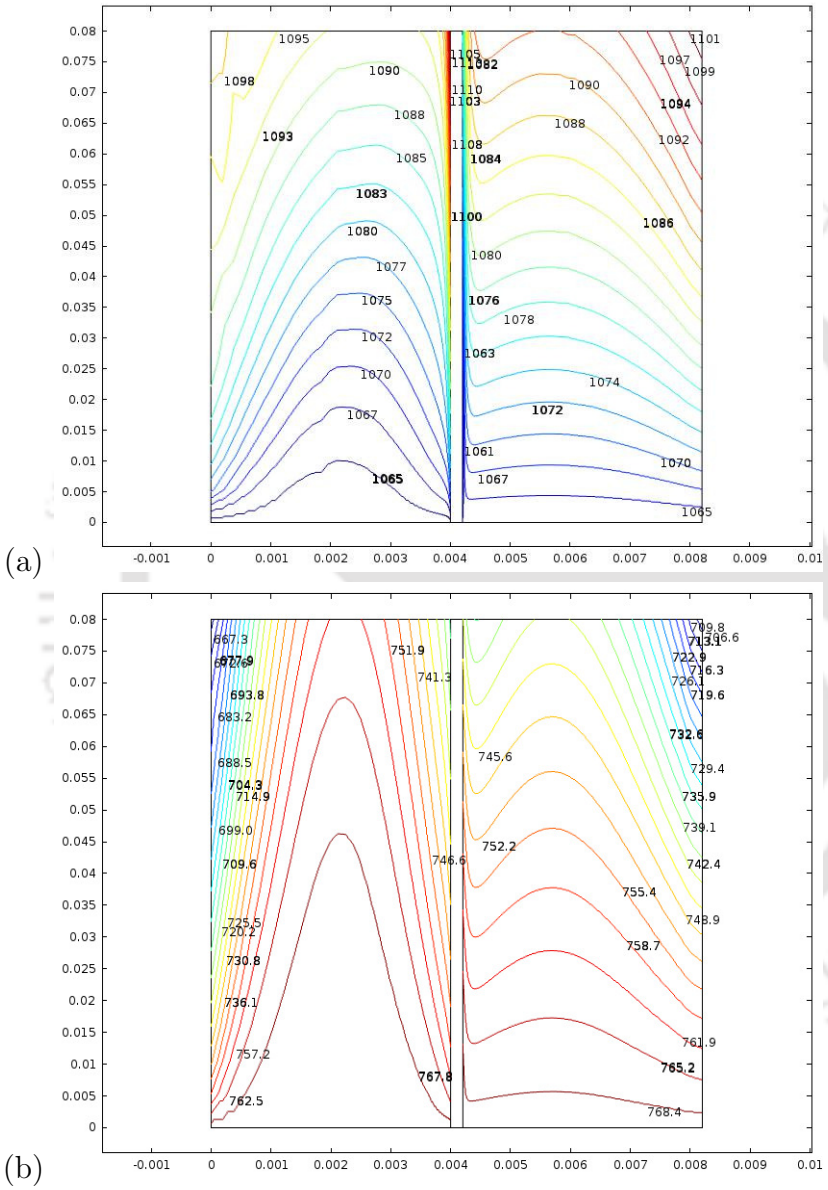

Figure 6.6: Contours of the V(III) and V(IV) concentration while charge (a) and during discharge (b), in the negative and positive electrode at *t=2034 s* (end of charge) for $\omega = 2\, mL/s$.

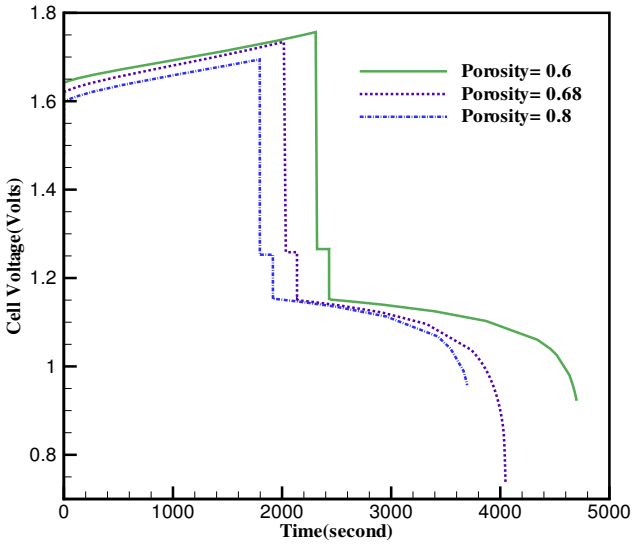

Figure 6.7: Simulated charge-discharge curves for three electrode porosity values, with initial concentration of $C_3^0 = 1080\ mol/m^3$, These charge times are 2298 s for $\varepsilon = 0.6$, *2010 s* for $\varepsilon = 0.68$ and *1788 s* for $\varepsilon = 0.8$.The other parameter values are given in B.5-B.7

as coulombic efficiency. The performance increase is similar to that due to increase of concentration of V(III), which is seen by comparing Fig. 6.3 and Fig. 6.7. Effects with an increased porosity are increased bulk diffusion, decreased bulk conductivity coefficients, increased permeability and greater electrolyte volume in the electrode. The increasing volume in the electrode leads to an increased bulk reaction rate and therefore a more rapid reduction of V(III) while charge. If the electrode porosity is low, uniform distribution of concentration is observed throughout the electrode; so current density and overpotential are considerably higher on average. If the porosity of the electrode is high, it leads to lower concentration of V(III) and decreased bulk conductivity therefore greater the polarization. It leads to higher rate of side reactions during charging for higher porosity of electrode.

6.4.4 Effects of applied current

Figure 6.10 shows charge-discharge curves for three applied currents $I = 5\ A$, $I = 10\ A$, $I = 15\ A$. The sign of the current is reversed during discharge. The charge time is defined by an equivalent SOC for each applied current. There is increase in

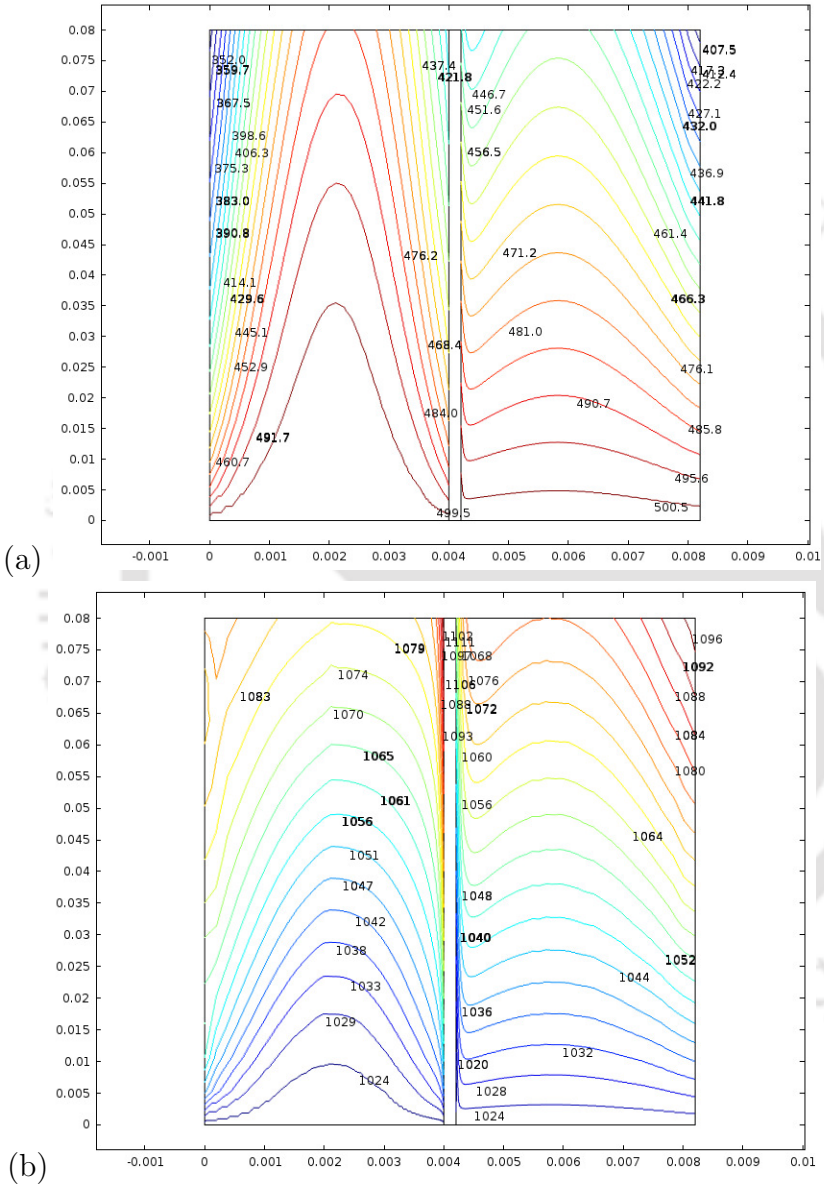

Figure 6.8: Contours of the V(III) and V(IV) concentration while charge (a) and during discharge (b) corresponding to the cycle, porosity $\varepsilon = 0.6$at t=*2298 s* (end of charge).

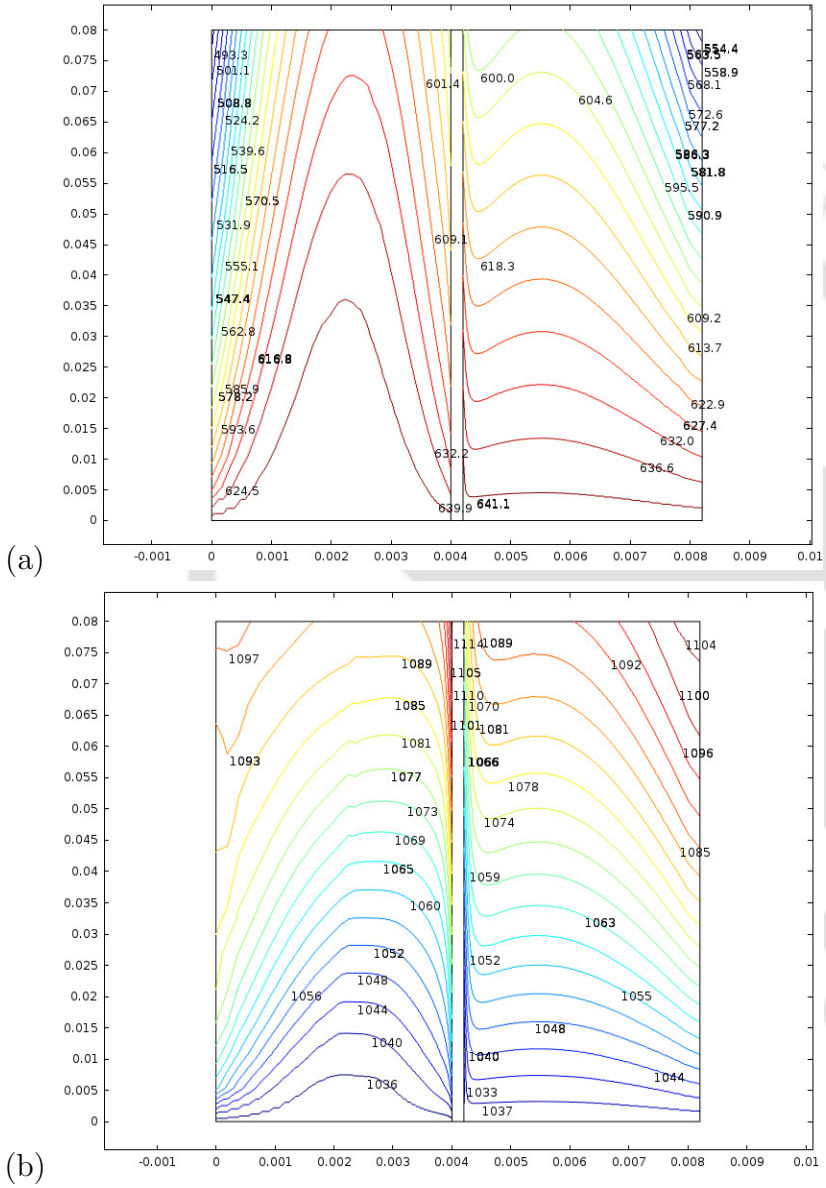

Figure 6.9: Contours of the V(III) and V(IV) concentration while charge (a) and during discharge (b) corresponding to the cycle, porosity $\varepsilon = 0.8$ at *t=1788 s* (end of charge).

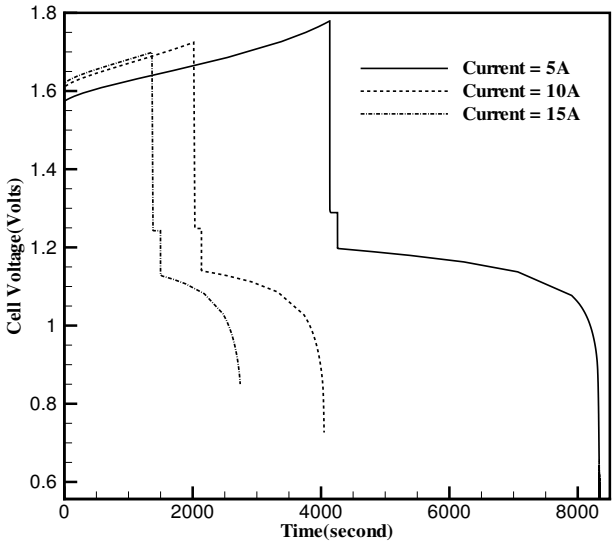

Figure 6.10: Simulated charge-discharge curves for three current values, with initial concentration of $C_3^0 = 1080\ mol/m^3$, These charge times are *4137 s* for $I = 5\ A$, *2010 s* for $I = 10\ A$ and *1379 s* for $I = 15\ A$. The other parameter values are given in B.5-B.7

the maximum cell voltage with decrease in applied current. The coulombic efficiency increases if the applied current decreases, fixing the end of discharge as the point at which the cell voltage reaches a value of 0.2 V. Figure 6.11 shows contours of V(III) concentration in the negative electrode at the end of the charging process for the case $I = 5\ A$. Comparing the V(III) concentration in Fig. 6.11 with the contour plots in Fig. 6.12 for $I = 10\ A$, it shows that the concentration is more uniform at the lower value of I. This is because for current $I = 5\ A$, the lower rates of reaction are required to maintain a lower current.

6.5 Results including the effects of losses into the model

In this case the structural dimensions of the VRFB cell has taken to be, 10 $cm \times$ 10 $cm \times 4\ mm$. In the model 2940 elements are used in the simulation. The effect of considering the concentration overpotential and ohmic losses can be observed in

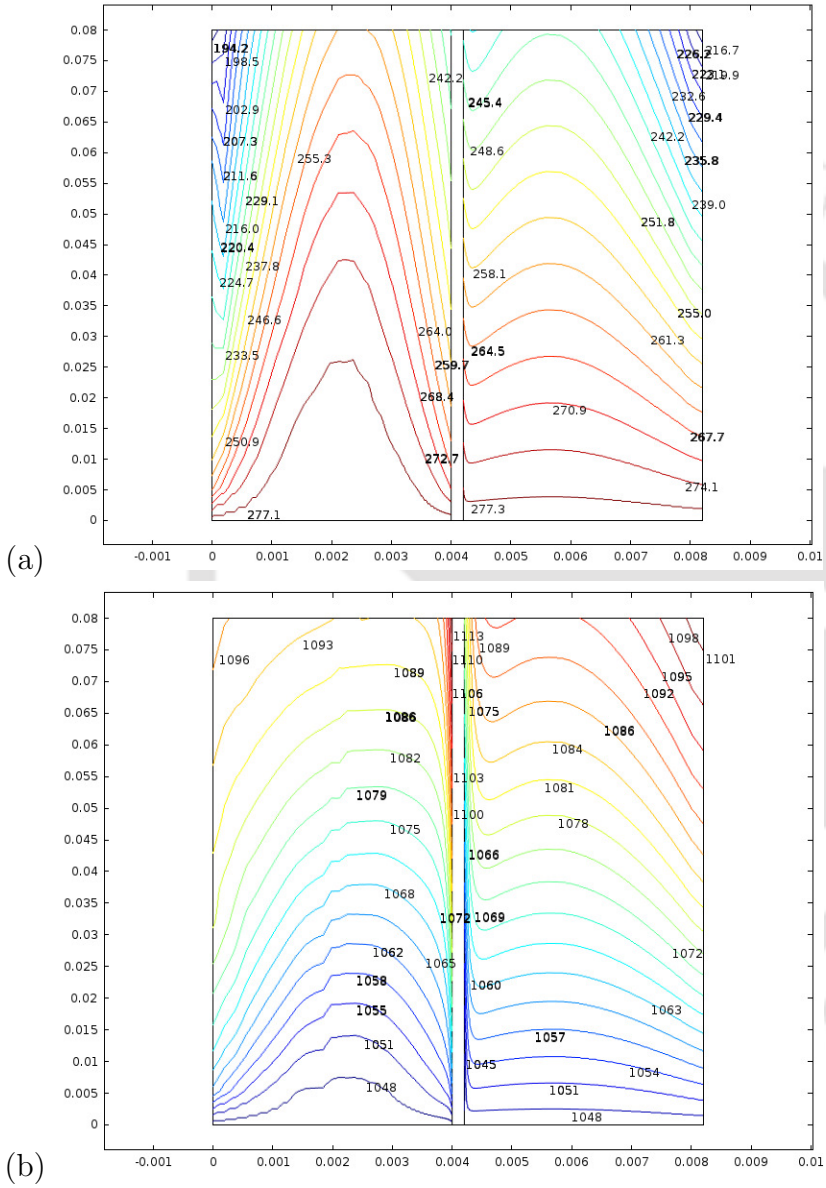

Figure 6.11: Contours of the V(III) and V(IV) concentration while charge (a) and during discharge (b) in the positive and negative electrode at *t=4137 s* (end of charge) for current $I = 5\ A$.

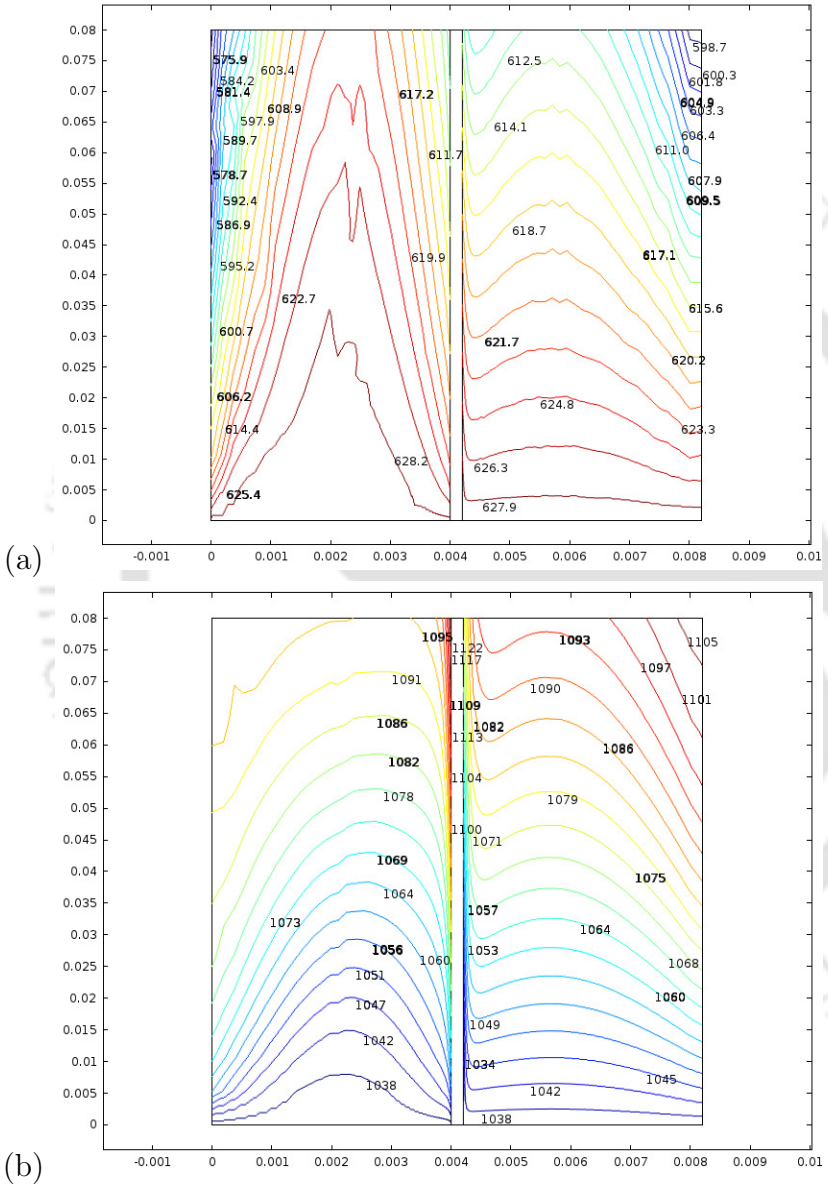

Figure 6.12: Contours of the V(III) and V(IV) concentration while charge (a) and while discharge (b) in the positive and negative electrode at *t=2010 s* (end of charge) for current $I = 10\ A$.

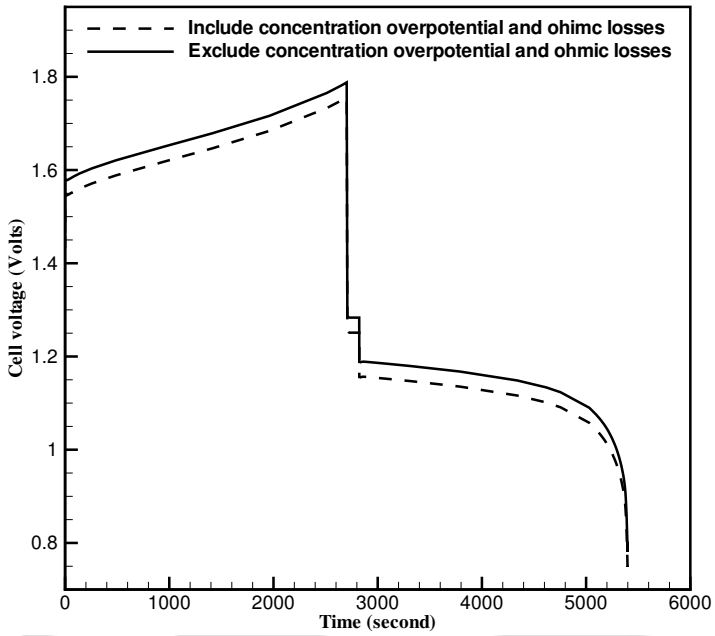

Figure 6.13: A comparison of simulated charge-discharge curves including and excluding, the concentration overpotential and ohmic losses. In this case initial concentration was $C_3^0 = 1440\ mol/m^3$.

Fig. 6.13. Due to these losses there is considerable drop in the cell voltage which results in decrease in voltage and energy efficiency. Therefore, there is drop in performance of the cell. By considering these losses the performance of the cell can be predicted very accurately. Figure 6.14 shows contour plots of the V(III) and V(IV) concentration at times while charge and discharge for the case $C_3^0 = 1440\ mol/m^3$. The inlet surface is denoted by the line $y = 0$ and the outlet by $y = 10\ cm$. While charging (Fig. 6.14(a)) the reduction of V(III) increases with height above the inlet surface along any vertical line. The magnitude of variation of concentration in this direction is calculated by the rate at which the electrolyte is passed through the electrode through the pump, i.e., the volumetric electrolyte flow rate ω and as we predict, the highest concentration takes place along the inlet surface.

6.5.1 Effects of electrolyte concentration

Figure 6.15 shows variation of coulombic, voltage and energy efficiency for three different concentrations, $C_3^0 = 1080\ mol/m^3$, $C_3^0 = 1260\ mol/m^3$ and $C_3^0 = 1440\ mol/m^3$. The results show an increased coulombic efficiency for increased concentration but

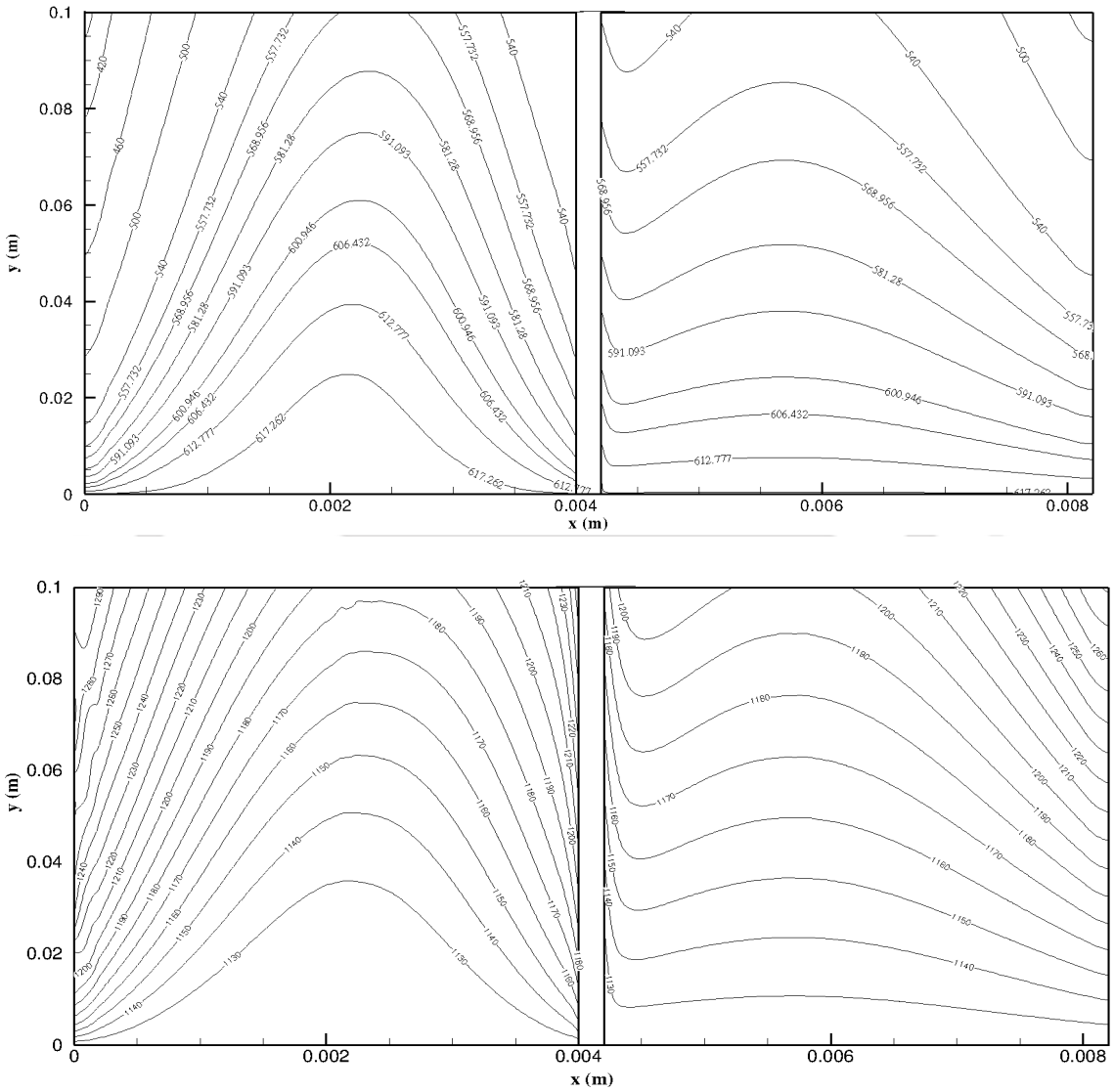

Figure 6.14: Contours of the V(III) and V(IV) concentration while charge (a) and while discharge (b) corresponding to the cycle $C_3^0 = 1440\ mol/m^3$ shown in Fig. 6.2(b).

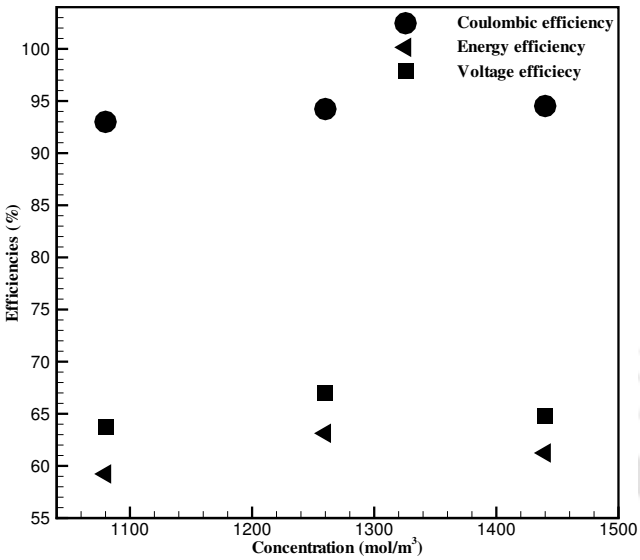

Figure 6.15: Coulombic, voltage and energy efficiencies for electrolyte concentration $C_3^0 = 1080\ mol/m^3$, $C_3^0 = 1260\ mol/m^3$ and $C_3^0 = 1440\ mol/m^3$. The flow rate was $\omega = 1\ mL/s$ and current density, $j_{app} = 1000\ A/m^2$. The other parameter values are given in Table B.5-B.7

voltage efficiency decreases for concentration $C_3^0 = 1440\ mol/m^3$, therefore in this case energy efficiency decreases. From Fig. 6.15 it is understood that optimum concentration is achieved for concentration, $C_3^0 = 1260\ mol/m^3$ in which voltage and energy efficiency is high.

6.5.2 Effects of electrolyte flow rate

An vital parameter to improve the performance of the battery is the flow rate. If the flow rate is too low, the electrolyte is not circulated uniformly therefore stagnant regions will be formed in the electrode. If the electrolyte flow rate is high,there is risk of leakage leads to reduction in performance for the extra power required. Figure 6.16 shows the simulated results of coulombic, voltage and energy efficiencies for three volumetric flow rates. From the simulation result it is understood that coulombic, voltage and energy efficiencies increases with the flow rate. This is because higher the flow rate concentration is more uniformly distributed in the electrode. Also higher flow rate minimizes the contact time for reaction in the electrode, which results in little longer time for the exit solution to reach the required state of charge. Conclusion from this result higher the flow rate all three efficiencies increases and

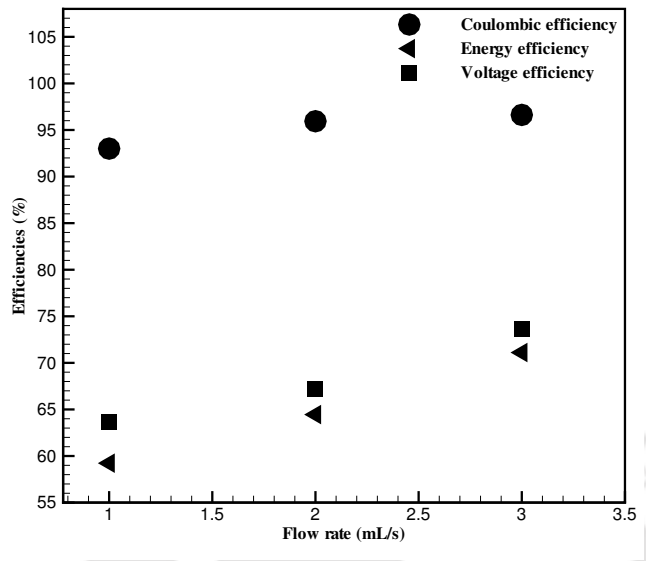

Figure 6.16: Coulombic, voltage and energy efficiencies for volumetric flow rates, $\omega = 1\ mL/s$, $\omega = 2\ mL/s$ and $\omega = 3\ mL/s$. The initial concentration was, $C_3^0 = 1080\ mol/m^3$ and current density, $j_{app} = 1000\ A/m^2$. The other parameter values are given in Table B.5-B.7

lower the rates of hydrogen and oxygen gas evolution side reactions.

6.5.3 Effects of electrode porosity

For three different porosity values $\epsilon = 0.6$, $\epsilon = 0.68$ and $\epsilon = 0.8$ variation of coulombic, voltage and energy efficiencies are shown in Fig. 6.17. The total volume of electrolyte was same in all cases. There is change in efficiency even for small change in porosity as observed from Fig. 6.17. Lower the porosity of electrode gives higher the coulombic efficiency, due to uniform distribution of concentration throughout the electrode therefore current density and overpotential are considerably higher on average. If the porosity of the electrode is high, it leads to decrease concentration of V(III) and reduced bulk conductivity therefore greater the polarization. It leads to higher rate of side reactions during charging for higher porosity of electrode. It is observed from the result, for porosity $\epsilon = 0.68$, voltage and energy efficiency are maximum, beyond that these efficiencies decrease. Therefore $\epsilon = 0.68$ is the optimum porosity value, which gives maximum efficiency.

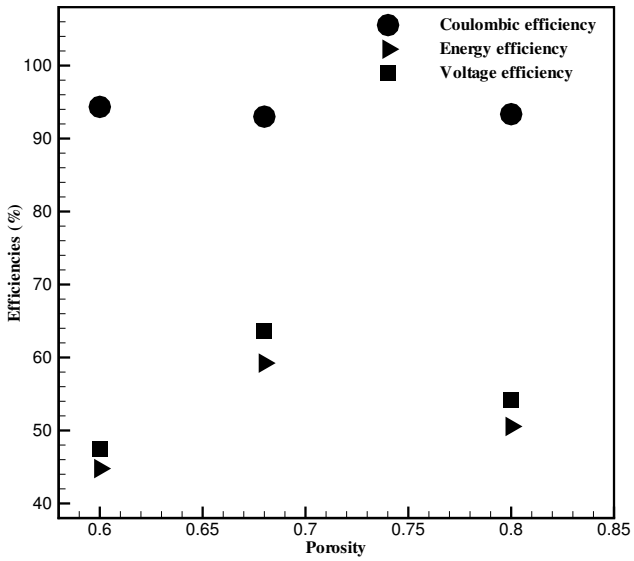

Figure 6.17: Coulombic, voltage and energy efficiencies for electrode porosity values, $\epsilon = 0.6$, $\epsilon = 0.68$ and $\epsilon = 0.8$. The initial concentration was, $C_3^0 = 1080\ mol/m^3$, flow rate, $\omega = 1\ mL/s$ and current density, $j_{app} = 1000\ A/m^2$. The other parameter values are given in Table B.5-B.7

6.5.4 Effects of applied current

Figure 6.18 shows variation of coulombic, voltage and energy efficiencies with three applied current values. The charge times are defined by an equivalent SOC for each applied current. If the applied current decreases both coulombic efficiency and voltage efficiency increase, hence energy efficiency increases. If the applied current decreases maximum cell voltage increases therefore good performance of the cell can be attained for lower applied current. The efficiencies reduce if the applied current increases due to magnitude of overpotentials in the both electrode increases leads to oxygen and hydrogen gas evolution side reactions taking place inside the cell. Due to oxygen and hydrogen bubble formation, the active surface area for electrochemical reaction in the electrode decreases. So the effective ionic and thermal conductivities and the effective diffusion coefficients decrease, therefore the performance of the cell decreases.

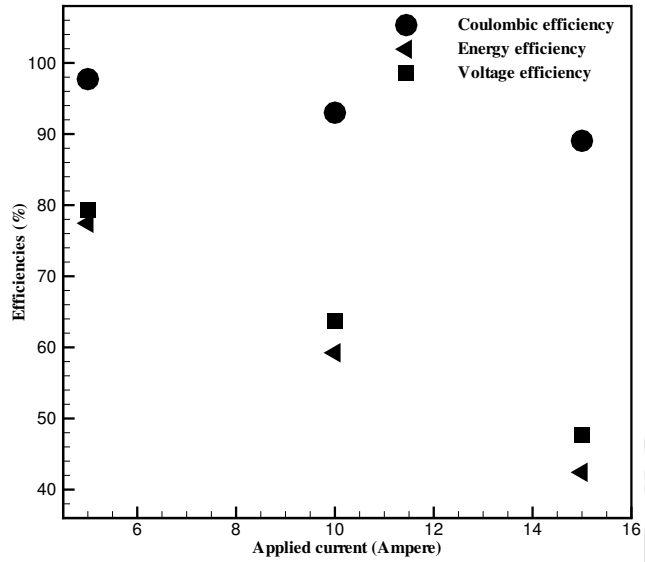

Figure 6.18: Coulombic, voltage and energy efficiencies for applied current values, $j_{app} = 5\ A$, $j_{app} = 10\ A$ and $j_{app} = 15\ A$. The initial concentration was, $C_3^0 = 1080\ mol/m^3$, flow rate, $\omega = 1\ mL/s$. The other parameter values are given in Table B.5-B.7

6.6 Closure

A two-dimensional, transient, isothermal model for the all-vanadium redox flow battery is developed. This model used to predict the effects of change in electrolyte concentration, flow rate, electrode porosity and applied current. Numerical model results are validated with the available experimental result which shows good agreement.

Also same model is extended by including various losses into the model formulation. The coulombic, voltage and energy efficiencies are analyzed to predict the effects of change in electrolyte flow rate, concentration, electrode porosity and applied current. There is need to optimize the cell parameters to predict various efficiencies very accurately to improve the performance. Results indicate that there is an optimal concentration and electrode porosity at which maximum efficiency can be achieved. The model also predicts that cell efficiencies increase with increase of electrolyte flow rate and cell efficiencies decrease with increase of applied current.

Chapter 7

Effects of Different Parameters on Performance of a 3-D All-Vanadium Redox Flow Battery

7.1 Introduction

Industrialization and increase in global population lead to increasing demand for energy. Renewable energy is an alternative to conventional energy due to its diversification and sustainability. The solar and wind energy belongs to renewable energy which are random and intermittent nature therefore electricity energy storage (EES), which is capable of storing and releasing electricity temporarily is available to resolve those problems [74]. Among all the EES technologies all-vanadium redox flow battery (VRFB) is a better option, which was initially proposed by Skyllas-Kazacos and co-researchers in the mid-1980s [1]. The VRFBs have many advantages including long cycle life, independent of capacity and power, elimination of electrolyte cross contamination, active thermal management, high energy efficiency, low capital cost for large energy storage capacity, etc. Therefore, VRFBs have been used for emergency backup, load leveling, peak shaving, uninterruptible power supply and facilitation of wind and photovoltaic energy delivery [54]. The challenges include optimization and scale-up in order to implement commercial application. Modeling and simulation are economical methods to resolve these challenges, which helps in

minimizing the costs and time related with experiments. Up to now there are only a few number of comprehensive models are proposed for VRFBs for understanding system characteristics and performance under different operating conditions.

A complete two dimensional transient model was first developed by Shah et al. [29]. The present model was based on laws of conservation of mass, momentum and charge adding with the fundamental models of transport and a kinetic model for reactions including vanadium ions. The model is used to study the effects of variation in electrolyte flow rate, concentration, electrode porosity, on the performance. A three-dimensional model studied by Yin and co-researchers [44] for single and multi inlet designs on the performance. Xu et al. [45] developed three-dimensional model to study different flow field configurations. Qiu et al. [43] studied 3-D pore scale resolved model to analyze the physical processes at the microscopic level. In this chapter we consider a three-dimensional isothermal model for VRFBs. The main objective of the multidimensional modeling and simulation is to study of VRFBs in detail. The model considers the effect of concentration overpotential and ohmic losses. There is a scope to study the variation of cell voltage with state of charge for various operating parameters. The effects of species concentration, electrolyte flow rate, electrode porosity and applied current density on the performance are also studied.

7.2 Problem Description

The model is based on three-dimensional, steady, isothermal for the geometry shown in Fig. 1.2. The main components of the battery are electrodes, current collectors, membrane, reservoirs and pumps. The model is based on the conservation laws of charge, mass, momentum along with a kinetic model for reaction containing soluble vanadium species. Also, the model includes concentration overpotential and ohmic losses for the all-vanadium redox flow battery. Due to reduction and oxidation reaction in the cell the variation in concentration of vanadium species takes place, therefore, the performance of the cell changes. The assumptions considered during modeling are given below.

1. The dilute solution approximation is used for simplification and the flow is considered as laminar and incompressible.

2. Physical properties of the electrode and membrane are homogeneous and isotropic.

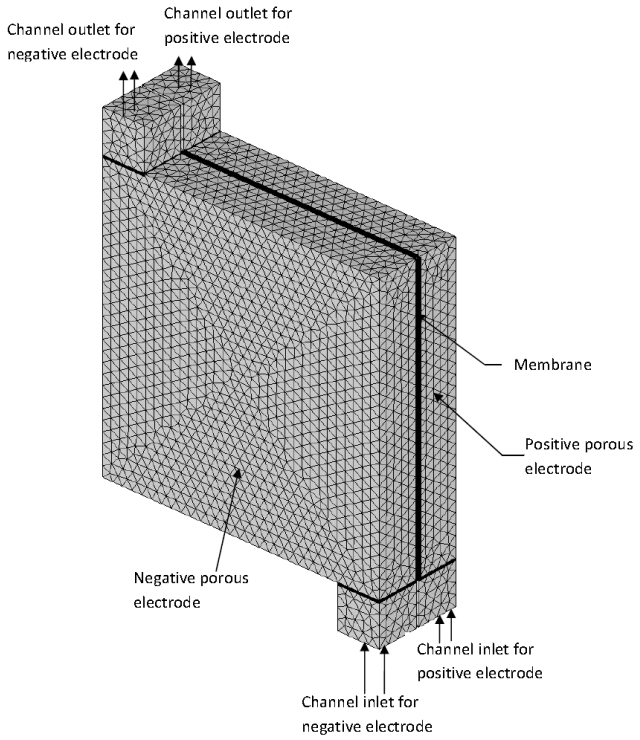

Figure 7.1: The three-dimensional geometry includes computational meshes.

3. There is no self discharge of vanadium species through the membrane because there is no leakage of charge or reactant through the external surfaces of the cell.
4. The transport of the charged species takes place by convection and diffusion and migration terms are neglected for simplification.
The performance of the cell is studied for different parameters. It includes concentration, electrolyte flow rate, electrode porosity and applied current density.

7.3 Numerical Details

The present three-dimensional model was solved using the package COMSOL Multiphysics, which is based on the finite element method. Figure 7.1 shows three-dimensional computational mesh, which has 114019 tetrahedral elements used in all of the simulations. The relative tolerance is set to 1.0×10^{-5}. The governing equations with initial and boundary conditions are shown in sections 3.9 to 3.14. The structural dimensions of the battery and other default parameters are given in Tables B.8-B.11 in appendix B.

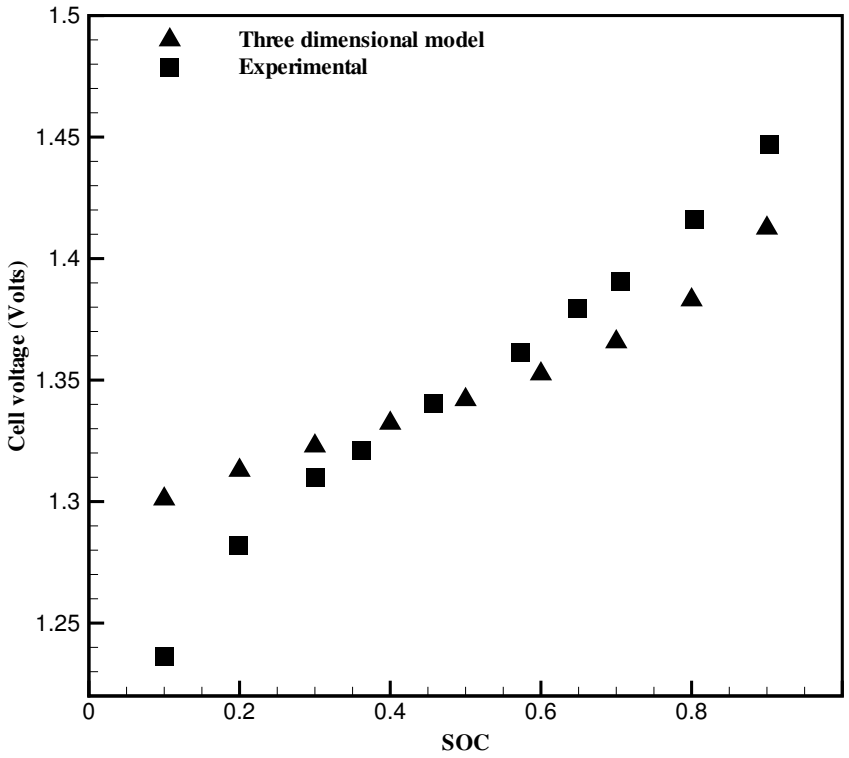

Figure 7.2: Comparison of simulated overall cell voltage values by experimental result and present simulation result at different SOC for applied current density of 40 mA/cm^2

7.4 Results and Discussion

Figure 7.2 shows the comparison of simulated cell voltage with experimental result available in literature [13] and the present simulation result is computed at different SOC for applied current density of 40 mA/cm^2. The initial vanadium electrolyte was 1500 mol/m^3. The result shows in good agreement with the experimental result. The average error is less than 2.2 %. The little deviation between the two results are due to the effect of crossover of vanadium species through membrane which was not considered in this model. The velocity distribution in three-dimension is complex compared to two- dimensional one. Figure 7.3 shows the variation of velocity in the porous electrode. The magnitude of velocity in two-dimensional geometry in porous electrode is almost constant due to its simple rectangular geometry. In three-dimensional geometry variation of velocity is entirely different. The electrolyte flow is taking place from inflow channel to porous electrode. The velocity of the electrolyte decreases due to expansion in the porous electrode then increases when

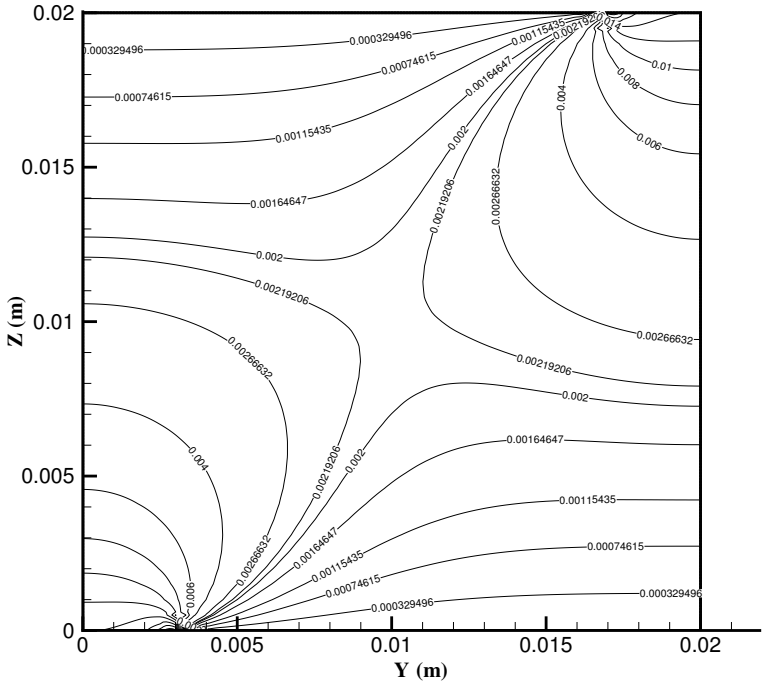

Figure 7.3: Velocity contour plot on current collector and electrode interface

the electrolyte leaves the outflow channel. The flow is taking place in the porous electrode in the diagonal direction from inlet to outlet flow channel. The minimum velocity occurs at the two corners corresponds to the axis of ($Y = 0.02\ m$ and $Z = 0$) and ($Y = 0$ and $Z = 0.02\ m$), respectively. The symmetric velocity distribution is found in the region of ($Y > 0.004\ m, Z > 0, X \in (0, 0.003\ m)$) and ($Y > 0, Z > 0.013\ m, X \in (0, 0.003\ m)$). Also, symmetric pattern is observed in the region of ($Y < 0.009\,m, Z < 0.013\,m, X \in (0, 0.003\,m)$) and ($Y > 0.012\,m, Z > 0.008\,m, X \in (0, 0.003\ m)$). The velocity in X direction is very small as compared with Y and Z direction velocity.

7.4.1 Effects of electrolyte flow rate

Figure 7.4 shows variation of concentration of V(III) ions during charging and during discharging at 50% SOC. Due to redox reactions of vanadium ions V(III) it decrease toward the downstream region of the cell. In the negative electrode a relatively higher depletion of discharged species V(III) is observed near the interface of the negative electrode and membrane, so it results in higher concentration of charged

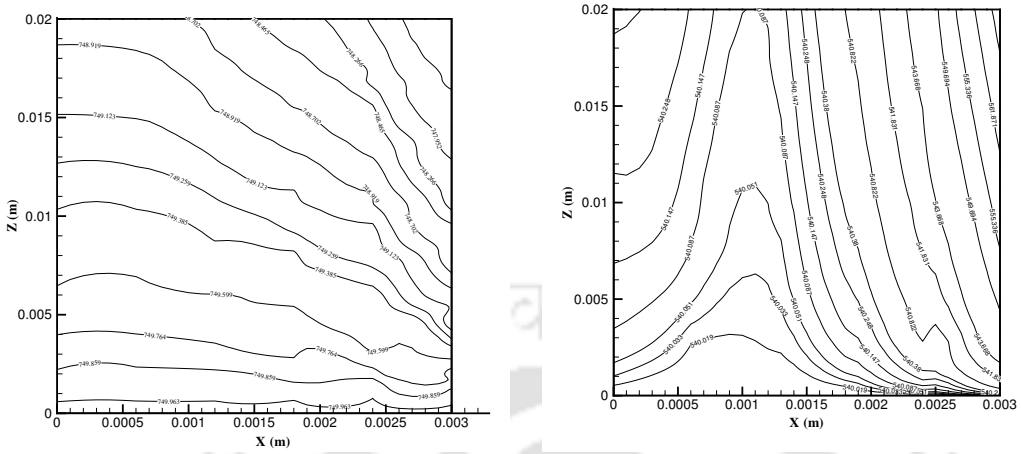

(a) (b)

Figure 7.4: Contour of V(III) (a) during charging, (b) while discharging.

species V(II) there. Also, it is observed that concentration V(III) decreases during charging, during discharging reverse trend is observed as shown in Fig. 7.4(b). Most important parameter is electrolyte flow rate in which the performance of the battery depends. If flow rate of electrolyte is high, there is high risk of leakage of electrolyte which leads to decrease in performance due to extra power required for pumping. If flow rate is too low, stagnant regions are formed due to non-uniform distribution of electrolyte in the porous electrode. Figure 7.5 shows the cell voltage variation with state of charge for three different volumetric flow rates. The result shows that for flow rate 3 mL/s cell voltage variation is maximum during charging and discharging process. Even though coulombic efficiency difference is small, voltage efficiency is higher, therefore, energy efficiency increases. This is due to more evenly distribution of vanadium concentration in the porous electrode for higher flow rate. Also, it is understood that higher flow rate decreases the contact time for reaction in the electrode, which results in little longer time for the exit solution to reach the required state of charge. It can be concluded that higher the flow rate, lower the rate of oxygen and hydrogen gas evolution side reactions, therefore, efficiency of the cell increases.

7.4.2 Effects of concentration

Figure 7.6 shows variation of overall cell voltage with soc for three different concentrations, $C^0_{III} = 1080\ mol/m^3$, $C^0_{III} = 1260\ mol/m^3$ and $C^0_{III} = 1440\ mol/m^3$.

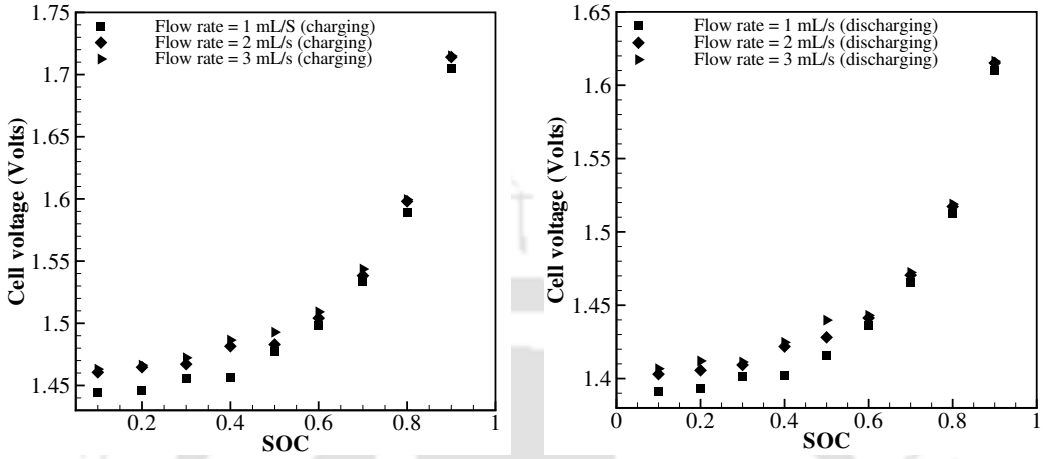

(a) (b)

Figure 7.5: Simulated cell voltage values at different soc for three electrolyte flow rates, 1 mL/s, 2 mL/s and 3 mL/s : (a) charging (b) discharging, the other default parameter values are given in Tables B.8-B.11 in appendix B.

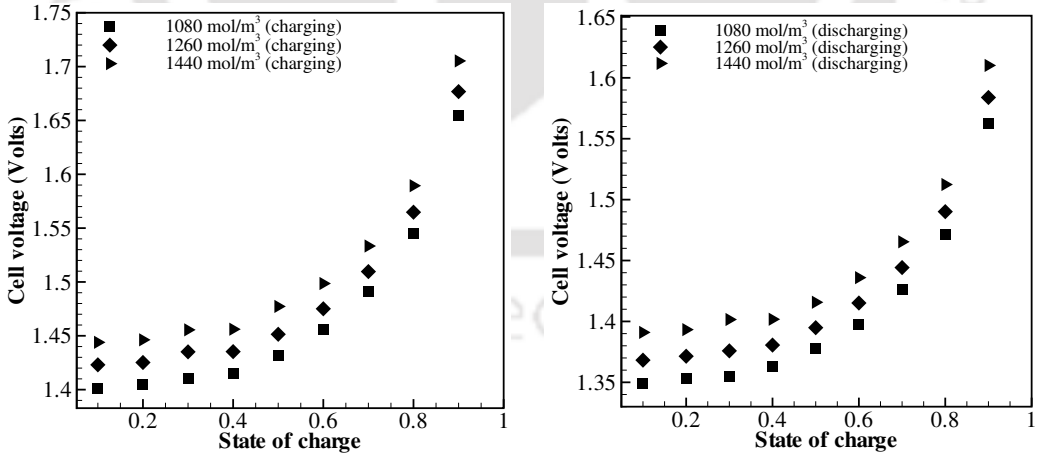

(a) (b)

Figure 7.6: Cell voltage variation with soc for three different concentration values, 1080 mol/m^3, 1260 mol/m^3 and 1440 mol/m^3 : (a) charging (b) discharging, the other default parameter values are given in TablesB.8-B.11 in appendix B.

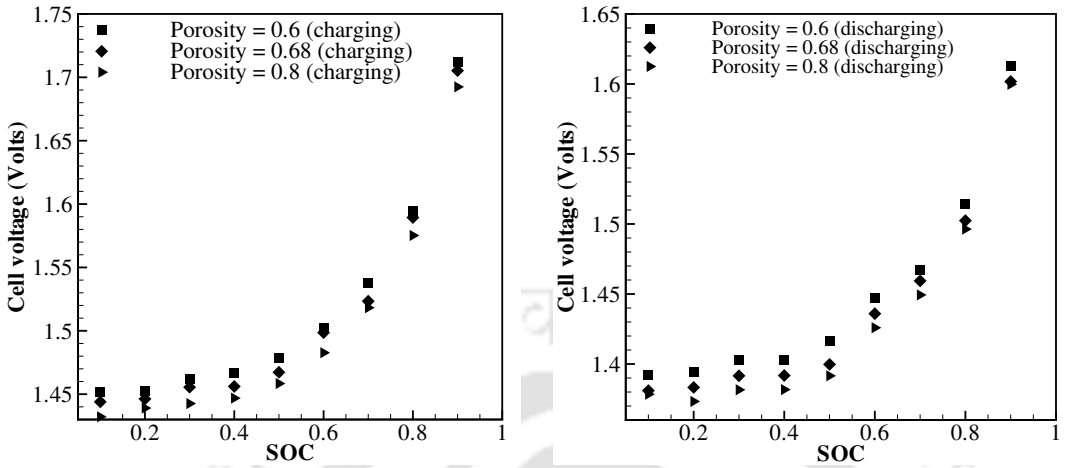

Figure 7.7: Variation of overall cell voltage with soc for three different values of electrode porosity values, 0.6, 0.68 and 0.8 : (a) charging (b) discharging, the other default parameter values are given in Tables B.8-B.11 in appendix B.

The results show that higher voltage efficiency is observed at concentration $C^0_{III} = 1440\ mol/m^3$ for both charging and discharging process. From Fig. 7.6 it is understood that for the given geometry optimum concentration is achieved for concentration, $C^0_{III} = 1440\ mol/m^3$ in which voltage and energy efficiency are high.

7.4.3 Effects of electrode porosity

Factors to be added for selecting the electrode material are porosity, specific surface area, electrical conductivity, and resistance to corrosion. Figure 7.7 shows cell voltage variation with soc for three porosity values. The difference in the cell voltage variation is observed even for small difference in porosity. The effects of increase in electrode porosity are bulk diffusion coefficients increases, bulk conductivity decreases, higher volume of electrolyte in the electrode and permeability increases.

The increasing electrolyte volume in the electrode results in increased bulk reaction rate, therefore, $V(III)$ concentration decreases rapidly during charging. From Fig. 7.7 it is understood that lower the value of porosity of electrode gives better performance due to uniform distribution of concentration throughout the electrode, therefore, values of overpotential and current density are higher on an average. For higher porosity electrode the performance of the cell decreases because of lower concentration of $V(III)$ and bulk conductivity decreases, therefore, higher the po-

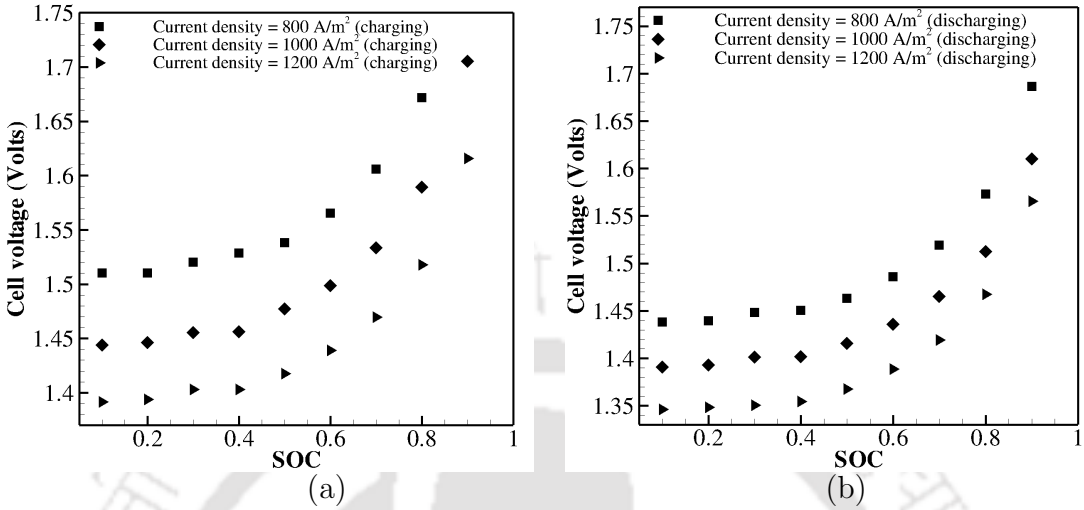

Figure 7.8: Simulated overall cell voltage variation with soc for different current density values, 800 A/m^2, 1000 A/m^2 and 1200 A/m^2 : (a) charging (b) discharging, the other default parameter values are given in Tables B.8-B.11 in appendix B.

larization. Also, higher porosity of the electrode leads to higher rate of hydrogen and oxygen evolution side reactions.

7.4.4 Effects of applied current density

Figure 7.8 shows cell voltage variation with soc with three applied current density values for charging and discharging process. It is seen from the results that if the applied current density decreases, voltage increases with soc, therefore, voltage and energy efficiency increases. The performance of the cell decrease with increase in applied current density due to increase in magnitude of overpotentials in the both electrode and it leads to hydrogen and oxygen gas evolution side reactions inside the cell. Due to hydrogen and oxygen bubble formation, the active surface area for reaction decreases in the electrode and the diffusion coefficients and the effective thermal and ionic conductivities decrease, and therefore, the performance of the cell decreases.

7.5 Closure

A three-dimensional steady VRFB model due to Shah et al. [29] is used to predict the VRFB performance. The model is able to predict the effects of concentration, electrolyte flow rate, electrode porosity, applied current density with state of charge has been studied. It is observed that higher electrolyte flow rate gives better performance due to uniform distribution of concentration in the porous electrode. Also, high concentration of vanadium shows good performance. The lower porosity values of electrode shows higher energy efficiency and the lower applied current density ensure higher performance due to no side reactions.

Chapter 8

Three Dimensional, Isothermal, Unsteady Numerical Simulation of All-Vanadium Redox Flow Battery

8.1 Introduction

The all-vanadium redox flow battery is a most promising, cost effective large-scale electro chemical energy storage device. There are various applications of the all-vanadium redox flow battery (VRFB), which include emergency backup, uninterruptible power supplies and peak load levelling [1]. VRFB is used in renewable energy applications as it enhances the effectiveness of utilizing and delivering the intermittent renewable energy sources such as photovoltaic and wind energy. Three-dimensional studies of VRFB are done by Ma et al. [41] who accounted only for negative half cell conditions. It was further extended including the effect of non-isothermal based on a full cell configuration [51]. One more 3-D model was developed by Xu et al. [45] to evaluate the suitability of different flow field configuration. Also 3-D pore scale stationary isothermal model was studied to study the physical processes at the microscopic level [43, 42]. Many challenges have to be overcome for the commercial applications of the vanadium redox flow battery such as, optimization and scale-up which include flow geometries and operation conditions.

8.2 Problem Specification

In this chapter we study a three-dimensional dynamic, isothermal model based on conservation laws which include the fundamental modes of transport and kinetic model for reactions involving the vanadium species. The diffusion of ions across the membrane and electrolyte flow through the porous electrodes can be modeled by the conservation laws of mass, momentum. By solving of Poisson's equations the distribution of electric potential inside the cell can be calculated. The electrochemical interaction of species in the cell is obtained by the Butler Volmer law and Nernst equation. The computational geometry is shown in Fig. 1.2. Referring to Fig. 1.2, the line $x1$ represents the electrode/current collector interface and $x2 = 0.003\ m$ represents the electrode/membrane interface. The dimensions in x and y direction represents in meters. Also the present model includes concentration overpotential and ohmic losses for the all-vanadium redox flow battery. The description of each term related with structural dimensions are shown in nomenclature. The performance of the cell is studied for different parameters, which includes concentration, electrolyte flow rate and electrode porosity.

8.3 Numerical Details

The present three-dimensional model is solved using the COMSOL Multiphysics package. To choose the number of computational mesh grid independence study has been carried out. From the Table 8.1 it is evident that the difference in maximum cell voltage with elements 3.022 lacs and 4.01 lacs is very small. Therefore, 3.022 lacs elements are used in all simulations. The relative tolerance for all variables is set to 1.0×10^{-6}. The default set of parameters is listed in Table B.12 of appendix B. The other input parameters taken from Shah et al. [29].

8.4 Results and Discussion

Figure 8.1 shows a comparison of the simulation result with the experimental result of Shah et al. [29] for validation. In this case concentration was, $C^0_{III} = C^0_{IV} = 1440\ mol/m^3$, the model captures good trends. The comparison of V(II) and V(III)

Table 8.1: Grid independence test

Number of elements	**Maximum cell voltage (Volts)**
2.01×10^5	1.6759
3.022×10^5	1.67577
4.01×10^5	1.67578

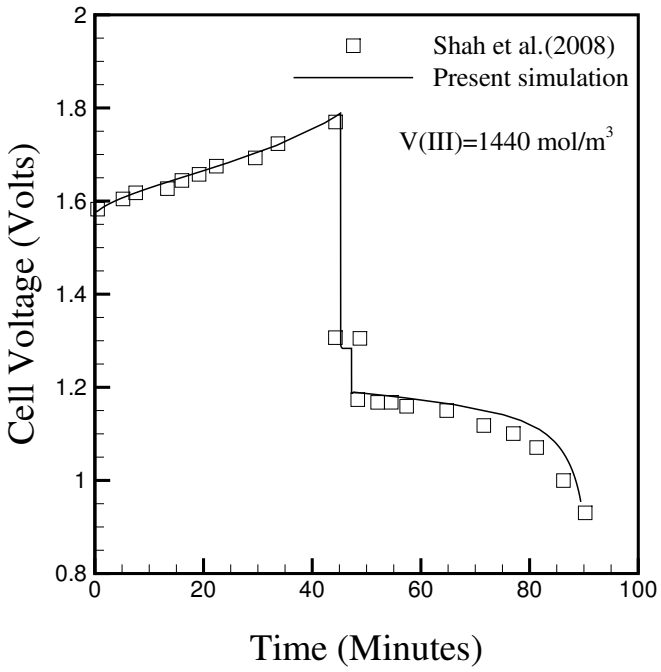

Figure 8.1: A comparison of simulated and experimental charge-discharge curves for $C_3^0 = 1440\ mol/m^3$.

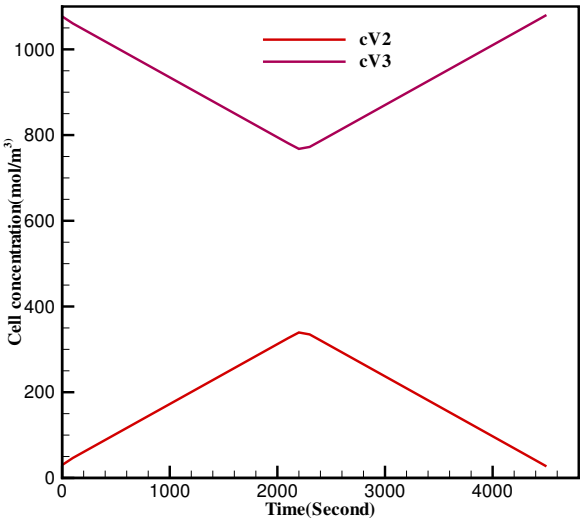

Figure 8.2: Cell concentration V(II) and V(III) variation with time during the full charge-discharge cycle

cell concentration variation for $T = 300\ K$, $C_3^0 = C_4^0 = 1080\ mol/m^3, \omega = 1\ mL/s$, and $j_{app} = 1000\ A/m^2$ is shown in Fig. 8.2. The other parameter values are given in Table B.12 in appendix B. During charging V(II) concentration increases from initial value but V(III) decreases from initial value, while discharging V(II) decreases and V(III) increases. This is because of reduction and oxidation reactions. Figure 8.3 shows isosurface of electrolyte pressure variation inside negative half of the cell. The similar pressure variation is expected in positive half of the cell because almost same fluid properties of fluid. The pressure is higher at the inlet and it decreases gradually from inlet to outlet of the cell. This pressure variations calculated by using the Darcy's law for porous electrode.

8.4.1 Concentration effects

Figure 8.4 shows a comparison between the simulations for two different concentrations $C_3^0 = 1080\ mol/m^3$ and $C_3^0 = 1440\ mol/m^3$, the model captures the trends very well. The results show an increased coulombic efficiency for increased concentration. In the calculations, the charge times are, approximately, 2210 s and 2903 s for the cases $C_3^0 = 1080\ mol/m^3$ and $C_3^0 = 1440\ mol/m^3$, respectively. Figure 8.5 shows contour plots of the V(III) and V(IV) concentration at times during charge

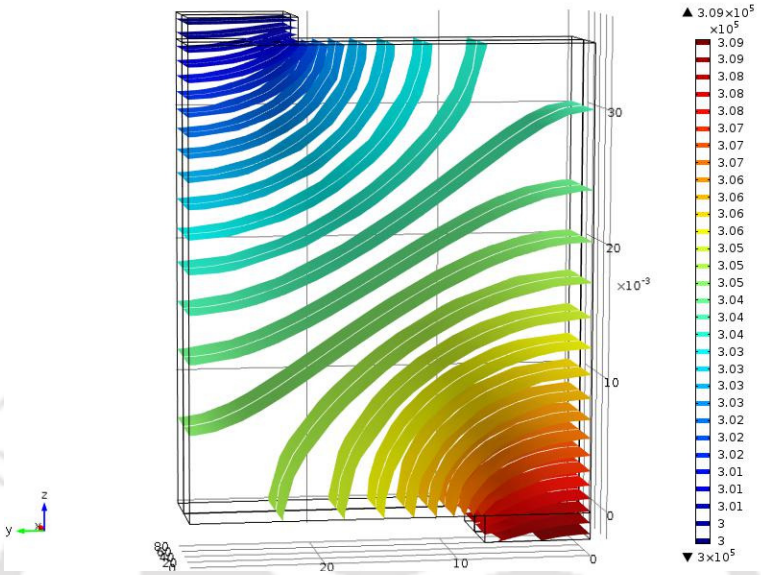

Figure 8.3: Isosurface of pressure variation of electrolyte for consider negative half of the cell of the VRFB

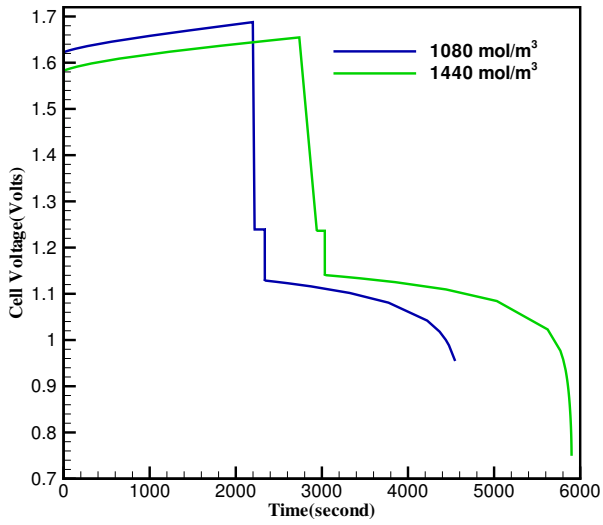

Figure 8.4: A comparison of simulated charge-discharge curves for $C_3^0 = 1080\ mol/m^3$ and $C_3^0 = 1440\ mol/m^3$, The other parameter values are given in Table B.12 in appendix B.

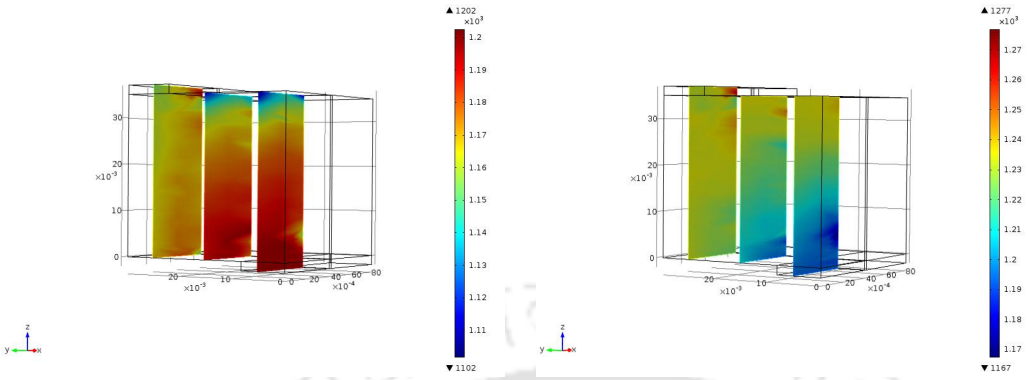

(a) (b)

Figure 8.5: Contours of the V(III) concentration while charging (a) and during discharging (b) corresponding to the cycle $C_3^0 = 1440\ mol/m^3$ shown in Fig. 8.4.

and discharge for the case $C_{III}^0 = 1440\ mol/m^3$. The inlet surface is represented by the line $y = 0$ and the outlet by, $y = 3.5\ cm$. During charging (Fig. 8.5.(a)) the reduction of V(III) increases with height above the inlet surface increases along any vertical line. The magnitude of concentration variation in this direction is calculated by the rate at which the electrolyte is passed through the electrode through the pump, i.e. the volumetric flow rate and it is expected that the highest concentration takes place along the inlet surface. Along any horizontal line, the reduction of V(III) during charge increases as the current collector surface x1 is reached, since it is the surface along which the current enters. Therefore, concentration V(III) lies at the intersection of the upper surface, $y = 0.035\ m$, and the electrode/current-collector interface, x1. These similar effects can be seen in the V(II) concentration while discharge, the evolution of which can be deduced from the V(III) profiles shown on the bottom row. Also, we can observe that the concentration V^{3+} decreases along the width of the electrode shown in Fig. 8.5.

8.4.2 Effects of electrolyte flow rate

Electrolyte flow rate is most vital parameter to control the operation of a VRFB. If the electrolyte flow rate is too low, the electrolyte is not uniformly circulated, therefore stagnant regions will be formed in the electrode. There is also a risk of leakage which leads to reduction in performance for the extra power required if the flow rate is too high. Figure 8.6 shows the comparison of simulated results at three volumetric flow rates in the case of $C_{III}^0 = 1080\ mol/m^3$. The trends and magnitude

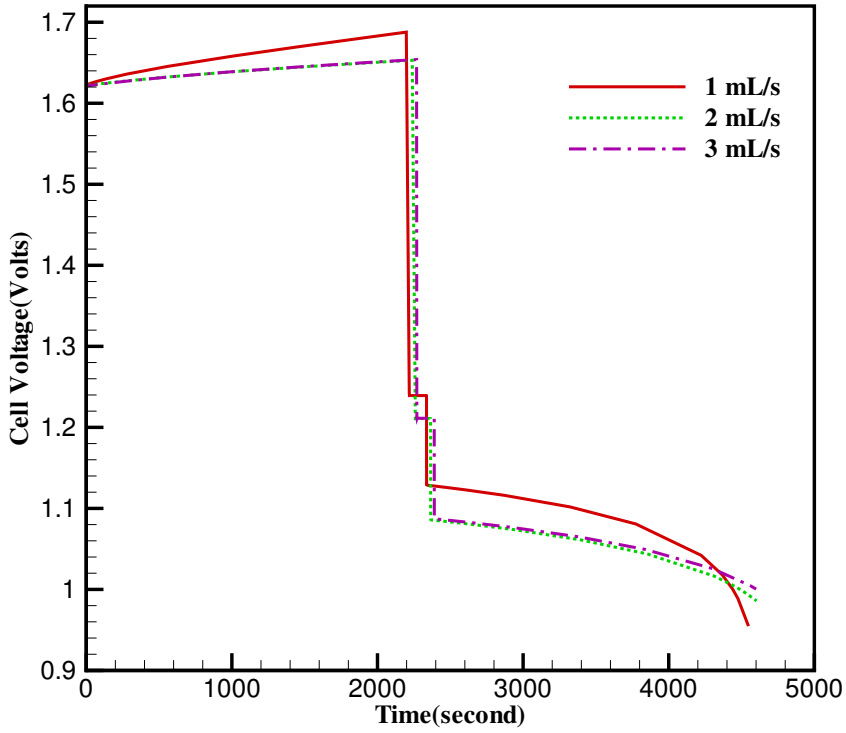

Figure 8.6: A comparison of simulated charge-discharge curves for three volumetric flow rates with initial concentration of $C_3^0 = 1080\ mol/m^3$. The charge times are 22100 s for $\omega = 1\ mL/s$, 2234 s for $\omega = 2\ mL/s$ and 2258 s for $\omega = 3\ mL/s$.The other parameter values are given in Table B.12 in appendix B.

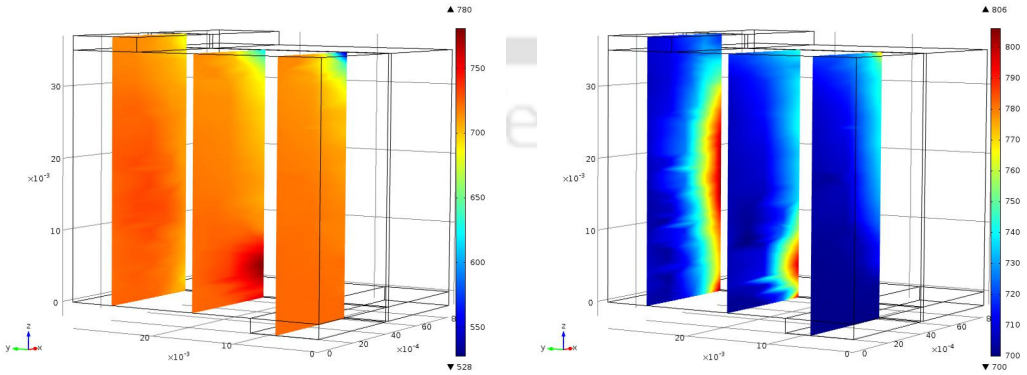

(a) (b)

Figure 8.7: Simulated surface contour of V(III) concentration, in the negative electrode at $t = 2234\ s$ (end of charge) for $\omega = 2\ mL/s$.

of variation are captured well. From the simulation result for $\omega = 3\ mL/s$, it is understood that the relative increment in coulombic efficiency decreases as the flow rate increases, therefore, there is optimum flow rate in which the performance is maximum. Figure 8.7 shows contours of the V(III) and V(IV) concentration in the negative and positive electrode at the end of the discharge period at $t = 2034\ s$. If we compare Fig. 8.5 (concentration contour for $\omega = 1\ mL/s$) and Fig. 8.7 (concentration contour for $\omega = 2\ mL/s$), it is understood that for $\omega = 2\ mL/s$, the concentration in the electrode is more uniformly distributed at the higher flow rate. This is because a higher flow rate decreases the contact time for reaction in the electrode and hence it results in little longer time for the exit solution to reach the required state of charge. From the above results it is understood that as the flow rate increases, coulombic efficiency increases and the rate of oxygen and hydrogen evolution decreases.

8.5 Effects of electrode porosity

Factors to be considered for selecting the electrode material are resistance to corrosion, specific surface area, electrical conductivity, and porosity. Figure 8.8 shows charge-discharge curves for three different values of electrode porosity. The total volume of electrolyte was equal in all cases. The difference in the curves can be observed in Fig. 8.8 even for small difference in porosity. If we compare Fig. 8.9 and Fig. 8.10, it is evident that the bulk reaction rate is going from $\epsilon = 0.8$ to $\epsilon = 0.6$, therefore, it increases the time taken to reach an equivalent state of charge and coulombic efficiency. Effects with an increased porosity are increased permeability, decreased bulk conductivity, greater electrolyte volume in the electrode and increased bulk diffusion coefficients. If the volume in the electrode increases, bulk reaction rate also increases, therefore a more rapid depletion of V(III) occurs during charging process. Lower the porosity of electrode, uniform distribution of concentration throughout the electrode and therefore, overpotential and current density are significantly higher on an average.

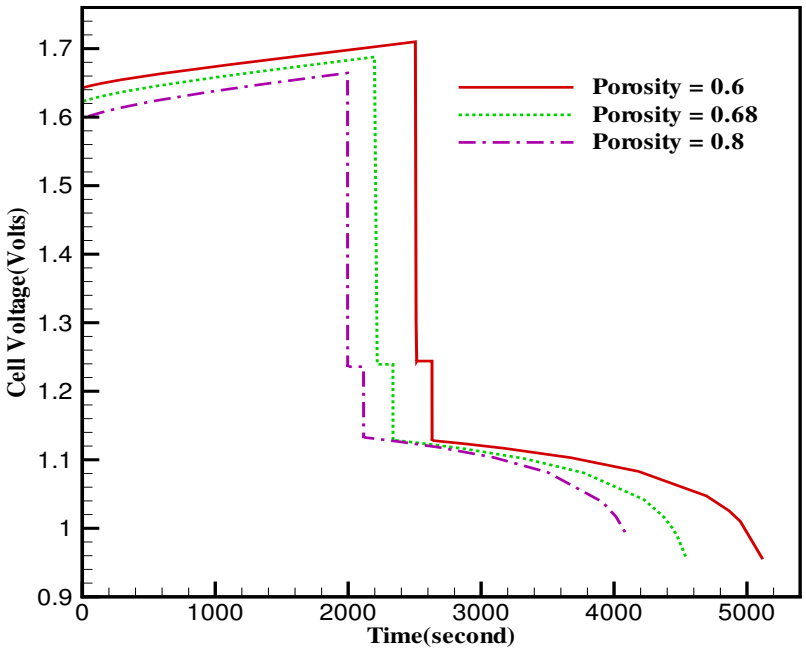

Figure 8.8: Simulated charge-discharge curves for three electrode porosity values, with initial concentration of $C_3^0 = 1080\ mol/m^3$, These charge times are 2498 s for $\epsilon = 0.6$, 2210 s for $\epsilon = 0.68$ and 1988 s for $\epsilon = 0.8$.The other parameter values are given in Table B.12 in appendix B.

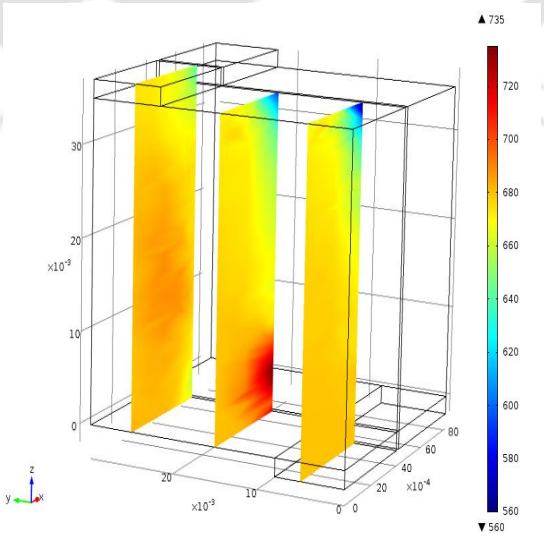

Fig. (a)

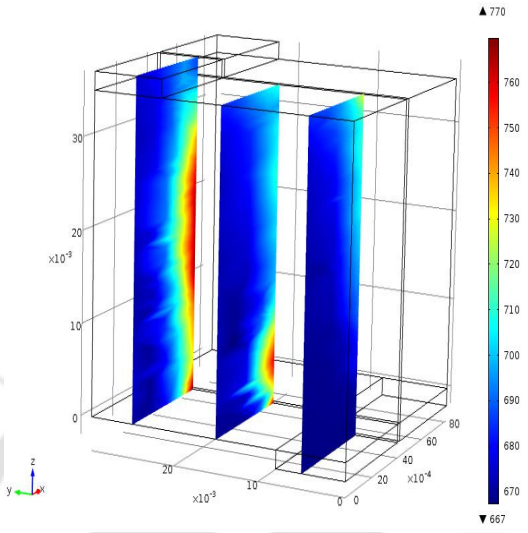

Fig. (b)

Figure 8.9: Surface contour of the V(III) concentration during charge (a) and during discharge (b) corresponding to the cycle, porosity $\epsilon = 0.6$ at $t = 2298\ s$ (end of charge).

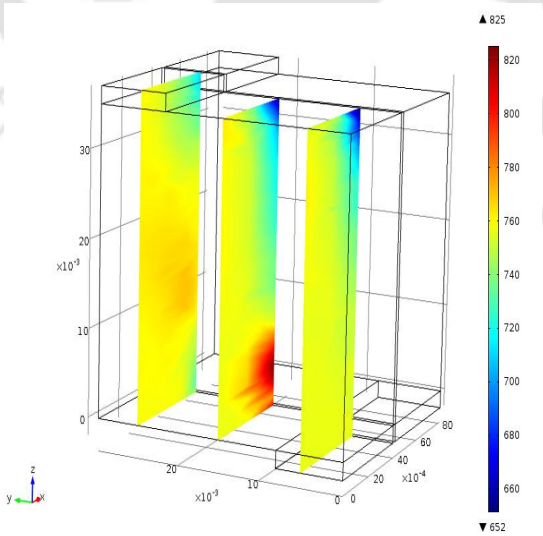

Fig. (a)

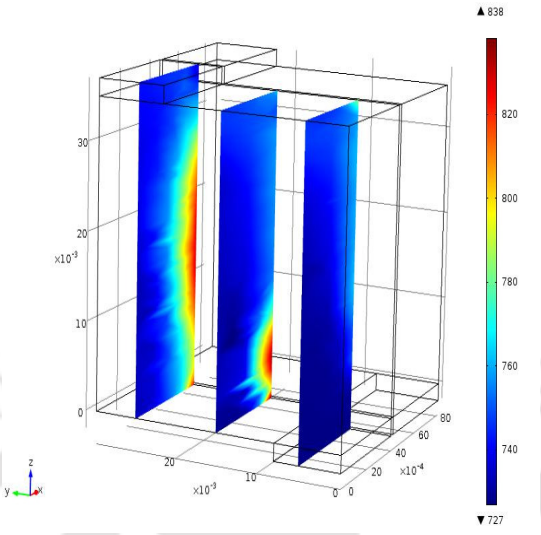

Fig. (b)

Figure 8.10: Surface contour of the V(III) concentration during charge (a) and during discharge (b) corresponding to the cycle, porosity $\epsilon = 0.8$ at $t = 1988\ s$ (end of charge).

8.6 Closure

The performance of the battery is also studied numerically with the three-dimensional isothermal unsteady model. This model is employed to predict the effects of change in electrolyte flow rate, concentration and electrode porosity. It is observed from the results that higher vanadium concentration shows uniform distribution of concentrations inside the cell and increase in cell voltage which leads to high performance. The higher electrolyte flow rate gives longer charging time, higher the coulombic efficiency and also better cell performance. It is also observed that decreasing the electrode porosity by a very small amount results in significant increase in coulombic efficiency and decrease in the rates of hydrogen and oxygen gas evolution reactions.

Chapter 9

Conclusions and Future Work

9.1 Conclusions

In the thesis thermo-electro-hydrodynamic investigations of all-vanadium redox flow battery (VRFB) have been studied using lumped model and numerical simulation. Initially the investigation was started with solving lumped model to see the effect of different parameters on the performance of the battery. From this study it was felt to see the distribution of electrolyte velocity and concentration inside the battery, so the investigations were extended to two- and three-dimensional numerical study using commercial software COMSOL of VRFB to know more about the physics of the problem. The results from the numerical simulation not only provide useful information about limiting mechanisms in the battery reaction, but also can be readily used to optimize battery design. The numerical results provide an improved estimate of the state of charge, offer a useful tool for proposing new charging algorithms and allow the prediction of the power consumption profile associated with a driving cycle. These can be further used in developing protocols for optimization, power management and control in a real-life situation.

A lumped dynamic model due to Shah et al. [27] has been implemented to predict the effects of flow rate, porosity, temperature, concentration and applied current density on the performance of an all-vanadium redox flow battery. It is observed that the higher electrolyte flow rate gives longer charging time and higher cell performance. The lower applied current density yields better potential difference than higher applied current densities. The higher vanadium concentration shows increase

in cell voltage which leads to high performance. The lower porosity of the electrode gives little less potential difference than higher porosity electrode during charging, while discharging it gives higher performance. The higher operating temperature leads to poor performance of the cell.
Then the lumped dynamic model was extended considering the effects of mass transfer and crossover of vanadium ions through the membrane. The model is used to predict the capacity loss of the battery due to the crossover of vanadium ions through the membrane over many cycles at different temperatures. The effect of temperature and porosity on concentration change is studied for three membrane materials such as, Selemion AMV membrane, Selemion CMV membrane and Nafion 115 membrane, and the temperature ranging from 10° C and 40° C. Also effects of temperature on diffusion coefficients and reaction rate constants have been studied. It is observed that for Selemion AMV membrane and Selemion CMV membrane capacity loss shows linear variation with number of cycles. In the case of Nafion 115 membrane capacity loss is experienced for initial 77 cycles then it stabilizes with increase in number of cycles. It is observed that the crossover and mass transfer effects have significant impact on the performance of the cell potential response. The new MTL approximations are used and have predicted well the cell voltage response for higher density ratio.

To consider the effect of temperature in the model, a lumped thermal model based on energy conservation has been developed for the VRFB system. The simulations are performed employing a stack with 19 cells and two cylindrical electrolyte external reservoirs under different air temperatures and operating conditions. It is observed that electrolyte temperatures in both the stack and tanks are very much sensitive to the effects of surrounding air temperature, heat generation by cell and flow rate. The thermal model can be used to predict the battery temperature variation in stack at the particular place of the installation and changes can be made in design of the VRFB materials and structure. In addition to this, the model is more useful for efficient temperature management system to ensure the battery temperature can be controlled to ensure better performance.

Then a transient, two-dimensional, isothermal model for the all-vanadium redox flow battery is solved to get better insights about the physics. With the same condition the present model results are compared with available experimental results and it

shows good agreement with the experimental results. It is observed from the results that higher vanadium concentration shows increase in cell voltage and it leads to high performance. The higher electrolyte flow rate gives longer charging time, higher coulombic efficiency and higher cell performance. The lower applied current yields better potential difference than higher applied current. Also it is observed that decreasing the electrode porosity by very small amount leads to a significant increase in coulombic efficiency and a reduce in the rates of oxygen and hydrogen gas evolution. One of the main feature of the numerical model is the ability to predict many quantities like, profiles of velocity, concentration, pressure etc. By experimental measurements of these quantities are difficult to measure and in some cases not possible, therefore this information can be most important both good performance and long life of the battery.

A dynamic, two-dimensional, isothermal model incorporating concentration overpotential and ohmic losses for the all-vanadium redox flow battery is developed. Due to adding the concentration overpotential and ohmic losses in the model, there is significant value of voltage drop. The effect of electrolyte flow rate, concentration, electrode porosity and applied current on the performance of the cell is also analyzed. The present model is validated with the available experimental result, which shows a good degree of accuracy. Simulation results have predicted that it gives maximum voltage and energy efficiency for concentration $C_3^0 = 1260\ mol/m^3$, therefore it can be considered as optimum value. Also it is observed that increasing the electrolyte flow rate gives better performance of the cell. Lesser value of electrode porosity values shows higher the efficiencies of the cell due to uniform distribution of concentration inside the porous electrode. If the applied current value is less, higher coulombic, voltage and energy efficiencies can be observed due to no side reactions.

One of the major advantage of three-dimensional model is that it can provide the detailed information about the distributions of overpotential, transfer current density and concentration on membrane/electrode interface, which cannot be obtained by two-dimensional model. From the three-dimensional modeling of the vanadium redox flow battery one can predict the performance and optimize the vanadium redox flow battery by studying the distribution of the velocity, concentration, overpotential and transfer current density. A three-dimensional steady stationary VRFB model is solved to predict the VRFB performance in this thesis. The three-dimensional model

is able to predict well the effects of concentration, electrolyte flow rate, electrode porosity, applied current density with state of charge. It is observed that electrolyte distribution has evenness pattern in the porous electrode domain. The higher velocity of electrolyte leads to lower overpotential, therefore there are less chances of side reactions. The flow rate 3 mL/s shows higher energy efficiency due to more uniform distribution of vanadium ions in the porous electrode. Also it is observed that for initial concentration 1440 mol/m^3, it gives higher voltage for both charging and discharging conditions. From the result it is seen that lower electrode porosity gives better performance due to lower polarization and lower hydrogen and oxygen gas evolution side reactions. The higher current density increases the overpotentials in both half of the cell and it leads to side reactions, therefore performance decreases. The three-dimensional numerical model is used to optimize the VRFB cell design and performance. From the results it can be concluded that electrode properties and current density vary with state of charge and these parameters have significant impact on the energy efficiency.

Finally, a dynamic, isothermal, three-dimensional model is solved to see the transient effects. It is observed from the results that higher vanadium concentration shows increase in cell voltage and uniform distribution of concentrations inside the cell, which leads to high performance. The higher electrolyte flow rate gives longer charging time, higher coulombic efficiency and better cell performance. It is also observed that decreasing the electrode porosity by very small amount can lead to a significant increase in coulombic efficiency and decrease in the rates of oxygen and hydrogen gas evolution.

9.2 Future Scope of Work

Even though a lot of research efforts have been put for the development of the lumped model and comprehensive numerical model, there are still more opportunities to improve its performance of VRFB with some more additional features. In this thesis considerable progress has been made on the modeling of the complex multiphysics process in VRFB. However, there is a huge scope to study these effects by doing experiments. The present work can also be extended to study the following numerically.

1. A three-dimensional numerical simulation involving the effects of hydrogen evo-

lution gas reactions can be studied. Analysis may involve the effects of vanadium concentrations, temperature on bubble diameter, applied current and electrolyte flow rate.

2. A three-dimensional numerical model involving the effects of oxygen evolution gas reactions can be studied. More detail analysis involves multi-phase mixture model to study the effects of temperature on oxygen bubble formation.

3. A three-dimensional unsteady non-isothermal model including the effects of crossover of vanadium ions through membrane can be studied. In-depth study of the species crossover within the membrane and the dependency of membrane properties and operating parameters of VRFB can be determined.

4. A numerical model for the zinc-cerium redox flow battery and the vanadium chloride/polyhalide redox flow battery can be developed. The study includes a half-cell reaction requiring the efficient deposition and stripping of zinc metal.

5. A multi-scale three-dimensional pore scale model can be developed to determine the behavior of charge, mass, momentum, energy transport and the performance for different pore geometries and also are to investigate the effective material properties.

References

[1] Skyllas-Kazacos M., Rychick M., and Robins R. (1988) 'All vanadium redox battery', *US Patent*, (4,786,567), pp. 1–22.

[2] Sekiguchi S., Furusato K., Miyabayashi M., Satou K., Tanimoto T., and Naitou S. (2004) 'Redox flow battery', *US Patent*, (6,764,789 B1), pp. 1–14.

[3] Sum E. and Skyllas-Kazacos M. (1985) 'A study of the v(ii)/v(iii) redox couple for redox flow cell applications', *Journal of Power sources*, vol. 15, pp. 179–190.

[4] de Leon P., Frias-Ferrer A., Gonzalez-Garcia J., Sz'nto D.A., and Walsh F.C. (2006) 'Review redox flow cells for energy conversion', *Journal of Power sources*, vol. 160, pp. 716–732.

[5] de Leon P. and Walsh F.C. (2009) 'Secondary batteries zinc systems,zinc bromine', *Encyclopedia of Electrochemical Power sources*, pp. 487–496.

[6] Bae C.H., Roberts E., and Dryfe R.A.W. (2002) 'Chromium redox couples for application to redox flow batteries', *Electrochimica Acta*, vol. 48, pp. 279–287.

[7] Leung P.K., de Leon C.P., Low C.T.J., Shah A.A., and Walsh F.C. (2011) 'Characterization of a zinc-cerium flow battery', *Journal of Power Sources*, vol. 196, pp. 5174–5185.

[8] Scamman D.P., Reade G.W., and Roberts E.P.L. (2009) 'Numerical modelling of a bromide-polysulphide redox flow battery part 1: Modelling approach and validation for a pilot-scale system', *Journal of Power Sources*, vol. 189, pp. 1220–1230.

[9] Skyllas-Kazacos M. and kazacos M. (2011) 'State of charge monitoring methods for vanadium redox flow battery control', *Journal of Power Sources*, vol. 196, pp. 8822–8827.

[10] Wills R.G.A., Collins J., Stratton-Campbell D., Low C.T.J., Pletcher D., and Walsh F.C. (2010) 'Developments in the soluble lead-acid flow battery', *Journal of Applied Electrochemistry*, vol. 40, pp. 955–965.

[11] Vafiadis H. and Skyllas-Kazacos M. (2006) 'Evaluation of membranes for the novel vanadium bromine redox flow cell', *Journal of Membrane Science*, vol. 279, pp. 394–402.

[12] Vynnycky M. (2011) 'Analysis of a model for the operation of a vanadium redox battery', *Energy*, vol. 36, pp. 2242–2256.

[13] You D., Zhang H., and Chen J. (2009) 'A simple model for the vanadium redox battery', *Electrochimica Acta*, vol. 54, pp. 6827–6836.

[14] Bayanov M. and Vanhaelst R. (2011) 'The numerical simulation of vanadium redox flow batteries', *J. Math. Chem.*, vol. 49, pp. 2013–2031.

[15] Sum E., Rychcik M., and Skyllas-Kazacos M. (1985) 'Investigation of the v(v)/v(iv) system for use in the positive half cell of a redox battery', *Journal of Power sources*, vol. 16, pp. 85–95.

[16] Hwang G.J. and Ohya H. (1997) 'Cross linking of anion exchange membrane by accelerated electron radiation as a separator for the all vanadium redox flow battery', *Journal of Membrane Science*, vol. 132, pp. 55–61.

[17] Fabjan C., Garche J., Harrer B., Jorissen L., Kolbeck C., Philippi F., Tomazic G., and Waner F. (2001) 'The vanadium redox-battery: an efficient storage unit for photovoltaic systems', *Electrochimica Acta*, vol. 47, pp. 825–831.

[18] Fang B., Wei Y., Arai T., Iwasa S., and Kumagai M. (2003) 'Development of a novel redox flow battery for electricity storage system', *Journal of Applied Electrochemistry*, vol. 33, pp. 197–203.

[19] Sukkar T. and Skyllas-Kazacos M. (2003) 'Water transfer behaviour across cation exchange membranes in the vanadium redox battery', *Journal of Membrane Science*, vol. 222, pp. 235–247.

[20] Zhao P., Zhang H., Zhou H., Chen J., Gao S., and Yi B. (2006) 'Characteristics and performance of 10 kw class all-vanadium redox-flow battery stack', *Journal of Power sources*, vol. 162, pp. 1416–1420.

[21] Zhang D., Liu Q., Shi X., and Li Y. (2012) 'Tetrabutylammonium hexafluorophosphate and 1-ethyl-3-methyl imidazolium hexafluorophosphate ionic liquids as supporting electrolytes for non-aqueous vanadium redox flow batteries', *Journal of Power sources*, vol. 203, pp. 201–205.

[22] Agar E., Dennison C., Knehr K., and Kumbur E. (2013) 'Identification of performance limiting electrode using asymmetric cell configuration in vanadium redox flow batteries', *Journal of Power Sources*, vol. 225, pp. 89–94.

[23] Chen D., Hickner M., Agar E., and Kumbur E.C. (2013) 'Selective anion exchangemembranes for high coulombic efficiency vanadium redox flow batteries', *Electrochemistry Communications*, vol. 26, pp. 37–40.

[24] Hsieh W., Leu C., Wu C., and Chen Y. (2014) 'Measurement of local current density of all-vanadium redox flow batteries', *Journal of Power Sources*, vol. 271, pp. 245–251.

[25] Jeong S., Kim L., Kwon Y., and Kim S. (2014) 'Effect of nafion membrane thickness on performance of vanadium redox flow battery', *Korean Journal of Chemical Engineering*, vol. 31(11), pp. 2081–2087.

[26] LI M. and Hikihara (2008) 'A coupled dynamical dodel of redox rlow battery based on chemical reaction, fluid flow, and electrical circuit', *IEICE TRANS. FUNDAMENTALS*, vol. E91-A(7), pp. 1741–1747.

[27] Shah A.A., Tangirala R., Singh R., Wills R.G.A., and Walsh F.C. (2011) 'A dynamic unit cell model for the all-vanadium flow battery', *Journal of The Electrochemical Society*, vol. 158(6), pp. A671–A677.

[28] Chen J., Wang B., and Lv H. (2011) 'Numerical simulation and experiment on the electrolyte flow distribution for all vanadium redox flow battery', *Advanced Materials Research*, vol. 236-238, pp. 604–607.

[29] Shah A.A., Watt-Smith M.J., and Walsh F.C. (2008) 'A dynamic performance model for redox-flow batteries involving soluble species', *Electrochimica Acta*, vol. 53, pp. 8087–8100.

[30] Chen C., Yeoh H., and M.H.Chakrabarti (2014) 'An enhancement to vynnyckys model for the all-vanadium redox flow battery', *Electrochimica Acta*, vol. 120, pp. 167–179.

[31] Sharma A., M.Vynnycky, C.Y.Ling, E.Birgersson, and M.Han (2014) 'The quasi-steady state of all-vanadium redox flow batteries: A scale analysis', *Electrochimica Acta*, vol. 147, pp. 657–662.

[32] Turker B., Klein S.A., Hammer E., Lenz B., and Komsiyska L. (2013) 'Modeling a vanadium redox flow battery system for large scale applications', *Energy Conversion and Management*, vol. 66, pp. 26–32.

[33] Xu Q., Zhao T., and Zhang C. (2014) 'Effects of soc-dependent electrolyte viscosity on performance of vanadium redox flow batteries', *Applied Energy*, vol. 130, pp. 139–147.

[34] Tian C., Chein R., Hsueh K., Wu C., and Tsau F. (2011) 'Design and modeling of electrolyte pumping power reduction in redox flow cells', *Rare Metals*, vol. 30, pp. 16–21.

[35] Bromberger K., Kaunert J., and Smolinka T. (2014) 'A model for all-vanadium redox flow batteries: Introducing electrode-compression effects on voltage losses and hydraulics', *Energy Technology*, vol. 2, pp. 64–76.

[36] Ontiveros L. and Mercado P.E. (2014) 'Modeling of a vanadium redox flow battery for power system dynamic studies', *International Journal of Hydrogen Energy*, vol. 39, pp. 8720–8727.

[37] Latha T.J. and Jayanti S. (2014) 'Hydrodynamic analysis of flow fields for redox flow battery applications', *Journal of Applied Electrochemistry*, vol. 44, pp. 995–1006.

[38] Rudolph S., Schroder U., Bayanov I., and Hage D. (2014) 'Measurement, simulation and in situ regeneration of energy efficiency in vanadium redox flow battery', *Journal of Electroanalytical Chemistry*, vol. 728, pp. 72–80.

[39] Latha T.J. and Jayanti S. (2014) 'Ex-situ experimental studies on serpentine flow field design for redox flow battery systems', *Journal of Power Sources*, vol. 248, pp. 140–146.

[40] Rudolph S., Schroder U., Bayanov R., Blenke K., and Bayanov I. (2015) 'Optimal electrolyte flow distribution in hydrodynamic circuit of vanadium redox flow battery', *Journal of Electroanalytical Chemistry*, vol. 736, pp. 117–126.

[41] Ma X., Zhang H., and Xing F. (2011) 'A three dimensional model for negative half cell of the vanadium redox flow battery', *Electrochimica Acta*, vol. 58, pp. 238–246.

[42] Qiu G., Dennison C., Knehr K., Kumbur E., and Sun Y. (2012) 'Pore-scale analysis of effects of electrode morphology and electrolyte flow conditions on performance of vanadium redox flow batteries', *Journal of Power Sources*, vol. 219, pp. 223–234.

[43] Qiu G., A.S.Joshi, Dennison C., Knehr K., Kumbur E., and Sun Y. (2012) '3d pore-scale resolved model for coupled species/charge/fluid transport in a vanadium redox flow battery', *Electrochimica Acta*, vol. 64, pp. 46–64.

[44] Yin C., Y.Gao, S.Guo, and H.Tang (2014) 'A coupled three dimensional model of vanadium redox flow battery for flow field designs', *Energy*, vol. 74, pp. 886–895.

[45] Xu Q., Zhao T., and Leung P. (2013) 'Numerical investigations of flow field designs for vanadium redox flow batteries', *Applied Energy*, vol. 105, pp. 47–56.

[46] Tang A., Ting S., Bao J., and Skyllas-Kazacos M. (2012) 'Thermal modelling and simulation of the all-vanadium redox flow battery', *Journal of Power Sources*, vol. 203, pp. 165–176.

[47] Al-Fetlawi H., Shah A.A., and Walsh F.C. (2009) 'Non-isothermal modelling of the all-vanadium redox flow battery', *Electrochimica Acta*, vol. 55, pp. 78–89.

[48] Xiong B., Zhao J., Tseng K., Skyllas-Kazacos M., Lim T.M., and Zhang Y. (2013) 'Thermal hydraulic behavior and efficiency analysis of an all-vanadium redox flow battery', *Journal of Power Sources*, vol. 242, pp. 314–324.

[49] Xiong B., Zhao J., Wei Z., and Skyllas-Kazacos M. (2014) 'Extended kalman filter method for state of charge estimation of vanadium redox flow battery using thermal-dependent electrical model', *Journal of Power Sources*, vol. 262, pp. 50–61.

[50] Wei Z., Zhao J., Skyllas-Kazacos M., and Xiong B. (2014) 'Dynamic thermal-hydraulic modeling and stack flow pattern analysis for all-vanadium redox flow battery', *Journal of Power Sources*, vol. 260, pp. 89–99.

[51] Zheng Q., Zhang H., Xing F., Ma X., Li X., and Ning G. (2014) 'A three-dimensional model for thermal analysis in a vanadium flow battery', *Applied Energy*, vol. 113, pp. 1675–1685.

[52] Wei Z., Zhao J., and Xiong B. (2014) 'Dynamic electro-thermal modeling of all-vanadium redox flow battery with forced cooling strategies', *Applied Energy*, vol. 135, pp. 1–10.

[53] Oh K., H.Yoo, J.Ko, S.Won, and H.Ju (2014) 'Three-dimensional, transient, nonisothermal model of all-vanadium redox flow batteries', *Energy*, pp. 1–12.

[54] You D., Zhang H., Sun C., and Ma X. (2011) 'Simulation of the self-discharge process in vanadium redox flow battery', *Journal of Power Sources*, vol. 196, pp. 1578–1585.

[55] Tang A., Bao J., and Skyllas-Kazacos M. (2011) 'Dynamic modelling of the effects of ion diffusion and side reactions on the capacity loss for vanadium redox flow battery', *Journal of Power Sources*, vol. 196, pp. 10737–10747.

[56] Badrinarayanan R., J.Zhao, Tseng K., and Skyllas-Kazacos M. (2014) 'Extended dynamic model for ion diffusion in all-vanadium redox flow battery including the effects of temperature and bulk electrolyte transfer', *Journal of Power Sources*, vol. 270, pp. 576–586.

[57] Agar E., Knehr K., Chen D., Hickner M., and Kumbur E. (2013) 'Species transport mechanisms governing capacity loss in vanadium flow batteries: Comparing nafion and sulfonated radel membranes', *Electrochimica Acta*, vol. 98, pp. 66–74.

[58] Benjamin A., Agar E., Dennison C., and Kumbur E. (2013) 'On the quantification of coulombic efficiency for vanadium redox flow batteries: Cutoff voltages vs. state-of-charge limits', *Electrochemistry Communications*, vol. 35, pp. 42–44.

[59] Knehr K.W. and Kumbur E.C. (2012) 'Role of convection and related effects on species crossover and capacity loss in vanadium redox flow batteries', *Elecrochemical Communications*, vol. 23, pp. 76–79.

[60] Agar E., Benjamin A., Dennison C., Chen D., Hickner M., and Kumbur E. (2014) 'Reducing capacity fade in vanadium redox flow batteries by altering charging and discharging currents', *Journal of Power Sources*, vol. 246, pp. 767–774.

[61] Tang A., J.Bao, and M.Skyllas-Kazacos (2012) 'Thermal modelling of battery configuration and self-discharge reactions in vanadium redox flow battery', *Journal of Power Sources*, vol. 216, pp. 489–501.

[62] Won S., Oh K., and Ju H. (2015) 'Numerical analysis of vanadium crossover effects in all-vanadium redox flow batteries', *Electrochemistry Communications*, vol. EA 24218, pp. 1–11.

[63] Shah A.A., Al-Fetlawi H., and Walsh F.C. (2010) 'Dynamic modelling of hydrogen evolution effects in the all-vanadium redox flow battery', *Electrochimica Acta*, vol. 55, pp. 1125–1139.

[64] Al-Fetlawi H., Shah A.A., and Walsh F.C. (2010) 'Modelling the effects of oxygen evolution in the all-vanadium redox flow battery', *Electrochimica Acta*, vol. 55, pp. 3192–3205.

[65] Patankar S.V., *Numerical heat transfer and fluid flow* (McGraw-Hill book company, 1980).

[66] Sun C., Chen J., Zhang H., Han X., and Luo Q. (2010) 'Investigations on transfer of water and vanadium ions across nafion membrane in an operating vanadium redox flow battery', *Journal of Power Sources*, vol. 195(3), pp. 890–897.

[67] Springer T., Zawodzinski T., and Gottesfeld S. (1991) 'Polymer electrolyte fuel cell model', *Journal of Electrochemical Society*, vol. 138(8), pp. 2334–2342.

[68] Newman J. and Thomas-Alyea K.E., *Electrochemical Systems* (A John Wiley and Sons, Inc Publication, 2004).

[69] Yu V. and Chen D. (2014) 'Dynamic model of a vanadium redox flow battery for system performance control', *Journal of Solar Energy Engineering*, vol. 136, pp. 0210051–0210057.

[70] Bernadi D. and Verbrugge M. (1992) 'A mathematical model of the solidpolymerelectrolyte fuel cell', *Journal of Electrochemical Society*, vol. 139(9), pp. 2477–2491.

[71] (2013) 'Introduction to comsol multiphysics', *Version 4.3a*, pp. 1–147.

[72] Skyllas-Kazacos M. (2003) 'Novel vanadium chloride/polyhalide redox flow battery', *Journal of Power sources*, vol. 124, pp. 299–302.

[73] Skyllas-Kazacos M. and Goh L. (2012) 'Modeling of vanadium ion diffusion across the ion exchange membrane in the vanadium redox battery', *Journal of Membrane Science*, vol. 399-400, pp. 43–48.

[74] G.Kear, A.A.Shah, and F.C.Walsh (2012) 'Development of the all-vanadium redox flow battery for energy storage: a review of technological, financial and policy aspects', *International Journal of Energy Research*, vol. 36, pp. 1105–1120.

Appendix A

Variation of cell and reservoir concentration

The mass balance of species i in the reservoirs can be expressed as,

$$V_r \frac{dC_i^{res}}{dt} = -\varepsilon A_{in} u (C_i^{res} - C_i) \tag{A.1}$$

Substitute, $V_r = \frac{V_e}{\delta} = \frac{A_{in} h_e}{\delta}$, into above equation

$$\frac{dC_i^{res}}{dt} = -\frac{\varepsilon A_{in} u}{\left(\frac{A_{in} h_e}{\delta}\right)} (C_i^{res} - C_i)$$

$$\frac{dC_i^{res}}{dt} = -\frac{\varepsilon \delta u}{h_e} (C_i^{res} - C_i)$$

The mass balance of species i in the electrode include recirculation and electrochemical reaction,

$$\varepsilon V_e \frac{dC_i}{dt} = \varepsilon u A_{in} (C_i^{res} - C_i) - A_s \frac{j_{app}}{F} \; for\; V(III)\; and\; V(IV) \tag{A.2}$$

$$\varepsilon V_e \frac{dC_i}{dt} = \varepsilon u A_{in} (C_i^{res} - C_i) + A_s \frac{j_{app}}{F} \; for\; V(II)\; and\; V(V) \tag{A.3}$$

Add the equation A.1 and A.3 to eliminate recirculation terms,

$$V_r \frac{dC_i^{res}}{dt} + \varepsilon V_e \frac{dC_i}{dt} = -\varepsilon A_{in} u (C_i^{res} - C_i) + \varepsilon u A_{in} (C_i^{res} - C_i) - A_s \frac{j_{app}}{F} \tag{A.4}$$

$$V_r \frac{dC_i^{res}}{dt} + \varepsilon V_e \frac{dC_i}{dt} = -A_s \frac{j_{app}}{F} \tag{A.5}$$

Substitute $A_s = SV_e$, into above equation

$$\frac{dC_i^{res}}{dt} + \frac{\varepsilon V_e}{V_r} \frac{dC_i}{dt} = -\frac{SV_e j_{app}}{V_r F} \tag{A.6}$$

Substitute $\delta = \frac{V_e}{V_r}$, into above equation

$$\frac{d}{dt}\left(C_i^{res} + \varepsilon\delta C_i\right) = -\frac{\delta S j_{app}}{F} \tag{A.7}$$

Integrate above equation,

$$C_i^{res} + \varepsilon\delta C_i = -\frac{\delta S j_{app}}{F} t + constant \tag{A.8}$$

Use the initial condition, $t = 0$ and $C_i = C_i^{res} = C_i^0$ to determine the value of constant,

$$\varepsilon\delta C_i^0 + C_i^0 = constant$$

$$constant = C_i^0(1 + \varepsilon\delta) \tag{A.9}$$

$$C_i^{res} = (\varepsilon\delta + 1)C_i^0 - \frac{\delta S j_{app}}{F} t - \varepsilon\delta C_i \tag{A.10}$$

Substitute C_i^{res} into equation

$$\varepsilon V_e \frac{dC_i}{dt} = \varepsilon u A_{in} \left(\left((\varepsilon\delta + 1)C_i^0 - \frac{\delta S j_{app}}{F} t - \varepsilon\delta C_i \right) - C_i \right) - A_s \frac{j_{app}}{F} \tag{A.11}$$

$$\frac{dC_i}{dt} = \frac{\varepsilon u A_{in}}{\varepsilon V_e} \left(\left((\varepsilon\delta + 1)C_i^0 - \frac{\delta S j_{app}}{F} t - \varepsilon\delta C_i \right) - C_i \right) - A_s \frac{j_{app}}{F \varepsilon V_e} \tag{A.12}$$

Substitute $A_{in} = \frac{V_e}{h_e}$ into above equation

$$\frac{dC_i}{dt} = \frac{\varepsilon u \left(\frac{V_e}{h_e}\right)}{\varepsilon V_e} \left(\left((\varepsilon\delta + 1)C_i^0 - \frac{\delta S j_{app}}{F} t - \varepsilon\delta C_i \right) - C_i \right) - A_s \frac{j_{app}}{F \varepsilon V_e} \tag{A.13}$$

Substitute $\tau = \frac{h_e}{u}$ into above equation

$$\frac{dC_i}{dt} = \frac{1}{\tau}\left((\varepsilon\delta + 1)C_i^0 - C_i(\varepsilon\delta + 1) - \frac{\delta S j_{app}}{F}t\right) - \frac{A_s j_{app}}{F\varepsilon V_e} \tag{A.14}$$

$$\frac{dC_i}{dt} = \frac{1}{\tau}(\varepsilon\delta + 1)C_i^0 - \frac{C_i(\varepsilon\delta + 1)}{\tau} - \frac{\delta S j_{app}}{F}t - \frac{A_s j_{app}}{\varepsilon V_e F} \tag{A.15}$$

Substitute $\tilde{\varepsilon} = \frac{1}{\tau}(\varepsilon\delta + 1)$ and $A_s = SV_e$ into above equation

$$\frac{dC_i}{dt} + \tilde{\varepsilon}C_i = \tilde{\varepsilon}C_i^0 - \frac{\delta S j_{app}t}{\tau F} - \frac{SV_e j_{app}}{\varepsilon V_e F} \tag{A.16}$$

$$\frac{dC_i}{dt} + \tilde{\varepsilon}C_i = \tilde{\varepsilon}C_i^0 - \frac{S j_{app}}{\varepsilon F}\left(1 + \frac{\varepsilon\delta}{\tau}t\right) \tag{A.17}$$

$$\frac{dC_i}{dt} + \tilde{\varepsilon}C_i = \tilde{\varepsilon}C_{_i}^0 - \frac{S j_{app}}{\varepsilon F}\left(1 + \frac{\varepsilon\delta}{\tau}t\right) \tag{A.18}$$

Integrate above equation, which is in the form of first-order non homogeneous differential equation. Rewrite this differential equation in the usual form $C_i' + \tilde{\varepsilon}C_i = f(t)$

$$C_i' + \tilde{\varepsilon}C_i = \tilde{\varepsilon}C_{_i}^0 - \frac{S j_{app}}{\varepsilon F}\left(1 + \frac{\varepsilon\delta}{\tau}t\right) \tag{A.19}$$

Also notice that the variable is t, so now C_i is a function of t. Solve the homogeneous part of the differential equation

$$C_i' + \tilde{\varepsilon}C_i = 0 \tag{A.20}$$

$$C_i' = -\tilde{\varepsilon}C_i \tag{A.21}$$

$$C_{h,i}(t) = Ae^{-\tilde{\varepsilon}t} \tag{A.22}$$

Find a particular solution of governing equation. The non homogeneous part of the equation is $f(t) = \tilde{\varepsilon}C_{_i}^0 - \frac{S j_{app}}{\varepsilon F}\left(1 + \frac{\varepsilon\delta}{\tau}t\right)$, a quadratic polynomial, so we look for a particular solution in the form of a quadratic polynomial $C_i(t) = Bt^2 + Ct + D$.

Substituting this to the differential equation,

$$(Bt^2 + Ct + D)^1 + \tilde{\varepsilon}(Bt^2 + Ct + D) = \tilde{\varepsilon}C_i^0 - \frac{Sj_{app}}{\varepsilon F}\left(1 + \frac{\varepsilon\delta}{\tau}t\right) \tag{A.23}$$

$$2Bt + C + \tilde{\varepsilon}Bt^2 + \tilde{\varepsilon}Ct + \tilde{\varepsilon}D = \tilde{\varepsilon}C_i^0 - \frac{Sj_{app}}{\varepsilon F}\left(1 + \frac{\varepsilon\delta}{\tau}t\right) \tag{A.24}$$

Compare the coefficients. The coefficients of t^2:
B=0
The coefficients of t:
$2B + \tilde{\varepsilon}C = -\frac{Sj_{app}}{\varepsilon F}\left(\frac{\varepsilon\delta}{\tau}\right)$
The constant terms are:

$C + \tilde{\varepsilon}D = \tilde{\varepsilon}C_i^0 - \frac{Sj_{app}}{\varepsilon F}$ So, $B = 0$, $C = -\frac{Sj_{app}\delta}{\tilde{\varepsilon}F\tau}$, $D = C_i^0 + \frac{Sj_{app}}{\tilde{\varepsilon}F}\left(\frac{\delta}{\tilde{\varepsilon}\tau} - \frac{1}{\varepsilon}\right)$ and the particular solution is

$C_{p,i}(t) = 0.t^2 + \left(-\frac{Sj_{app}\delta}{\tilde{\varepsilon}F\tau}\right)t + \left(C_i^0 + \frac{Sj_{app}}{\tilde{\varepsilon}F}\left(\frac{\delta}{\tilde{\varepsilon}\tau} - \frac{1}{\varepsilon}\right)\right)$

$C_{p,i}(t) = \left(-\frac{Sj_{app}\delta}{\tilde{\varepsilon}F\tau}\right)t + C_i^0 + \frac{Sj_{app}}{\tilde{\varepsilon}F}\left(\frac{\delta}{\tilde{\varepsilon}\tau} - \frac{1}{\varepsilon}\right)$

The general solution of the non homogeneous equation

$$C_i(t) = C_{h,i}(t) + C_{p,i}(t) = Ae^{-\tilde{\varepsilon}t} + \left(-\frac{Sj_{app}\delta}{\tilde{\varepsilon}F\tau}\right)t + C_i^0 + \frac{Sj_{app}}{\tilde{\varepsilon}F}\left(\frac{\delta}{\tilde{\varepsilon}\tau} - \frac{1}{\varepsilon}\right) \tag{A.25}$$

$$C_i(t) = Ae^{-\tilde{\varepsilon}t} + C_i^0 + \frac{Sj_{app}}{\varepsilon\tilde{\varepsilon}F}\left(\frac{\varepsilon\delta}{\tilde{\varepsilon}\tau} - 1 - \frac{\varepsilon\delta}{\tau}t\right) \tag{A.26}$$

Use the initial condition $C_i(0) = C_i^0$ to determine the value of A and so the solution of the initial value problem.

$$C_i^0 = A + C_i^0 + \frac{Sj_{app}}{\varepsilon\tilde{\varepsilon}F}\left(\frac{\varepsilon\delta}{\tilde{\varepsilon}\tau} - 1\right) \tag{A.27}$$

$$A = -\frac{Sj_{app}}{\varepsilon\tilde{\varepsilon}F}\left(\frac{\varepsilon\delta}{\tilde{\varepsilon}\tau} - 1\right) \tag{A.28}$$

The solution of the initial value problem is,

$$C_i(t) = -\frac{Sj_{app}}{\varepsilon\tilde{\varepsilon}F}\left(\frac{\varepsilon\delta}{\tilde{\varepsilon}\tau} - 1\right)e^{-\tilde{\varepsilon}t} + C_i^0 + \frac{Sj_{app}}{\varepsilon\tilde{\varepsilon}F}\left(\frac{\varepsilon\delta}{\tilde{\varepsilon}\tau} - 1 - \frac{\varepsilon\delta}{\tau}t\right) \tag{A.29}$$

$$C_i(t) = C_i^0 + \frac{Sj_{app}}{\varepsilon\tilde{\varepsilon}F}\left(\frac{\varepsilon\delta}{\tilde{\varepsilon}\tau} - 1 - \frac{\varepsilon\delta}{\tau}t - \left(\frac{\varepsilon\delta}{\tilde{\varepsilon}\tau} - 1\right)e^{-\tilde{\varepsilon}t}\right) \tag{A.30}$$

$$C_i(t) = C_i^0 + \frac{Sj_{app}}{\varepsilon\tilde{\varepsilon}F}\left(\frac{\varepsilon\delta}{\tilde{\varepsilon}\tau} - \left(\frac{\varepsilon\delta}{\tilde{\varepsilon}\tau} - 1\right)e^{-\tilde{\varepsilon}t} - 1 - \frac{\varepsilon\delta}{\tau}t\right) \tag{A.31}$$

Let $\tilde{\varepsilon}\tau = \varepsilon\delta + 1$,

$$C_i(t) = C_i^0 + \frac{Sj_{app}}{\varepsilon\tilde{\varepsilon}F}\left(\frac{\varepsilon\delta}{\varepsilon\delta+1} - \left(\frac{\varepsilon\delta}{\varepsilon\delta+1} - 1\right)e^{-\tilde{\varepsilon}t} - 1 - \frac{\varepsilon\delta}{\tau}t\right) \tag{A.32}$$

$$C_i(t) = C_i^0 + \frac{Sj_{app}}{\varepsilon\tilde{\varepsilon}F}\left(\frac{\varepsilon\delta}{\varepsilon\delta+1} - \left(\frac{\varepsilon\delta-\varepsilon\delta-1}{\varepsilon\delta+1}\right)e^{-\tilde{\varepsilon}t} - 1 - \frac{\varepsilon\delta}{\tau}t\right) \tag{A.33}$$

$$C_i(t) = C_i^0 + \frac{Sj_{app}}{\varepsilon\tilde{\varepsilon}F}\left(\frac{\varepsilon\delta + e^{-\tilde{\varepsilon}t}}{1+\varepsilon\delta} - 1 - \frac{\varepsilon\delta}{\tau}t\right) \tag{A.34}$$

Appendix B

Default parameter values used for simulation

Table B.1: Default values of geometrical parameters used in the model

Symbol	Description	Value
w_e	Width of the electrode	0.004 m
w_m	Width of the membrane	125 μm
w_c	Width of the current collector	0.005 m
b_c	Breadth of the electrode	0.1 m
h_e	Height of the electrode	0.1 m
S	Specific surface area for reaction	420 m^{-1}
ε	Porosity of the electrode	0.67
V_r	Volume of the electrolyte in the reservoir	$2.232\times10^{-4}m^3$

Table B.2: Default values of electrochemical parameters used in the model

Symbol	**Description**	**Value**
E_1^0	Reference potential for reaction 1	-0.26 V
E_2^0	Reference potential for reaction 2	1.004 V
$k_{1,ref}$	Reference rate constant for reaction 1	$3.56 \times 10^{-6}\ m/s$
$k_{2,ref}$	Reference rate constant for reaction 2	$3{\times}10^{-9}$ m/s
σ_e	Ionic conductivity (both positive/negative half cells)	100 s m^{-1}

Table B.3: Default values of operating parameters used in the model

Symbol	**Description**	**Value**
w	Electrolyte flow rate	$1 \times 10^{-6}\ m^3/s$
T	Temperature	297 K
j_{app}	Current density	1000 A/m^2
$C_{H^+}^0$	Initial proton concentration	4200 mol/m^3
C_{H_2O}	Initial H_2O concentration	$4.23 \times 10^4\ mol/m^3$
$C_{V(II)}^0$	Initial V(II) concentration	60 mol/m^3
$C_{V(III)}^0$	Initial V(III) concentration	1140 mol/m^3
$C_{V(IV)}^0$	Initial V(IV) concentration	1140 mol/m^3
$C_{V(V)}^0$	Initial V(V) concentration	60 mol/m^3

Table B.4: Values of diffusion coefficients for three different membrane materials

Membrane	k_2 **(dm/s)**	k_3 **(dm/s)**	k_4 **(dm/s)**	k_5 **(dm/s)**
Selemion AMV	3.53×10^{-8}	2.18×10^{-8}	0.91×10^{-8}	2.57×10^{-8}
Selemion CMV	3.17×10^{-7}	0.716×10^{-7}	2×10^{-7}	1.25×10^{-7}
Nafion 115	6.9×10^{-7}	2.54×10^{-7}	5.37×10^{-7}	4.64×10^{-7}

Table B.5: Default values of geometrical parameters used in the model

Symbol	Description	Value
w_e	Width of the electrode	0.004 m
w_m	Width of the membrane	125 μm
w_c	Width of the current collector	0.005 m
S	Specific surface area for reaction	420 m^{-1}
ε	Porosity of the electrode	0.68
V_r	Volume of the electrolyte in the reservoir	2.232 $\times 10^{-4} m^3$

Table B.6: Default values of electrochemical parameters used in the model

Symbol	Description	Value
E_1^0	Reference potential for reaction 1	-0.26 V
E_2^0	Reference potential for reaction 2	1.004 V
$k_{1,ref}$	Reference rate constant for reaction 1	3.56 $\times 10^{-6}$ m/s
$k_{2,ref}$	Reference rate constant for reaction 2	3 $\times 10^{-9}$ m/s
σ_e	Ionic conductivity (both positive/negative half cells)	100 s m^{-1}

Table B.7: Default values of operating parameters used in the model

Symbol	Description	Value
w	Electrolyte flow rate	1×10^{-6} m^3/s
T	Temperature	297 K
j_{app}	Current density	1000 A/m^2
$C^0_{H^+}$	Initial protons concentration	4200 mol/m^3
$C^0_{H_2O}$	Initial H2O concentration	4.23 $\times 10^4$ mol/m^3
$C^0_{V(II)}$	Initial V(II) concentration	60 mol/m^3
$C^0_{V(III)}$	Initial V(III) concentration	1140 mol/m^3
$C^0_{V(IV)}$	Initial V(IV) concentration	1140 mol/m^3
$C^0_{V(V)}$	Initial V(V) concentration	60 mol/m^3

Table B.8: Default initial and boundary values

Symbol	Description	Value
T	Operating temperature	27°C
C^0_{III}	Initial V(III) concentration	1080 mol/m^3
C^0_{II}	Initial V(II) concentration	27 mol/m^3
C^0_{IV}	Initial V(IV) concentration	1080 mol/m^3
C^0_V	Initial V(V) concentration	27 mol/m^3
$C_H SO_4^-$	Initial HSO_4^- concentration	1200 mol/m^3
$C_H SO_4^+$	Initial HSO_4^+ concentration	1300 mol/m^3
$C^0_{H^+}$	Initial H^+ concentration	1300 mol/m^3
$C^0_{H^-}$	Initial H^- concentration	1200 mol/m^3
p_{out}	Positive and negative electrode outlet pressure	300 KPa
I	Current density	1000 A/m^2
ω	Volumetric flow rate	1 mL/s

Table B.9: Default values of the constants related to current collectors, membrane and electrodes

Symbol	Description	Value
h_e	Electrode height	2 cm
w_e	Carbon electrode width	2 cm
b_c	Carbon electrode thickness	3 mm
w_m	Membrane thickness	180 μm
w_c	Collector thickness	6 mm
ϵ	Carbon electrode porosity	0.68
d	Carbon electrode inter-fibre distance	10 μm
d_f	Carbon electrode fibre diameter	10 μm
a	Specific surface area: electrode	2×10^6 m^{-1}
L_w	Electrode width	3 cm
V_T	Electrolyte volume (half cell)	250 mL

Table B.10: Default values of the constants related to electrochemistry

Symbol	Description	Value
k_1	Standard rate constant: reaction (1)	$1.75 \times 10^{-7}\ m/s$
k_2	Standard rate constant: reaction (2)	$3 \times 10^{-9}\ m/s$
$\alpha_{-,1}$	Cathodic transfer coefficient: reaction (1)	0.5
$\alpha_{+,1}$	Anodic transfer coefficient: reaction (1)	0.5
$\alpha_{-,2}$	Cathodic transfer coefficient: reaction (2)	0.5
$\alpha_{+,2}$	Anodic transfer coefficient: reaction (2)	0.5
$E_{0,1}$	Equilibrium potential: V(II)/V(III)	0.255 V
$E_{0,2}$	Equilibrium potential: V(IV)/V(V)	1.004 V
c_f	Fixed charge site (sulfonate) concentration	$1200\ mol/m^3$
z_f	Charge of fixed (sulfonate) sites	-1

Table B.11: Default values of the constants related to electrochemistry

Symbol	Description	Value
D_{II}	V(II) diffusion coefficient in electrolyte	$2.4 \times 10^{-10}\ m^2/s$
D_{III}	V(III) diffusion coefficient in electrolyte	$2.4 \times 10^{-10}\ m^2/s$
D_{IV}	V(IV) diffusion coefficient in electrolyte	$3.9 \times 10^{-10}\ m^2/s$
D_V	V(V) diffusion coefficient in electrolyte	$3.9 \times 10^{-10}\ m^2/s$
D_{H_2O}	Water diffusion coefficient in electrolyte	$2.3 \times 10^{-10}\ m^2/s$
D_w^{eff}	Water diffusion coefficient in the membrane	$5.75 \times 10^{-10}\ m^2/s$
$D_{H^+}^{eff}$	Proton diffusion coefficient in the membrane	$9.312 \times 10^{-9}\ m^2/s$
$D_H SO_4^-$	HSO_4^- diffusion coefficient in the membrane	$1.23 \times 10^{-9}\ m^2/s$
K	Kozeny-Carman constant: porous electrode	5.55
k_ϕ	Electrokinetic permeability: membrane	$1.13 \times 10^{-19}\ m^2$
k_p	Hydraulic permeability: membrane	$1.58 \times 10^{-18}\ m^2$
μ_{H_2O}	Water viscosity	$10^-3\ Pa\ s$
σ_s	Electronic conductivity of porous electrode	$500\ S/m$
σ_{coll}	Electronic conductivity of collectors	$1000\ S/m$

Table B.12: Default values of the constants related to current collectors, membrane and electrodes

Symbol	Description	Value
h	Electrode height	3.5 cm
L_w	Carbon electrode width	4 cm
L_t	Carbon electrode thickness	4 mm
L_m	Membrane thickness	180 μm
L_t	Collector thickness	6 mm
ϵ	Carbon electrode porosity	0.68

Table B.13: Default parameter values for the thermal modeling of the VRFB

Symbol	Description	Value
c	Concentration of Vanadium	1.6 mol/L
C_p	Specific heat of sulfate	3.2 J/gK
ρ	Density of electrolyte	1354 kg/m^3
num	Number of cells	19
V_c	Volume of each cell	0.9 L
V_{stack}	Volume of the stack	17.1 L
R_c	Average cell resistivity during charging	2.9 Ωcm^2
R_d	Average cell resistivity during discharging	3.13 Ωcm^2
S	Area of electrode	1500 cm^2
F	Faradays constant	96485 C/mol
h_{11}	Convection heat transfer coefficient for the inner cylinder surface	270.1 W/m^2K
h_{12}	Convection heat transfer coefficient for the inner top or bottom surface	405.2 W/m^2K
h_{21}	Convection heat transfer coefficient for the outer cylinder surface	3.5 W/m^2K
h_{22}	Convection heat transfer coefficient for the outer top or bottom surface	5.3 W/m^2K
z	Number of electrons transferred	1

Table B.14: Default parameter values for the thermal modeling of the VRFB

Symbol	**Description**	**Value**
eff	Coulombic efficiency	95%
V_s	Total electrolyte volume for one half-cell	10.95 L
r	Radius of the tank	0.252 m
H	Height of the tank	1 m
V_{tank}	Volume of each tank	200 L
θ	Polypropylene thickness	0.01 m
k	Polypropylene conductivity	0.16 W/m K

Table B.15: Default entropy values used in the simulation

Formula	$S_f(J/mol.K)$
V^{2+}	-130
V^{3+}	-230
VO^{2+}	-133.9
VO_2^+	-42.3
H_2O	69.9
H^+	0

Appendix C

Equations to calculate convective heat transfer coefficients and losses for the thermal modeling of the VRFB

The mode of natural convection heat transfer is assumed for both outer and inner layers of the tanks. The average natural convection heat transfer coefficients can be denoted as,

$$Nu_f = C(Ra)^m \tag{C.1}$$

Where, Nu is the Nusselt number, Ra is the Rayleigh number, C and m are the constant values specified for different cases empirically, f denotes the film temperature defined as the arithmetic mean between the wall and free-stream temperature.
Nusselt number is dimensionless number which is the ratio of convective heat transfer to conductive heat transfer.

$$Nu_f = \frac{hx}{k_f} \tag{C.2}$$

Where, h = convective heat transfer coefficient
x = characteristic length
k_f = thermal conductivity of the fluid

The Rayleigh number is the product of the Prandtl number and Grashof number,

$$Ra = GrPr \tag{C.3}$$

One more dimensionless number is Prandtl number is the ratio of kinematic viscosity to thermal diffusivity

$$Pr = \frac{C_p \mu}{k} \tag{C.4}$$

Where,
C_p =specific heat
μ = dynamic viscosity
k = thermal conductivity
Finally Grashof number is expressed as,

$$Gr = \frac{g\beta\Delta T x^3}{\nu^2} \tag{C.5}$$

Where,
g = acceleration due to gravity
β = volumetric thermal expansion coefficient
ΔT = temperature difference between free-steam and the wall
$\nu = \mu/\rho$ = kinematic viscosity
x = characteristic length
Assume that the film temperature of $27°C$, take the properties of air at atmospheric pressure from tables, calculate Grashof number and Prandtl number and then calculate Nusselt number. Knowing the value of Nusselt number convective heat transfer coefficients can be determined from Eq. (C.2).

C.1 Power losses (P_R) due to internal resistance

This losses is due to the ohmic resistance during charging or discharging, which is given by,
For charging process,

$$P_{Rc} = I^2 R_c \tag{C.6}$$

For discharging process,

$$P_{Rd} = I^2 R_d \tag{C.7}$$

The current I may be charging or discharging current. During charging process, I can be a positive value, while discharging process the current I can be a negative value. Resistance R varying depending on charging or discharging process.

C.2 Chemical power (P_{ch})

It is the heat generated during charging process and heat absorbed while discharging process. To determine the heat generation by chemical reactions change in entropy is considered. The minimum amount of heat generated during chemical reaction process, which is given by,

$$P_{ch} = qn \tag{C.8}$$

The minimum amount of heat can be released by the chemical reaction is calculated by:

$$\begin{aligned} q = T\Delta Sn &= T\left(\sum S_{products} - \sum S_{reactants}\right) \\ &= T\left(S_{VO^{2+}} + S_{V^{3+}} + S_{H_2O} - S_{VO_2{}^+} - S_{V^{2+}} - 2S_{H^+}\right) \end{aligned} \tag{C.9}$$

Consumption rate of vanadium n is given by,

$$n = \frac{I}{zF} \tag{C.10}$$

The values of entropy for reactants and products are given in the table B.15 (Appendix B)

C.3 Total pump power

Total pump power is given by,

$$P_{pump} = \Delta p \times Q \times 2 \tag{C.11}$$

where Q is the electrolyte flow rate.
where Δp is the total pressure drop given by,

$$\Delta p = \Delta p_{friction} + \Delta p_{form} \tag{C.12}$$

where $\Delta p_{friction}$ is the frictional pressure drop , Δp_{form} is the form pressure drop. Frictional pressure drop $\Delta p_{friction}$ is given by,

$$\Delta p_{friction} = f \frac{L}{D_h} \frac{\rho V_m^2}{2} \tag{C.13}$$

where f is coefficient of friction for pipe can be calculated by,

$$f = \frac{56}{R_e} \tag{C.14}$$

$$R_e = \frac{\rho D_h V_m}{\mu} \tag{C.15}$$

where L is the length of the pipe, ρ is the density of the electrolyte, V_m is the velocity of the electrolyte.
Hydraulic mean diameter of pipe D_h can be expressed as.

$$D_h = 4\frac{a_w}{p} \tag{C.16}$$

where a_w is the cross sectional area and p is the perimeter.
Form pressure drop Δp_{form} is given by,

$$\Delta p_{form} = K \frac{\rho V_m^2}{2} \tag{C.17}$$

where K is the form loss coefficient for pipe.